

University of South Bohemia in České Budějovice
Faculty of Science

**Computational modeling of
biomolecular interactions in proteins
using MD simulations**

Ph.D. thesis

Zeenat Zara

Supervisor: Dr. David Reha PhD

České Budějovice 2023

This thesis should be cited as:

Zara, Z., 2023: Computational modeling of biomolecular interactions in proteins using MD simulations. PhD Thesis. University of South Bohemia, Faculty of Science, České Budějovice, Czech Republic, 230 pp.

Annotation

Biomolecular interactions are fundamental for protein structural stability, functional activities, and cellular localization. Non-covalent interacting forces present in proteins such as electrostatic interactions, hydrophobic interactions, hydrogen bonding, and Van der Waals forces are important for protein folding, for holding their 3D structure, proper conformation, and stability, but also to establish intermolecular interactions, involving ligands, substrates, or regulatory molecules. In this thesis, molecular modeling tools and molecular dynamic simulations were used to investigate the interaction of biomolecular systems.

GPCRs (G protein-coupled receptors) encompass the largest family of membrane proteins that are involved in transmitting signals from the extracellular surroundings to the inter regions of the cell. GPCR interaction with G protein is of vital importance in cellular signaling and plays a vital function in numerous physiological processes. A diverse array of ligands, such as neurotransmitters, sensory stimuli, and hormones, can activate these receptors. These receptors are activated by a wide range of ligands, including neurotransmitters, hormones, and sensory stimuli. Using molecular modeling and molecular dynamics simulations, I investigated the interface interactions of 5-hydroxytryptamine receptor type 7 (5HT7R) and its downstream partner G protein.

PETase is an enzyme derived from bacteria (*Ideonella sakaiensis*) that can degrade polyethylene terephthalate (PET), a widely used plastic in bottles and packaging. BHET (bis (2-hydroxyethyl) terephthalate) is an intermediate compound in the degradation pathway of PET. The interaction between PETase and BHET in the presence of an ionic liquid (ILs) has significant importance for improving PET degradation and recycling.

The molecular dynamics simulations in the presence of a solution of ILs offer insights into the enzymatic hydrolysis site of PETase with BHET and hold opportunities for developing an efficient sustainable strategy for plastic bioremediation, waste management, and industrial applications.

Declaration

I hereby declare that I am the author of this dissertation and that I have used only those sources and literature detailed in the list of references.

České Budějovice

.....03/06/2023.....

.....Zeenat Zara.....

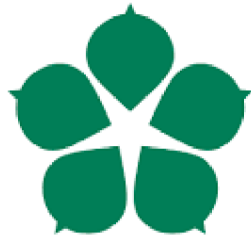
Name and Surname

zeenat zara

.....

Zeenat Zara

This thesis originated from a partnership of **the Faculty of Science, University of South Bohemia**, and the Center for Nanobiology and Structural Biology, Institute of Microbiology of the Czech Academy of Sciences, supporting doctoral studies in the Biophysics study program.



University of South Bohemia
in České Budějovice
Faculty
of Science

Financial support

e-INFRA LM2018140

GAJU 017/2019/P

GA21-15936S

Acknowledgment

I would like to express my gratitude to my supervisor Dr. David Reha and co-supervisor Dr. Babak Minofar for giving me this chance to work on several different projects. It was a wonderful experience to work in your supervision and learn from you how to tackle different scientific problems. Thank you so much for always being so supportive and always believing in me.

I would also like to acknowledge Dr. Alexey Bonder for his insightful contributions to the project. You are a great person who always tries to accommodate not only their colleagues but also their juniors. I would like to thank Dr. Antonella Di Pizio for her continuous guidance and assistance she gave me during this journey. I have been extremely lucky to have you as my host supervisor who always took care of my work and promptly answered any questions I had. I would like to thank Alessesder, Saurabh, and Depti with whom I worked on different projects and for learning many new things. Thank you for helping me during this time, for valuable discussions and for creating a friendly environment.

I would also like to express my deepest gratitude to my husband Muhammad Haseeb for his unwavering love, encouragement, and support throughout this journey. I am profoundly grateful to my parents and family for their unconditional love, support, and invaluable guidance throughout my academic pursuits, including the completion of this degree. I would like to extend my heartfelt appreciation to my dear friend Sana and others. Their friendship has been an invaluable source of inspiration and encouragement throughout my academic journey.

List of papers and author's contribution

1. Zeenat Zara., Deepti Mishra, Saurabh Kumar Pandey, Eva Csefalvay, Fatemeh Fadaei, Babak Minofar, and David Řeha, 2022. Surface Interaction of Ionic Liquids: Stabilization of Polyethylene Terephthalate Degrading Enzymes in Solution. *Molecules*, 27(1), p.119. (IF=4.927). Her contribution was performing all computational parts of the project with 80. %. Involvement.
2. Zeenat Zara, Alessandro Nicoli, Natalia Kulik, David Reha, Alexey Bondar, Antonella Di Pizio, 2023. Preassembly and coupling of 5-hydroxytryptamine receptor type 7 (5-HT7R) and the stimulatory G_s protein: dynamics of the protein-protein interface models. *Journal of Chemical Information and Modeling* (IF=6.162). (submitted). Her contribution was performing major computational parts of the project with 70. %. Involvement.
3. Zeenat Zara, Saurabh K. Pandey, Babak Minofar, 2020. Ionic Liquid-Based Nano-Materials for Drug Delivery, *Encyclopedia of Ionic Liquids*. Springer, Singapore. https://doi.org/10.1007/978-981-10-6739-6_71-1. Her contribution was writing this book chapter with 50. %. Involvement.

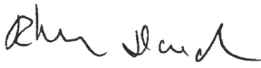
Papers not included in thesis:

Priyakshree Borthakur, Meysam Aryafard, Zeenat Zara, Řeha David, Babak Minofar, Manas h R. Das, Meththika Vithanage, 2021. Computational and experimental assessment of pH and specific ions on the solute solvent interactions of clay-biochar composites towards tetracycline adsorption: Implications on wastewater treatment. *Journal of Environmental Management*, 1(4), article: 111989. (IF=8.910). Her contribution was some computational parts of the project with 25. %. Involvement.

Zeenat Zara, Alessandro Nicoli, Alexandra Steuer, Antonella Di Pizio, 2023. Structural investigations of G protein-coupled receptors: turning challenges into opportunities (manuscript in preparation for the themed issue of the *British Journal of Pharmacology* https://onlinelibrary.wiley.com/pbassets/assets/14765381/Call_ComplexityofGPCRModulationSignalling-1675093013.pdf). Her contribution was some writing of this review with 50. %. Involvement.

Co-author agreement

Dr. David Reha, the supervisor of this Ph.D. thesis and co-author of the following papers [1-2], fully acknowledges the stated contribution of "Zeenat Zara" to these manuscripts.

Signature 

Name : Dr. David Reha

The papers:

1. Zeenat Zara., Deepti Mishra, Saurabh Kumar Pandey, Eva Csefalvay, Fatemeh Fadaei, Babak Minofar, and David Reha, 2022. Surface Interaction of Ionic Liquids: Stabilization of Polyethylene Terephthalate Degrading Enzymes in Solution. *Molecules*, 27(1), p.119.
2. Zeenat Zara, Alessandro Nicoli, Natalia Kulik, David Reha, Alexey Bondar, Antonella Di Pizio, 2023. Preassembly and coupling of 5-hydroxytryptamine receptor type 7 (5-HT7R) and the stimulatory G_s protein: dynamics of the protein-protein interface models. *Journal of Chemical Information and Modeling*. (submitted)
3. Zeenat Zara, Saurabh K. Pandey, Babak Minofar, 2020. Ionic Liquid-Based Nano-Materials for Drug Delivery, *Encyclopedia of Ionic Liquids*. Springer, Singapore. https://doi.org/10.1007/978-981-10-6739-6_71-1.

Contents

1. Introduction	13
1.1 Role of plastic in our world	14
1.1.1 Impact of plastic pollution on the marine environment	14
1.1.2 Degradation of plastic	15
1.1.3 Polyester polyethylene terephthalate (PET).....	17
1.1.4 PET degradation.....	18
1.1.5 PET recycling.....	19
1.2 Biodegradation approach.....	20
1.2.1 Cutinases	21
1.2.2 Lipase.....	22
1.2.3 Esterase	22
1.2.4 PETase	23
1.2.5 Ionic Liquid.....	26
1.3 GPCRs	29
1.3.1 Background of GPCRs	29
1.3.2 Background of G protein	31
1.3.3 Class A 5-hydroxytryptamine (5HT) receptors.....	32
1.3.4 5-hydroxytryptamine 7 receptor (5HT7R)	33
2. Material and methods	35
2.1 Homology modeling.....	36
2.1.1 GPCRdb database.....	37
2.1.2 Main template selection via GPCRdb.....	39
2.1.3 3D structural modeling of the 5HT7R inactive state	42
2.1.4 Template-based modeling:.....	43
2.1.5 <i>Ab initio</i> modeling	43
2.1.6 Active state 5HT7R --Experimental Structure	44
2.1.7 Refinement of the GDP-bound G _s protein.....	44
2.1.8 Refinement of the 5HT7R-G _s complex (active state)	45
2.1.9 Modeling of 5HT7R-G _s preassembled complex	45
2.1.10 Protein preparation of preassembly and coupling complexes	45
2.2 Molecular Dynamics (MD) simulations	46
2.2.1 Classical Molecular Dynamics simulation.....	46

2.2.2 Force fields	47
2.2.3 Bonded interactions	47
2.2.4 Non-bonded interactions	49
2.2.5 Integration algorithms for MD.....	50
2.2.6 Energy minimization.....	53
2.2.7 Equilibration and production of MD	54
2.2.8 MD simulation of PETase-BHET	56
2.2.9 MD simulation of GPCR-Gs protein.....	56
2.3 Analysis of MD Simulations	58
2.3.1 RMSD	58
2.3.2 RMSF calculations	58
2.3.3 SASA	59
2.3.4 Radius of Gyration.....	59
2.3.5 Hydrogen Bond	59
2.3.6 Radial distribution function (RDF).....	60
3. Results and discussions.....	61
3.1 MD simulation of PETase_PET ionic interaction.....	62
3.1.1 MD simulations	62
3.1.2 RMSD plot	63
3.1.3 Root Mean square Fluctuation (RMSF)	66
3.2 5HT7R Modeling Discussion	67
3.2.1 Active and inactive states of 5HT7R.....	67
3.2.2 Preassembled and active state complexes between 5HT7R and the G _s protein.....	71
3.2.3 Molecular Dynamics simulations of active and preassembly complexes	71
3.2.4 Interaction interfaces for the active and inactive complexes before and after MD simulation.....	72
4. Conclusion.....	77
5. References	80

Tables

TABLE 1 EXPERIMENTALLY SOLVED SEROTONIN RECEPTORS WITH ACTIVE (A), INTERMEDIATE (IM), AND INACTIVE (IA) CONFORMATIONS VIA GPCRDB.....	38
TABLE 2 AMINERGIC RECEPTORS FROM CLASS A COMPLEX WITH Gs PROTEIN (DATA FROM GPCRDB)	40
TABLE 3 SEROTONIN RECEPTOR: SEQUENCE IDENTITY/SIMILARITY WITH FULL SEQUENCE, C/N TERMINI, AND ALIGNMENTS. MSA WITH FULL SEQUENCE AND MSA AFTER CUTTING WITH 5HT7R VALUES	42
TABLE 4 SYSTEM DETAILS OF MD SIMULATION FOR GPCR-Gs PROTEIN	57

Figures

FIGURE 1 GENERAL PROCESS OF PLASTIC DEGRADATION UNDER AEROBIC CONDITIONS.	16
FIGURE 2 EUROPEAN UNION PLASTIC DEMAND.....	17
FIGURE 3 ASIA PACIFIC GLOBALLY DOMINATING THE PET MARKET IN 2021[37]	18
FIGURE 4 DIFFERENT METHODS OF PET DEGRADATION.....	19
FIGURE 5 MODEL OF PLASTIC- DEGRADING ENZYME PETASE	23
FIGURE 6 CHEMICAL STRUCTURES OF POLYETHYLENE TEREPHTHALATE (PET), BIS (2-HYDROXYETHYL) TEREPHTHALATE (BHET), MONO 2-HYDROXYETHYL TEREPHTHALATE (MHET), TEREPHTHALIC ACID (TPA), AND ETHYLENE GLYCOL (EG).	25
FIGURE 7 CHEMICAL STRUCTURES OF 1-ETHYL-3-METHYLIMIDAZOLIUM ACETATE [C2MIM][Ac], 1-BUTYL-3-METHYLIMIDAZOLIUM ACETATE [C4MIM][Ac] AND CHOLINIUM PHOSPHATE [Ch]3[PO4].....	28
FIGURE 8 TEMPLATE AND ACTIVE 5HT7R MODEL. A)4IAQ TEMPLATE FOR THE MODELING OF INACTIVE 5HT7R B)7WC4 TEMPLATE FOR THE MODELING OF INACTIVE 5HT7R C) 5HT7R CRYSTAL STRUCTURE IN THE ACTIVE STATE	33
FIGURE 9 PERIODIC BOUNDARY CONDITIONS (PBC)	53
FIGURE 10 SUPERIMPOSED PETASE BACKBONE STRUCTURE WITH DIFFERENT SOLVENTS (40%). BLUE COLOR DEPICTED THE WILD-TYPE, RED COLOR IS FOR WATER SIMULATION, SIMULATION WITH [Ch]3[PO4], [C4MIM][Ac] AND [C2MIM][Ac] ARE SHOWN IN YELLOW, GREEN, AND LIGHT BLUE, RESPECTIVELY.	62
FIGURE 11 ROOT MEAN SQUARE DEVIATION (RMSD) OF CA ATOMS OF WILD TYPE OF PETASE WITH WATER AND THREE DIFFERENT IONIC LIQUIDS SOLUTIONS.	63
FIGURE 12 ROOT MEAN SQUARE DEVIATION (RMSD) OF BHET WITH RESPECT TO PETASE IN WATER AND THREE DIFFERENT IONIC LIQUIDS SOLUTIONS	64
FIGURE 13 ROOT MEAN SQUARE FLUCTUATION (RMSF) OF WILD-TYPE OF PETASE WITH WATER AND IONIC LIQUID SOLUTIONS IN THE PRESENCE OF LIGAND BHET.	66
FIGURE 14 CONFORMATIONAL CLUSTER PLOT FOR SEROTONIN RECEPTORS. GREEN COLOR IS FOR ACTIVE STATE RECEPTORS, BLUE COLOR IS FOR INACTIVE STATE RECEPTORS AND ORANGE COLOR IS FOR INTERMEDIATE STATE RECEPTORS	68
FIGURE 15 MULTIPLE SEQUENCE ALIGNMENT (MSA) OF 5HT7R AND ALL SEROTONIN RECEPTORS (5HT4R, 5HT2A, 5HT1F, 5HT1B, 5HT5A, 5HT1D, 5HT2B, 5HT1A, 5HT1E, 5HT2C, AND 5HT6R. GREEN AND YELLOW COLORS ARE FOR IDENTICAL RESIDUES (GREEN) AND SIMILAR RESIDUES (YELLOW).....	69
FIGURE 16 MODELING OF 5HT7R IN THE A) ACTIVE AND B) INACTIVE STATE. THE REGION FROM THE ACTIVE STRUCTURE IS SHOWN IN GREEN, THOSE MODELED FROM TEMPLATES ARE SHOWN IN PURPLE AND THE AB INITIO REGIONS ARE DEMONSTRATED IN GRAY.	70
FIGURE 17 SEQUENCE OF OTHER SEROTONIN RECEPTORS WITH 5HT7R, ILLUSTRATING ONLY TM6, ECL3 AND TM7. THE GREEN COLOR SHOWS IDENTICAL RESIDUES, YELLOW COLOR SHOWS SIMILAR RESIDUES AND BLUE COLOR SHOWS ECL3 RESIDUES	71
FIGURE 18 IONIC LOCK TM6 (322), H5 (389) A) ACTIVE, B) PREASSEMBLY COMPLEX AFTER MD SIMULATION. THE YELLOW COLOR IS FOR INACTIVE 5HT7R, AND THE GREEN COLOR CARTOON REPRESENTS GA PROTEIN.	72
FIGURE 19 THE INTERACTION OF THE A) ACTIVE AND B) PREASSEMBLY 5HT7 RECEPTOR WITH THE A5 HELIX OF THE GAS PROTEIN DURING MD SIMULATION.	73

FIGURE 20 THE SIDECCHAIN-TO SIDECCHAIN INTERMOLECULAR CONTACTS BETWEEN A) ACTIVE AND B) PREASSEMBLY COMPLEXES AFTER MD SIMULATION. THE YELLOW COLOR CARTOON IS FOR 5HT7R, AND THE RED COLOR IS REPRESENTING THE GA PROTEINS. .. 74

FIGURE 21 A: UNIQUE INTERACTION WITH THE PERCENTAGE OF GPCR:G PROTEIN CONTACTS SPECIFIC TO THE STATIC ACTIVE STRUCTURE OF 5HT7R-Gs PROTEIN, B: UNIQUE INTERACTION WITH THE PERCENTAGE OF GPCR:G PROTEIN CONTACTS SPECIFIC TO THE STATIC ACTIVE STRUCTURE Gs PROTEIN WITH 5HT7R. 74

FIGURE 22 A: UNIQUE INTERACTION IN STATIC PREASSEMBLY COMPLEX % OF 5HT7R INTERACTIONS WITH Gs PROTEIN, B: THE PIE CHART DISPLAYS THE % OF GPCR:G PROTEIN CONTACTS SPECIFIC TO THE STATIC STRUCTURE Gs PROTEIN INTERACTIONS WITH 5HT7R..... 75

FIGURE 23 A: UNIQUE INTERACTION % OF ACTIVE COMPLEX 5HT7R-Gs PROTEIN AFTER MD. B: THE PIE CHART DISPLAYS % OF GPCR:G PROTEIN CONTACTS SPECIFIC TO Gs PROTEIN WITH 5HT7R..... 75

FIGURE 24 A: UNIQUE INTERACTIONS % OF PREASSEMBLY COMPLEX 5HT7R-Gs PROTEIN AFTER MD. B: THE PIE CHART DISPLAYS THE % OF GPCR:G PROTEIN CONTACTS SPECIFIC TO THE STRUCTURE Gs PROTEIN INTERACTIONS WITH 5HT7R. 76

LIST OF ABBREVIATIONS

PET	Polyethylene terephthalate
BHET	Bis (2-hydroxyethyl) terephthalate
MHET	Mono 2-hydroxyethyl terephthalate
TPA	Terephthalic acid
EG	Ethylene glycol
ILs	Ionic Liquids
GPCR	G-protein coupled receptor
5HT7R	5-hydroxytryptamine receptor type 7
AMBER	Assisted Model Building with Energy Refinement
BLAST	Basic Local Alignment Search Tool
CHARMM	Chemistry at HARvard Macromolecular Mechanics
GROMACS	GRoningen MAchine for Chemical Simulations
IP3	Inositol trisphosphate
MD	Molecular Dynamics
NMR	Nuclear Magnetic Resonance
PDB	Protein Data Bank
PLC	Phospholipase C

POPC	1-Palmitoyl-2-oleoylphosphatidylcholine
GAFF	Generalized Amber Force Field
OPLS	Optimized Potential for Liquid Simulations
PBC	Periodic Boundary Conditions
RDF	Radial Distribution Function
RMSD	Root Mean Square Deviation
RMSF	Root Mean Square Fluctuation
SASA	Solvent Accessible Surface Area
VMD	Visual Molecular Dynamics

1. Introduction

1.1 Role of plastic in our world

Plastics are ubiquitous in our modern world today. Approximately 380 million metric tons of plastic are manufactured each year. [1] It was estimated that during 1950 to 2015 [2], a total of 6300 million metric tons (Mt) of plastic was produced in the world. Out of this amount, 756 Mt became waste, 4977 Mt were set to landfills or ended up into the environment such as waterways and ocean [3]. In the modern economy, plastics have become global workhorse material-merging matchless functional asserts with low cost. Its consumption has increased in past to twentyfold and is anticipated to double in the next 20 years. Plastic is used in every human activity. They are mainly used for production of transportation vehicles (planes, trains as well as in cars) and in construction industrial and household materials. Now almost everywhere, every day, everyone meets with plastics-particularly packaging [4].

Although plastic has many useful applications, but the single-use plastic products have an advance effect on our environment, economy, and human health. Towards the end of twentieth-century, commodity production has opened commodity packaging company that itself one of the unsuited structures of our daily life. Globally, every minute 1 million plastic bottles are purchased, and approximately five trillion plastic bags are utilized annually [5]. Further in discount stores more than 80% of the merchandise is packaged unwontedly. When the items are straddled to present on the back of cardboard backing, almost every packaging includes plastic bubble or see-through windows. This package attracts the attention of consumers by using color or design, to a specific brand-name commodity [6].

1.1.1 Impact of plastic pollution on the marine environment

Numerous efforts have been considered to estimate the plastic pollution in marine life, most of these emphasize the abundance of plastic litter along the coastline [7]. Plastic can accumulate on the beaches because it is buoyant. The debris from the beaches is being studied and it has been found that three-quarter of all debris on the beaches are made of plastics. This significant level of plastic pollution in the environment shows the abundance of plastic products in the circulation [8, 9].

Unfortunately, most of the plastic we use can't biodegrade by itself, but it does physically break into smaller particles in marine life, where it becomes a part of the food chain and causes serious health effects [10]. Ultimately the collective amount of undesired plastic product end as waste, which is not easily degradable and resultant as accumulation in the environment. The

core hazards of plastic are for seawater animals mount involvement in and swallow of pronounced stuffs [11]. Mostly brood animals become entangled in plastic wreckages, resultantly creates serious problems in animal growth [12], hindrance in movement and adverting the animals from properly feeding. Plastic also effects the marine organism in other number of ways such as the release of plastic additives as plasticizer which can leak into the water, ingestion of plastics can also lead to physical blockage, internal damage, choking, stress problem and exposure of contamination can cause the persistent organic pollution [13]. These plastic additives as persistent organic pollutants can make changes in the metabolic process, endocrine disruption [14] or behavioral change. In the primary producer of food chain such as algae, it can also reduce photosynthesis and growth and it also affects the development and reproduction of crustaceans [15].

Moreover, The marine plastic rubbles consisting of biological insecticides likes dichlorodiphenyltrichloroethane (DDT), bisphenol A (BPA), polycyclic aromatic hydrocarbons (PAHs), and other toxic chemicals for examples nonylphenol (NP) and polychlorinated biphenyls (PCBs) [16-18]. These toxic agents are directly connected to health issues such as abnormal growth, imbalance of hormones, neurological impairment, breast cancer, diabetes, DNA hypomethylation and neurobehavioral changes [19-22].

The smaller pieces of plastic are even harmful as they can enter the biological systems (plants, bacteria, animals) and cause direct damage to organisms, further by entering the food chain they can approach the human being. Marine faunae can catch by the trash of plastic or ingest it-either by mistake it as pray or as the plastic tiny pieces presence in sea,bed [23]. Thus, the environmental challenges are increasing by large amount of unwanted plastic accumulation in the ecosystem.

1.1.2 Degradation of plastic

According to legislation, extensively used plastic when released in environment should not naturally degrade [24-27]. This might be the basic reason of admiration and prevalent approach of various polymers is their exceptional durability and firmness[24, 25]. Thus, by the four ways the plastic can be degrade in the atmosphere 1) thermooxidative degradation, 2) photodegradation 3) biodegradation by microorganisms 4) hydrolytic degradation.

Basically, the first step in plastic degradation is photodegradation, which subsequently results in thermooxidative degradation. The incorporation of oxygen atoms into the polymer is

initiated by ultraviolet radiation (UV) from the sun, as it provides the necessary activation energy [28, 29]. This process makes the polymer brittle and fractures it into smaller pieces, ultimately reaching a size that allows for its metabolism by microorganisms [25]. This process implies biological and physical forces leading to mineralization of the monomers is known as Bio-mineralization [30, 31]. These small pieces can certainly pass through semi-permeable bacterial membrane and serve as carbon and energy source for the organism, referred to as depolymerization [32] (Figure 1).

Nevertheless, this entire process is relatively slow, with complete degradation take up to 50 years to occur. There are number of factors due to that degradation in the ocean is hindered, including the fact that many polymers have slow rate of hydrolysis in the ocean, and the photodegradative is comparatively slow due to lower temperature and limited oxygen in the sea [7].

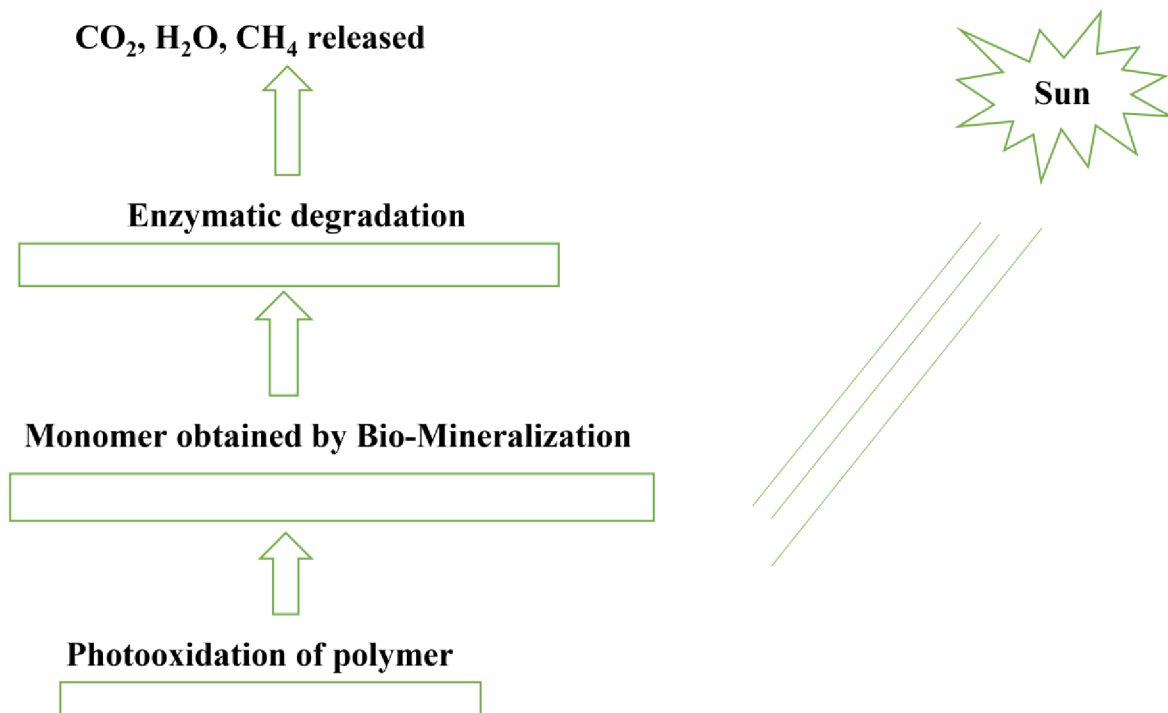


Figure 1 General process of plastic degradation under aerobic conditions.

Research has revealed that in the backbone of polylactic acid (PLA), polylactide-co-glycolide acid (PLGA), and polyglycolic acid (PGA), there is a chemical labile bond that is susceptible to bulk degradation. During this process the hydrolytically unstable ester backbone undergo random scission and break down into its monomer (glycolic acid (GA) or lactic acid) which

further break down into water and carbon dioxide that safely eliminate from the body via urine and tricarboxylic acid cycle [33].

1.1.3 Polyester polyethylene terephthalate (PET)

PET is a semi-crystalline biodegradable material that belong to thermoplastic polymer resin group within the polyester family. A major portion (60%) of PET production is used in polymer fiber and a lesser (30%) portion of it is used for PET bottles [34]. PET material is extensively considered as a primary choice for packaging beverages. It is lightweight, remarkably transparent, UV resistant, unbreakable in nature and water, gas barrier properties, make it ideal use as a PET bottle for beverages [35]. According to new regulations single-use plastic products will be prohibited from the market. However, we need additional alternates to stop the accumulation of thermoplastic polyester PET in the environment [36]. The predictable global market of PET is estimated to exceed US\$ 72.8 Bn by the end of 2030 with an annual growth rate of about 6.9%. Furthermore, the European plastic demand is expected to increase by 6.5% (Figure 2) [7]. Globally major share (48%) of PET came from the pacific Asia market in 2022 followed by Europe and North America (Figure 3).

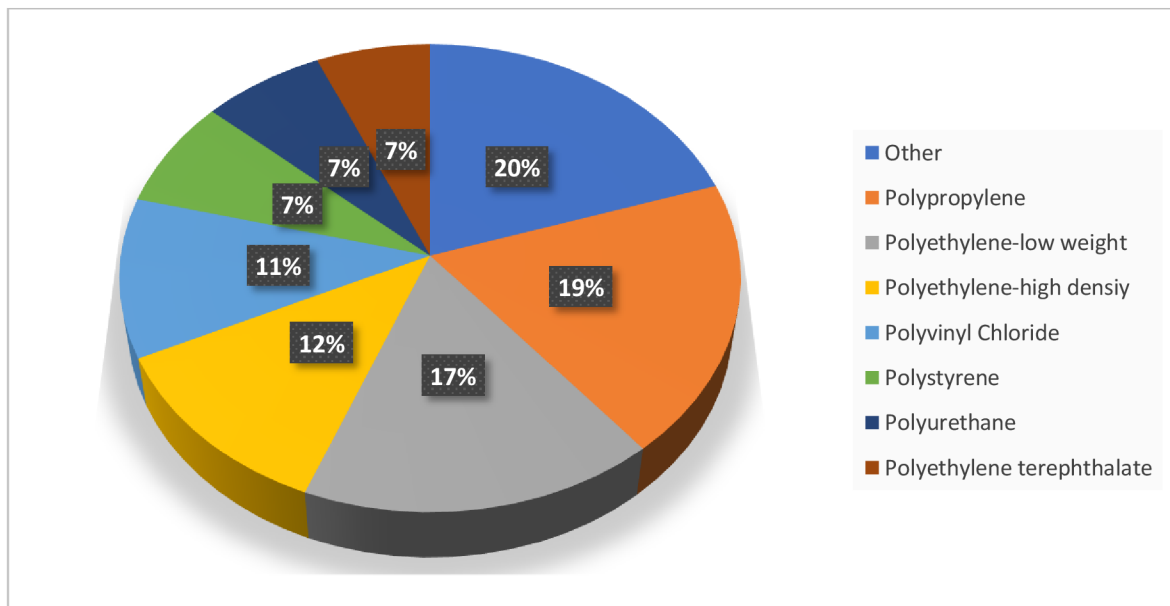


Figure 2 European Union plastic demand

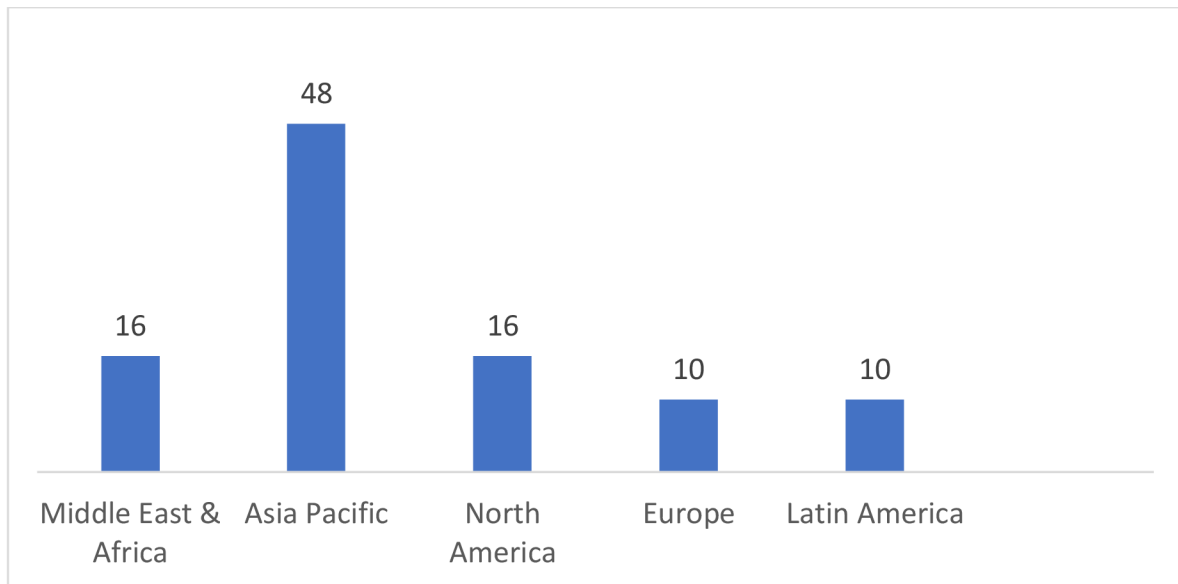


Figure 3 Asia pacific globally dominating the PET market in 2021[37]

1.1.4 PET degradation

There are numerous ways to deal with PET waste (Figure 4), like waste sorting followed by processing of plastic by recycling or destroying (disposing of, decomposing, or degrading). Some of the methods are very expensive while the other methods are not environmentally friendly. Although a significant quantity of PET is recycled to new products, a large portion of PET still ends up in landfills. In Iran, over 1 million m³ of landfill space is required annually to accommodate the disposal of PET bottles. The research on recycled PET in road pavement was started in 1990's [34]. There are several disadvantages of disposing PET in open land as it doesn't degrade rapidly. Sun rays don't affect the decay of plastic as PET polymer is resistant to UV radiation. When PET remains in the landfill for a longer time it creates anaerobic conditions that obstruct any kind of degradation [38].

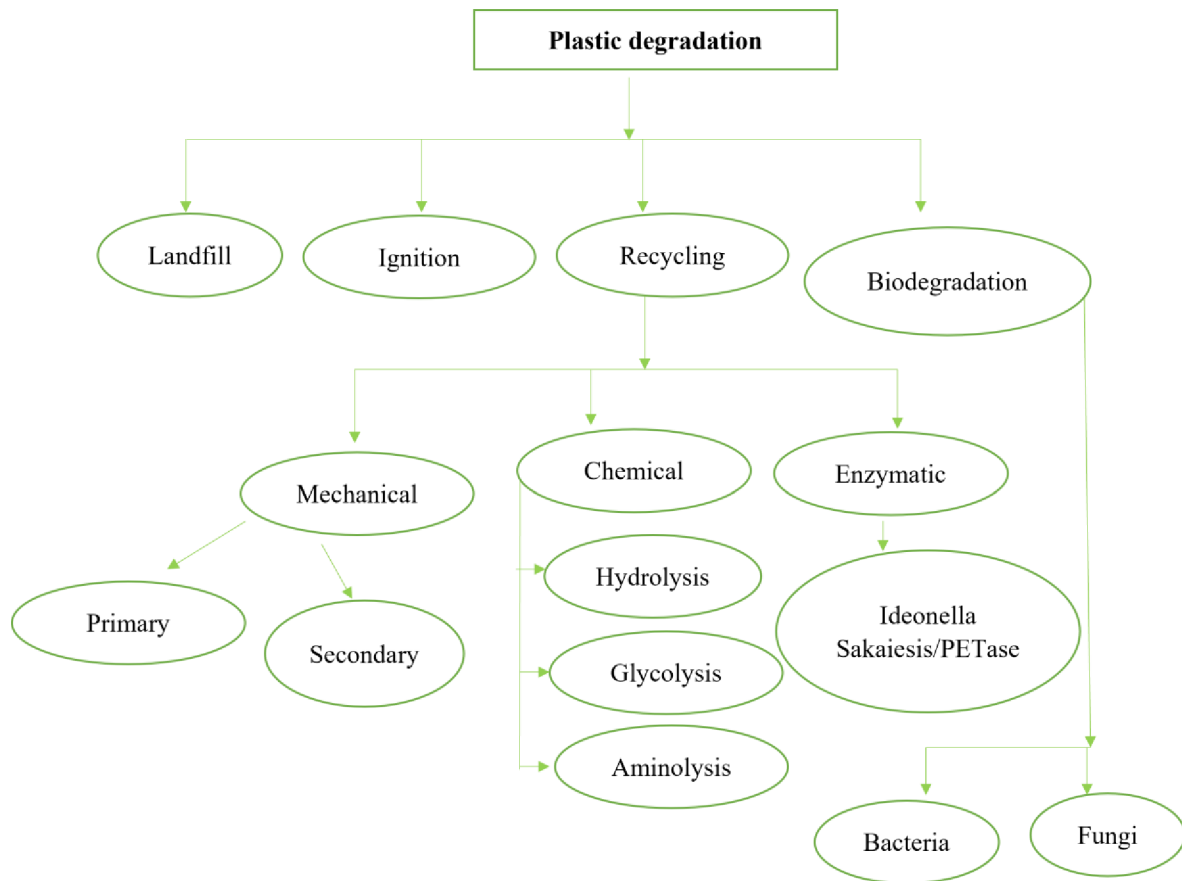


Figure 4 Different methods of PET degradation

The thermal degradation of PET not only requires a very high temperature to break down polymer material but also releases hazardous gases into the environment. Usually, Isothermal degradation of PET needed around 270-370 °C temperature to simulate the reaction process in an inert atmosphere (N₂) [39].

1.1.5 PET recycling

When we recycle material, it is engaged in a process known as “closing the loop”, where the materials are transformed into a usable form that can be repeatedly utilized. The utilization of new products derived from recycled materials not just brings environmental advantages, but it also saves energy that would otherwise be used during the mining or extraction of virgin materials. However, it is not a case of recycling plastic material where the loop is not closed. Recycled plastic can decrease its mechanical strength which degrades further upon reheating. However, partial recycling of PET can be obtained via chemical, mechanical, and biological processes.

During mechanical recycling, the PET material undergoes the following steps such as collecting, handling, sorting, shredding, melting, and granulation. In primary recycling, PET is collected from manufacturing industries, while in secondary recycling, the resulting new products may exhibit lower properties compared to the original products [40]. The ester group found in PET can be depolymerized through the use of various substances such as water (hydrolysis), alcohol (alcoholysis), glycols (glycolysis), acid (acidolysis), and amine (aminolysis). The product obtained because of chemical recycling depends on the reagent used.

In hydrolysis, the PET is recycled through a reaction of PET with water in the presence of either alkaline, neutral, or acidic environment to depolymerize it into its monomers such as terephthalic acid (TPA), and ethylene glycol (EG). These EG and TPA would be reused for the PET synthesis. In this way, the need for methanol production for synthesis of PET is eliminated. The main disadvantage of hydrolysis is to use high temperatures such as 200 to 250 °C and pressure 1.4 to 2 MPa for a longer time for complete depolymerization [41-43]. Commercially, hydrolysis is not extensively employed for food packaging PET due to high cost to purify recycled TPA.

During glycolysis, ethylene glycol (EG) is inserted into the PET chain to break down into bis (2-hydroxyethyl) terephthalate (BHET), a monomer of PET synthesis. This process requires a broad temperatures range of 180 to 240 °C for about 8 hours [41]. But in the absence of a catalyst, this process is very slothful [44-47]. However, researchers have investigated the glycolysis of PET using various catalysts. e.g. solid superacid [48], titanium-phosphate [49], metal acetates [49, 50] and few metal oxides such as TiO₂, Fe₂O₃, NiO [51] but these all catalysts are not only corrosive but also toxic and resulting in spartan pollution. Thus, the pursuit of extremely efficient and environmentally friendly catalysts or natural dilapidation ends in enzymatic degradation.

1.2 Biodegradation approach

The above-mentioned chemical degradation techniques have several drawbacks, which have posed significant challenges on a global scale. Technical hurdles for energy consumption, capital investments, the availability of resources and long taking time are important limiting factors. There are also various factors, such as the use of inorganic acids, the necessity for preliminary unit operations like filtration, crystallization, distillation, the control of elevated

temperature and pressure, contribute to the demand for more effective and environmentally friendly solutions.

Most polymers are resistant to degradation especially PET, polyethylene, polypropylene or polystyrene. As the result, the environmentalists build up an idea to use an approach that is both safer and economically viable for the society [52, 53]. The biodegradation of PET via enzymatic approach is an environmentally friendly method that is emerging as an economically viable recycling technique [43]. Biodegradation is recognized as an eco-friendly approach. There are various bacterial species and enzymes that have demonstrated promising potential for degrading PET. As the use of microorganisms is an economic approach, however, the maintenance of these microorganisms, cultivation and enzyme extraction indeed require precision.

During enzymatic activity the enzyme cleavages the polyester bond into its constituent monomers that can easily be processed further. The enzyme builds biofilm on the surface of PET due to cell surface hydrophilicity, where the enzyme uses carbon as an energy source and enhancing the degradation process [54]. There are different enzymes such as cutinases, lipases, esterases that can degrade PET to different extents.

1.2.1 Cutinases

In 2005, it was found that the PET film can be hydrolyze by enzymatic activity and it was first time purified by the enzymatic activity from the culture of *Thermobifida fusca* [55]. The enzymatic degradation of PET usually takes place with the enzyme cutinase, that can hydrolyze cutin and several other plastics at the temperature between 40 °C to 70 °C and within a pH range 7-9 [56]. There are different cutinases that are obtained from *Thermobifida fusca* cutinase (TfCut2), *Thermobifida fusca* cutinase (TfCut2) and they are known to effectively conduct hydrolysis [56-58]. The Cutinase belongs to α/β serine hydrolase family and it also consists of catalytic triad Ser-His-Asp residues that carrier out ester bond hydrolysis of PET. The high molecular weight PET can accommodate into the active site of cutinase and the hydrolysis of this polymer has been reported by many authors [59]. The catalytic activity of cutinase can be enhanced by adding cationic surfactant at 65 °C. The double mutations G62A/F209A have also been shown to have 12 times higher activity than the wild type cutinase [56]. Peculiarly, cutin and PET share slightly similar structural features apart from the easter bond, that is susceptible to cleavage by the cutinase enzyme [60].

1.2.2 Lipase

For the hydrolysis of PET, the lipase enzyme has also been employed. The enzyme employed for this process, is obtained from *Pseudomonas* sp. and *Candida cylindracea* [61, 62]. Likewise, for the degradation of PET, BHET/TPA-induced lipase has also been utilized from *Aspergillus oryzae*. For efficient hydrolysis of PET, the synergistic action of lipase from *Candida antarctica* (C. antarctica lipase IB CALB) and HiC has also been considered [63, 64]. Moreover, HiC has shown better degradation for PET as compared to degradation of mono 2-hydroxyethyl terephthalate (MHET) to its monomer unit TPA. Whereas CALB can't efficiently degrade PET unit, but it has better degradation of MHET into its monomer TPA. Nevertheless, the combination of lipase from HiC and CALB surprisingly showed better PET hydrolysis as compared to used them singly. However, there is still lack of information of used temperature, pH, and the effect of enzyme dosage. Cutinase and lipase have structural similarities such as hydrophobic surface [64]. Unlike other lipases, lipase B has a shallow catalytic site that allows it to access the substrate even in the absence of hydrophobic interface [65].

1.2.3 Esterase

Currently, only a few bacterial phyla are recognized to produce active PET esterase enzymes. There are two famous esterases which are characterized by *Aequorivita* genera and *Kaistella* within the Bacteroidetes phylum [66]. Bacteria from *Kaistella* are globally found in a variety of habitats such as sea water, the human gut, plant, soil, and fish [67]. Particularly, Bacteroidetes are known for producing very effective degraders of polymers and they are possessing a diverse array of hydrolyses [68-70].

The ester bond present in PET can also be cleaved into MHET and TPA using esterase enzyme from *Bacillus subtilis* nitrobenzylesterase (BsEstB) [38, 71]. During hydrolysis of PET, the presence of metal ions increases the productivity of the reaction. For example, the utilization of calcium ions in conjunction with thermostabilized esterase from *Saccharomonospora viridis* AHK190 enable the efficient hydrolysis of PET [72]. There are other recombinant esterases from *Thermobifida halotolerans* (Thh_Est) which are also employed for the degradation of PET into MHET and terephthalate (TA) [73, 74].

1.2.4 PETase

The above-mentioned enzymes e.g., cutinases, lipases, and esterases are being used as PET degrading microbes. Among these enzymes, cutinase is the most efficient PET degrading enzyme due to its efficiency, and it does not need a lid structure for its activation at lipid-water interface as lipases do for the water-lipid interface [75].

Recently, a new bacterium, *Ideonella sakaiensis* 201-F6, was isolated from a plastic-bottle recycling factory in Japan [76, 77] (Figure 5) .

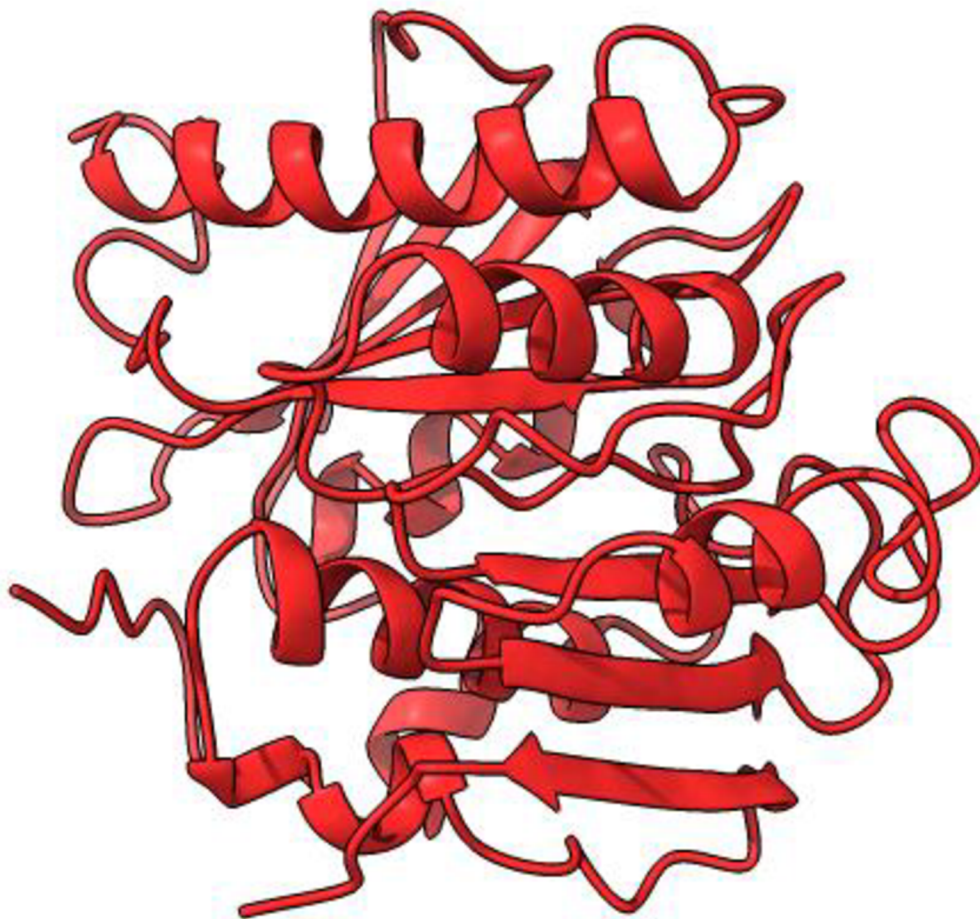


Figure 5 Model of plastic- degrading enzyme PETase

This bacterium utilizes PET as a source of carbon and energy. An improvement in the genomic databases shows that cutinase and PETase are homologues [78]. By biochemical and genetic analysis, scientists identified enzymes implicated in the intracellular pathway of PET hydrolysis and catabolism of extracellular PET hydrolytic products [77]. *Ideonella sakaiensis*

adhere on PET surface and secretes a unique cutinase-like enzyme that can degrade PET and known as PETase. This enzyme breaks down PET into smaller units i.e., BHET, MHET, TPA, and EG (Figure 6) at 30 °C and pH 7.0.

PETase exhibits significantly higher activity compared to previously mentioned PTE hydrolyzing enzymes, with an increase ranging from 5.5 to 120 folds. Additionally, PETase has preference for degrading PET rather than nitrophenol linked aliphatic esters which are surrogated compounds for activity determination of lipase and cutinase. PETase and cutinase enzymes show high sequence similarity that indicates the presence of similar structural features for PET binding [78, 79].

PETase is α/β -hydrolase enzyme that structurally comprises of 6 α -helices and 9 β -sheets. If we compare the active site of PETase with cutinase, it lacks a lid, much shallower, and wider. This active site character is responsible for an efficient binding of PET to the PETase surface. Cutinase has one disulfide bridge whereas PETase possesses an additional disulfide bridge responsible for connecting α and β loops, that participate in catalytic triad. There are also 3 extra residues (-Ser-131, His-208 and Asp-177) that extend the loop in the binding site of PETase and make some space for PET attachment [60]. The conformational flexibility of specific residues such as Trp residue and some other residues which are absent in cutinase, facilitate efficient binding of PET on PETase surface [80]. The PETase enzyme derived from *I. sakaiensis* got huge attention, and it also degrades another aromatic polyester such as polyethylene-2,5-furandicarboxylate. PETase has the specification to degrade only aromatic polyesters as it can't degrade aliphatic polyester [81]. There is another enzyme secreted by *I. sakaiensis* known as MHETase as it degrades MHET into smaller units such as TPA and EG. PETase and MHETase from this bacterium have an essential role in PET degradation [82].

The solubility of plastic materials in enzymatic medium is typically limited, causing challenges for their effective utilization in enzymatic processes. However, alternative media i.e., ionic liquids, organic solvents, and deep eutectic solvents (DES) can be used to overcome this limitation. These solvents improve the solubility of plastic materials and enable better interaction between ligand and the enzymes. On the other hand, these solvents can also influence the activity of enzymes, they can denature enzyme or change its secondary structure or make it to work better and enhance its activity. Morteza and coworkers have investigated the impact of co-solvents on the stability as well as the activity of the enzymes [83]. They investigated that various agricultural and industrial pollutants become a part of the environment to increase the

chemical contamination there. Most of them belong to haloalkanes, and various other enzymes are capable of hydrolytically breaking the C-X bond in haloalkanes [84-86]. They have done theoretical as well as experimental work to consider the activity and inhibitory effects of haloalkanes dehalogenase enzymes with different solvents such as acetone, formamide, and isopropanol. They demonstrated that organic solvents can easily enter the active sites of the enzymes without any competitive inhibition. Thus, organic solvents have an effect on enzyme stability.

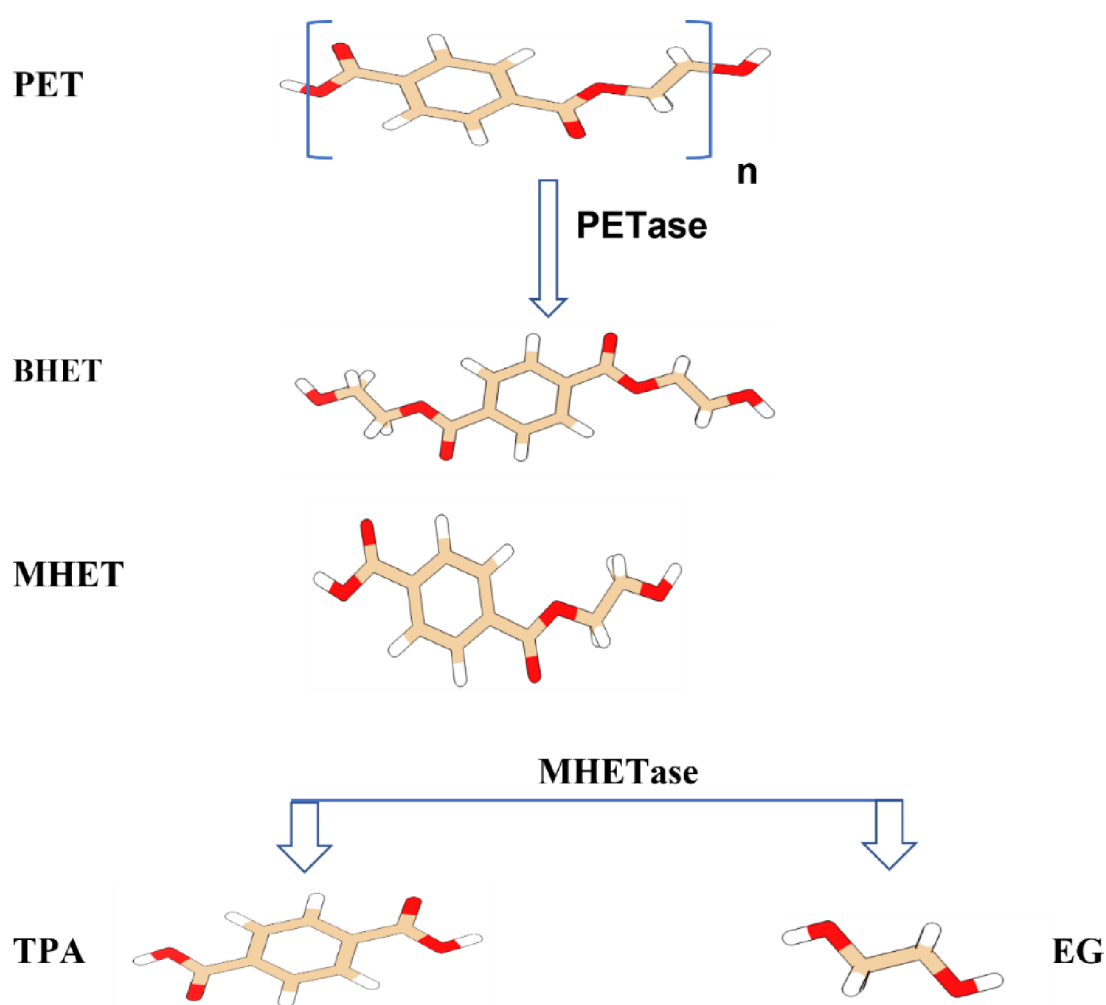


Figure 6 Chemical structures of polyethylene terephthalate (PET), bis (2-hydroxyethyl) terephthalate (BHET), mono 2-hydroxyethyl terephthalate (MHET), terephthalic acid (TPA), and ethylene glycol (EG).

1.2.5 Ionic Liquid

Ionic liquids (ILs) have emerged as a novel class of solvents that gained attention over volatile solvents due to their diverse properties in the field of biochemistry. These solvents which are characterized as ionic liquids have remarkable properties, for example non-flammability, lower vapor pressure, thermal stability, and excellent solvation capacity. These liquids or solvents, with melting point below 100 °C, are known as ionic liquids (salts). Ionic liquids have a wider liquid range: they are liquid at room temperature and this property provides flexibility in selecting a wide range of ionic liquids with desired properties for specific applications.

PET has hydrophobic nature and a crystalline structure that poses challenges for the solubility and recyclability of PET: thus, finding an eco-friendly solvent is demanding [87]. The use of ILs can solve this problem [88]. Certain ILs have the capacity to partially transform the crystalline structure of PET into an amorphous structure. Additionally, as a substitute for conventionally employed organic molecules, various ILs are eco-friendly and can enhance the catalytic activity and stability of the enzymes [89-91]. ILs have remarkable characteristics i.e., thermal stability, low flammability, electrochemical stability, non-volatility, and strong power of dissolution of inorganic and organic compounds [92-95]. We can mix ILs with water at different concentrations to form hydrated ILs, and these hydrated ILs have a function of co-solvents in the solution [96]. The advantages and versatility of ILs have captured the attention of numerous researchers. That can be obtained by optimizing the anion and cation combinations, influencing low flammability, and many other properties [97, 98]. ILs can be employed for the degradation of polymers such as cellulose, utilized by ILs [99-101]. In a recent publication, ILs have been shown to increase the degradation of PET in experimental investigations [36, 102]. The advantage of using ILs over a traditional catalyst such as metal acetates is the ease of purification of recycled PET from ILs. ILs change the crystalline structure of PET into the lower crystalline (amorphous) structure, that can be attacked by PET-eating enzyme (PETase) during catalytic degradation [103].

Ionic liquids have been playing a vital role in dissolving various solutes, rendering them valuable as carriers and drug delivery system. Likewise, ILs are easier to modify or combine with different ILs. based on specific drug molecule or the environment conditions it needs to transvers in order to reach its target site [104]. It can also be utilized as a surfactant in microemulsions that replaced traditional surfactants. The hydrophilic heads of ILs such as imidazolium ring, exhibit stronger interactions with drug molecules as co-surfactant.

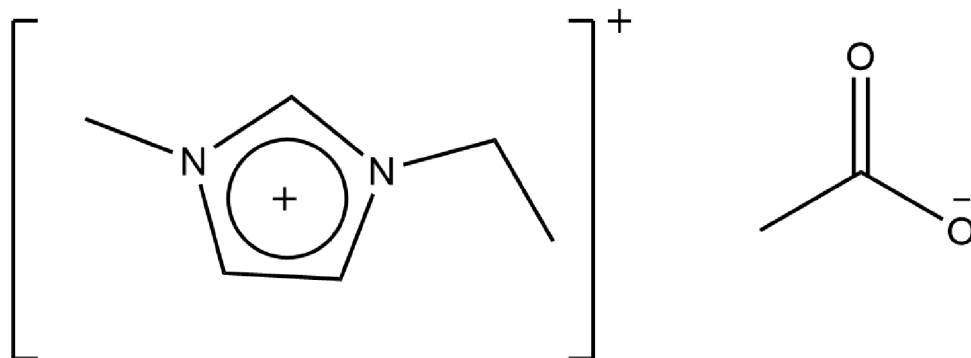
Additionally, these heads have a capacity to accommodate a larger number of solute molecules compared to smaller cationic head groups [105, 106]. Different properties of ILs for example, easy structural modifications, higher thermal or chemical stability, and solubility are proven to be handy in drug delivery when combined with nanoparticles.

It has also been shown that PET can dissolve in a few solvents such as dichloroacetic acid [107], phenol/1,1,2,2-tetrachloroethane solution [102], trifluoroacetic acid [108] and chlorophenol [108] but these solvents are so expensive and highly toxic. The PET degradation with ILs can occur easily with lower temperature and pressure without emission of toxic gases. Thus, the solubilization of PET in ionic liquids is quite demanding and valuable. Similarly, the solubilization of PET in ILs has been investigated by a few innovators led by Sun and his colleagues. They have explored that satisfactory solubility and effectual upgrading of polyethylene terephthalate and the depolymerization of PET have been done by the cheaper ionic liquids such as cholinium phosphate both in aqueous solution and in the pure form [36]. Another attractive character of this depolymerization is the easy separation of products from ILs by adding water and filtration, which allows ILs to be reused in further reactions. It has also investigated the PET degradation mechanism in 1-butyl-3-methylimidazolium chloride and determined that degradation is the first-order reaction kinetics. The activation energy for this reaction has been determined to be 232.79 kJ/mol. PET has also shown reliable solubility in ionic liquids (e.g. imidazolium) such as 1-butyl 3-methylimidazolium with various anions such as Br⁻, Cl⁻, CH₃COO⁻, CF₃COO⁻ and AlCl₄⁻ [102]. Furthermore, PET doesn't dissolve in those ionic liquids which have PF₆⁻ or BF₄⁻ anionic groups attached [102, 109].

The depolymerization of PET by glycolysis in a superlative ionic liquid such as 1-butyl-3-methylimidazole trichlorozincate ([Bmin]ZnCl₃) has been investigated [110]. Recently, Lewis acidic ionic liquids have become a hot topic. It has been found that these ionic liquids' catalytic properties are in the cycloaddition of carbon dioxide. And that the addition of Lewis acid to ionic liquids increases the epoxide yield [102]. The utilization of Lewis acidic ILs as catalysts have been shown to enhance the synthesis of α,β -unsaturated ketones in the cross-condensation of ketone and aldehyde, with a yield of up to 99% [111]. Thus for the depolymerization of PET, Lewis acidic ILs have been intensively used [112, 113].

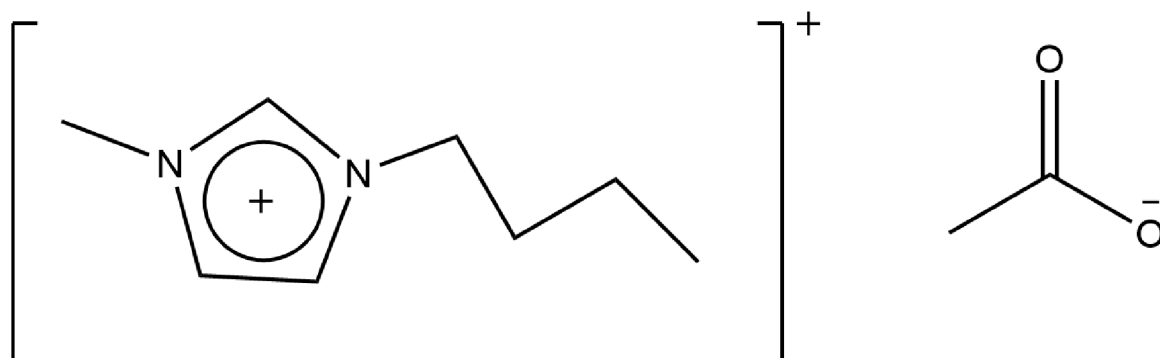
1-Ethyl-3-methylimidazolium acetate

[C2MIM][Ac]



1-Butyl-3-methylimidazolium acetate

[C4MIM][Ac]



Cholinium Phosphate

[Ch]₃[PO₄]

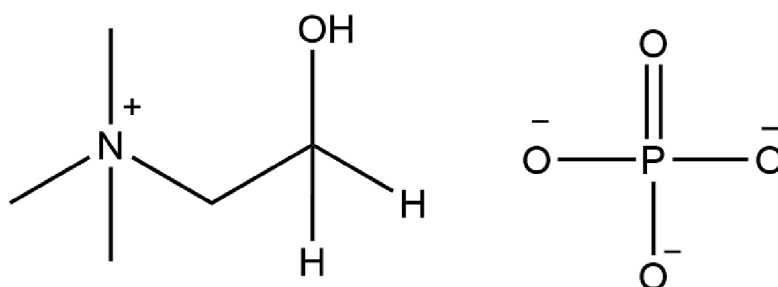


Figure 7 Chemical structures of 1-Ethyl-3-methylimidazolium acetate [C2MIM][Ac], 1-Butyl-3-methylimidazolium acetate [C4MIM][Ac] and Cholinium phosphate [Ch]₃[PO₄].

In this thesis, we have investigated PETase with various ILs such as Cholinium phosphate [Ch]₃[PO₄], 1-Butyl-3-methylimidazolium acetate [C4MIM][Ac], and 1-Ethyl-3-

methylimidazolium acetate [C2MIM][Ac] by molecular dynamics (MD) simulation to determine the effect of an aqueous solution of these ILs on the structure of PETase and to investigate the active site of PETase with ILs. The MD simulations were performed for the wild-type PETase and its ligand BHET in pure water and three distinctive concentrations 40%, 30%, and 20% of [C2MIM][Ac], [C4MIM][Ac], and [Ch]₃[PO₄] ILs that were used as a solvent to dissolve PET (Figure 7).

1.3 GPCRs

1.3.1 Background of GPCRs

G protein-coupled receptors (GPCRs) are essential membrane proteins that mediate a transmission of signals from extracellular environment to intracellular responses. GPCRs are responsible for responding to taste, olfaction, perception of visual signals, neurotransmitters, and hormones. [114, 115]. GPCRs are the main target for many therapeutic drugs and they cover around 35% of total market drugs [116].

GPCRs are comprising of 800 members, making them the largest surface receptor family that are encoded by human genomes [90]. The GPCRs have a shared structural arrangement, comprising of 7 transmembrane (TM) α -helices, an amino terminus located externally, and an intracellular carboxyl tail. There are 3 intracellular loops (ICL1, ICL2, and ICL3) and 3 extracellular loops (ECL1, ECL2, ECL3) that connect the seven TM [117]. These extracellular domains and intracellular domains play a crucial role in the binding of external stimuli i.e., ligands and an internal protein such as G protein. The extracellular loops and intracellular loops are particularly diverse in structure and sequence [118]. There are six classes of GPCRs stated as A-F. Class A, is called as rhodopsin-like, represents the largest group, comprising over 80% of all GPCRs. Class B is known as secretin-like receptor, while class C consists of metabotropic glutamate receptors. Class D includes pheromone receptors, class E as cAMP receptors, and class F is comprises the smoothened/frizzled family of receptors.[119-122]. Non-mammalian GPCRs belong to class D and class E receptors. These 6 families of GPCRs are subdivided into different sub-classes, primarily based on their different functions of GPCRs and their capacity to bind specific ligands [117]. These classes of GPCRs are implicated in numerous biological processes such as cardiovascular functions [123], cancer growth and development [124], and cognitive responses [125]. There is another naming system known as GRAFS system based on a phylogenetic tree that divides mammalian GPCRs into Rhodopsin (R), Frizzled/Taste2 (F),

Adhesion (A), Glutamate (G), Secretin (S) [122]. The main difference between class A-F and GRAFS is that in the GRAGS system, the class B family is further divided into two groups: 1. the Secretin family (B1) and 2. the Adhesion family (B2).

Class A GPCRs are the most numerous and several sequence numbering methods have been suggested to assign an immediate structural references to residues [126-130] [131]. The most widely used numbering scheme is Ballesteros–Weinstein (BW) scheme [131]. According to BW numbering scheme, the TM residues are numbered based on the position of highest conserved residue of each TM. This position is denoted as x.50, where x represents the helix number. From class A GPCRs, the most conserved residues are N^{1.50} (98%), D^{2.50} (90%), R^{3.50} (95%), W^{4.50} (97%), P^{5.50} (78%), P^{6.50} (99%) and P^{7.50} (88%) [132].

The class B, C, and F GPCRs use the same BW numbering for the residue positions but with distinctive reference position. The above-mentioned schemes use the same formatting for the residue numbering; therefore, it is recommended to use class A-F when classification of GPCRs is needed. For the comparison between class B GPCRs, Wootten numbering scheme is handy to use as it uses similar numbering scheme to BW numbering for highly conserved residue in the TM helices [133]. The most conserved residue position is X.50b, where X is TM helix, and b stands for class B GPCR [134]. This numbering scheme is most common for class B1 subclass. The reference TM x.50 residues are also highly conserved for B2 adhesion receptors, except for position 3.50 (frequency of E residue: 58%) and 4.50 (frequency of W residue: 42%).

The class C GPCRs exist mostly as dimers such as homodimer (mGlu and CaS receptors) and heterodimer (GABA_B receptors and T1Rs). The class C numbering scheme is named as Pin numbering scheme in 2003 after the name of ‘Jean-Philippe Pin’ [135, 136]. This numbering scheme also uses conserved residue position for each TM as a reference position, indicated with the x.50c number. The conserved positions are a G in the center of TM1, a middle F for TM2, a K near the end of TM3, a W at the end of TM4, a central L for TM5, a middle W for TM6 and a conserved motif in TM7 (xPKxY). Finally for class F GPCRs, the Wang scheme has been suggested [137].

In humans, there are only 17 members of Class F GPCRs and defining the conservation may be less intuitive. Therefore, if any helix has multiple fully conserved positions, then the position that is closest to the conserved position in Class A (Ballesteros-Weinstein), is employed as a reference position. Recently, Isberg and his colleagues developed a generic GPCR numbering

scheme based on conserved TM residues among all GPCRs, allowing structural comparison between GPCR subtypes [132].

Conserved residues have a vital functional role in GPCRs and are spread along the structure of GPCRs. Long-range intra-molecular and inter-molecular interactions, taking place between distant sites within the same receptor, play a vital role in modulating the signaling function of GPCRs. Furthermore, the Positive coupling or negative coupling between the extracellular domain, TM, and the intracellular domains facilitate cooperativity of activating “switches”, which are essential for the functional plasticity of GPCRs [138, 139]. The downstream signaling of GPCRs involves a combination of G protein-dependent and G protein-independent signaling pathways [140], which regulate diverse cellular responses.

1.3.2 Background of G protein

The extracellular ligands, such as hormones, bind and activate the TM protein e.g., the inactive GPCR. This interaction triggers a conformational change in the GPCRs, allowing it to bind to the G protein situated on the inner side of the cellular plasma membrane [141]. Activated GPCRs bind G protein heterotrimers ($G\alpha\beta\gamma$), and exchange the guanosine diphosphate (GDP) to guanosine triphosphate (GTP) followed by functional release of the G protein and stimulation of downstream pathways [142]. The G protein is categorized into four major groups based on their α subunit [143]: $G_{q/11}$ (activation of phospholipase C), G_s (adenylyl cyclase stimulation), $G_{12/13}$ (activation of small GTP-binding protein), and $G_{i/o}$ (adenylyl cyclase inhibition and activation of rectifying potassium, channels). The G_{12} subgroup consists of $G\alpha_{12}$ and $G\alpha_{13}$. The literature shows that the $G_{12/13}$ proteins are involved in various physiological processes, including cell growth, angiogenesis, the immune response and cell polarity and migration [144]. A typical cell consists about 100 types of GPCRs [145] that are bound to different G proteins. Similarly, within same family of G proteins, several G protein pools might occur, which may explain how receptors coupling to the same G protein family show different actions [146]. There are two main models of coupling between G protein and GPCRs. According to the first model, the GPCRs and G proteins move freely in the cell membrane and they interact after agonist activation which leads productive coupling with G proteins. This type of coupling is known as “collision coupling” and a majority of GPCRs act this way. The second type of association is known as “pre-assembly” in which GPCRs, and G proteins form stable complexes regardless of the activation state of GPCRs. When GPCRs are activated,

conformational changes occur in the GPCR-G protein complex which leads to the activation of the G protein [146].

Different techniques in living cells have been used for investigating the GPCR-G protein interactions. Fluorescence resonance energy transfer (FRET) studies have indicated that GPCRs exhibit interactions with G proteins only when they are in their active state (collision coupling) [147]. Whereas, other investigations (even with the same receptors) utilizing bioluminescence resonance energy transfer (BRET), or FRET suggested that receptors and G protein associated prior to ligand (pre-association) binding, and the activation of G protein occurs through conformational changes within a preformed complex [148-150]. Some additional investigations using fluorescence recovery after photobleaching (FRAP) suggested the differences between receptor and G protein by comparing their ability to form a pre-associated complex [151]. Pre-association of receptor-G protein has been generally reported for various G protein families including G_s , $G_{q/11}$, and $G_{i/o}$ [151-153].

1.3.3 Class A 5-hydroxytryptamine (5HT) receptors

In humans, the neurotransmitter 5-hydroxytryptamine (5HT, serotonin) and its receptors are involved in different behaviors such as sleep, mood, sex, anxiety, memory, and learning. They are also involved in several disease states related to autism, depression, drug addiction, mania, an eating disorder, obesity, and panic effects. Thus, the serotonin receptors are mainly targeted for numerous pharmaceutical drugs. The 5HT receptors are grouped into 7 families such as 5HT1R (1A,1B,1C,1D,1E,1F), 5HT2R (2A,2B,2C), 5HT3R (ligand-gated ion channel), 5HT4R, 5HT5R, 5HT6R and 5HT7R [154]. Three subfamilies (5HT4R, 5HT6R, and 5HT7R) of this 5HT family are coupled with G_s protein, followed by stimulation of adenylyl cyclase and increased cAMP production [155]. The 5HT2R family couples with $G_{q/11}$ of G protein and stimulates the activity of phospholipase C (PLC). 5HT5R and 5HT1R couple with $G_{i/o}$ of G protein to inhibit adenylyl cyclase activity. The 5HT3R is the only ligand-gated ion channel family which is not G protein-coupled receptor [154]. Receptors 5HT4R, 5HT6R, and 5HT7R are significantly different in their mode of coupling with G proteins in an inactive state. 5HT4R and 5HT6R couple with G_s protein only after activation, whereas the protein coupling between 5HT7R and G_s protein is a result of pre-association [147].

1.3.4 5-hydroxytryptamine 7 receptor (5HT7R)

The 5HT7R was cloned for humans, rats, mice, frogs, and guinea pigs independently in three different research labs in 1993 [156]. Alcohol and substance abuse have a profound effect on individual lives and greatly affect a large portion of society. The neurobiological system involved in the addiction process has been investigated by clinical research. There are some studies to investigate the possible connection between alcohol dependence and 5HT7R. Human genetic studies have revealed the presence of a 5HT7R polymorphism that is associated with a genetic predisposition to develop alcohol dependence. Event-related brain oscillations (ERO) are particularly found in alcohol-dependent and in those individuals who have a high risk of developing this disorder. Hence, these deficits are commonly led to alcoholism. Studies found a 5HT7R polymorphism that is associated with altered EROs [156, 157]. Therefore, for the cure of several psychiatric disorders, 5HT7R is particularly targeted [156]. The overall goal of this project was to analyze the pre-assembly complex formation between 5HT7R and G_s protein.

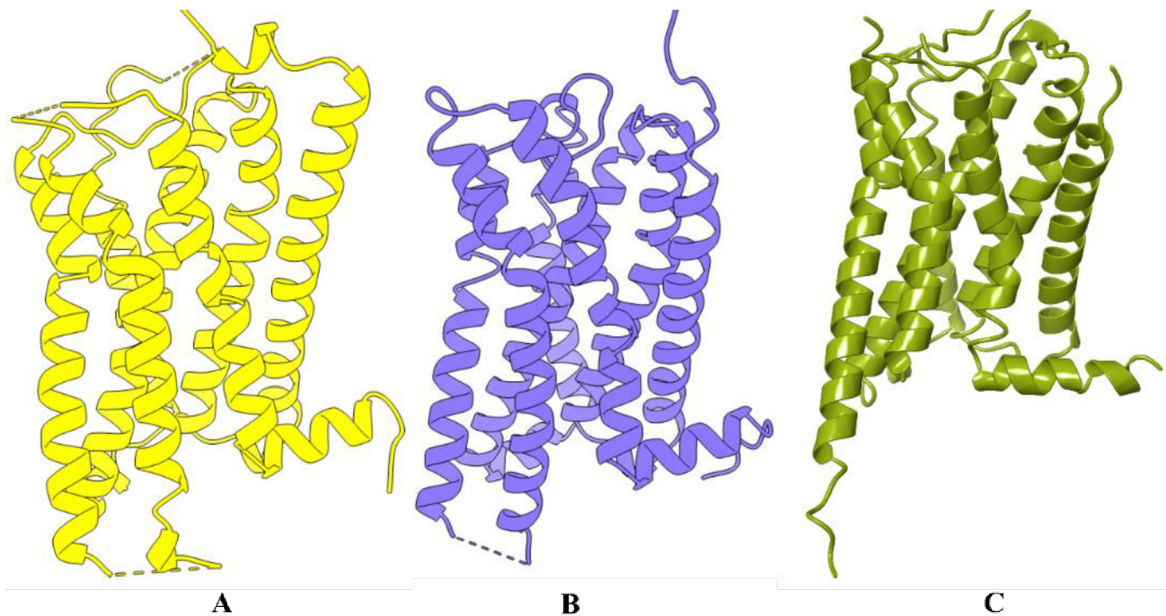


Figure 8 template and active 5HT7R model. A)4IAQ template for the modeling of inactive 5HT7R B)7WC4 template for the modeling of inactive 5HT7R C) 5HT7R crystal structure in the active state

The structural information of GPCRs is obtained from X-ray crystallography, and the number of GPCR structures in their inactive, active, or intermediate states were determined by this technique. The arrival of new structural determinants by cryo-electron microscopy has significantly increased the number of membrane protein structures. There are more structures

are resolved via cryo-electron microscopy than X-ray crystallography [158]. Unfortunately, currently, the inactive structure of 5HT7R has not been experimentally solved, therefore we must rely on computational prediction.

Multiple GPCRs, including 5HT_{1A}R, exhibit interactions with G proteins in the inactive state [147-149, 151, 159-161]. This coupling mode was known as precoupling, preassembly, and inverse coupling. Unlike other 5-HT receptors, 5HT₇R was found to have an inverse coupling with G_s protein by forming a long-lasting preassembled inactive complex [161, 162]. This inactive complex was proposed to downregulate 5HT₇R intrinsic basal activity [161]. However, in the absence of structures of preassembled complexes (I-5HT₇R-G_s protein), the structural determinants of the 5HT₇R and G_s structures required for the inactive complex formation remain unknown.

For this project, it was aimed to characterize the interaction interface between 5HT₇R and the G_s protein in the active (5HT₇R) and inactive states (I-5HT₇R). Recently, the structure of 5HT₇R in its active state (Figure 8 C) in complex with its downstream partner G_s protein was released [163]. However, the structure of 5HT₇R in the inactive state is still not available. Structures of only 15% GPCRs (120 unique receptors) are available at <https://gpcrdb.org/structure/statistics> [164]. Therefore, homology modeling is very important and continuously under development for successful GPCR structure-based drug design [165]. To design I-5HT₇R model, we used an integrated approach using the molecular modeling (Homology modeling) technique (Figure 8 A, B) with pdb structures 4IAQ, 7WC4 as templates. Molecular Dynamics (MD) simulations were used to uncover the structural determinants necessary for preassembled GPCR-G protein complex.

The goal of this project was to learn how to model a G protein-coupled receptor without a known structure (especially 5HT₇R) in a complex with a downstream partner (G_s protein). 5HT₇R share a low sequence similarity with available templates (5HT_{1A}R, 5HT_{1B}R, 5HT_{1E}R), making it a difficult target for modeling [166, 167]. The first challenge was to develop the protocol to accurately predict accurately the three-dimensional (3D) structure of I-5HT₇R and the modeling of complex I-5HT₇R-G_s protein. The second task was to add the missing parts of experimentally solved structure 5HT₇R and model its complex 5HT₇R-G_s protein and run MD simulation with 3 replicas.

2. Material and methods

There are various applications of computational methods to investigate membrane protein and plastic degradation enzymes and have been discussed in **Papers 1 and 2**. Different MD simulation methods are available to investigate membrane proteins, the interaction sites of two enzymes, drug sites on these proteins, and many others. A comparison of these methods, their limitations, and their applications with examples has been discussed. These MD simulation approaches are also employed to investigate any biomolecular system in general. The subsequent sections of our study provide an introduction to the computational methods employed and their applications.

2.1 Homology modeling

To investigate the structure, function, and interaction of a protein, it is crucial to possess a distinct 3D protein model.

There are three techniques which are used to crystalize the structure of macromolecules such as X-ray crystallography [168], electron microscopy [169], and nuclear magnetic resonance (NMR) [170]. Among these methods, X-ray crystallography is a technique, which has solved most of the macromolecular protein structures. A significant proportion of protein structures deposited in the Protein Data Bank (PDB) have been solved via X-ray crystallography [171]. Obtaining the structure of the protein in its highly pure form and at a good resolution can be challenging and it takes some time to achieve it via X-ray crystallography. For example, the structural determination of membrane protein via X-ray crystallography is difficult and needs extra effort and time as membrane proteins are insoluble in water which makes them challenging to get pure samples and then to get the crystal [171, 172]. In spite of recent developments in electro crystallography [173] and 25 other techniques such as neutron diffraction, the determination technique alone is not fast and sufficient enough to solve all the structures of proteins especially if we consider the vast size of solved structures to that of proteomes [174]. Here we use computational methods which play a crucial role in predicting the structure of protein and their complexes.

Comparative modeling or Homology modeling is one of the approaches of computational methods. When the crystal three-dimensional structure of a protein is unknown, different modeling methods may be used to predict its structure. The first method that can be used is homology modeling, this technique or method is used when homologs of a protein of interest (reference protein) or a certain part of a protein of interest have been solved experimentally

[175]. Homology modeling is based on two main assumptions: the homologous protein will have to share analogous protein structures and the protein folding pattern will be more conserved than the overall amino acid protein sequence [176]. It also says that the protein structures which have alike amino acid sequences, incline to make similar 3D protein structures [177]. For example, if we have more than 100,000 known proteins structures, we can categorize them into merely 500 unique folds [178, 179].

The initial and essential step of protein structure prediction through homology modeling is to identify the most relevant and suitable template with a known three-dimensional protein structure. Various online platforms can be utilized to search for reference protein templates, including protein-BLAST[180] [181, 182], UniprotBlast[183] [184], GPCR database[185] [186] and NCBI Blast [187] [188], which offer searches against PDB databases. To obtain a reliable structural model, it is important to have a reasonable sequence identity that exists between the target (reference) sequence and the template structure. This is significant as it minimizes the risk that can arise during automated sequence alignment, and this instills greater confidence that the reference and template both belong to the same protein fold. A sequence identity of more than 30% between the target sequence and the template sequence is generally considered a confidence point widely accepted in the field [178, 189]. It is always better to have multiple templates with a common three-dimensional structural pattern. Multiple sequence alignment (MSA) can be performed on them to resolve errors that may arise in local secondary structural alignment. MSA also provides reliability to the chosen templates when they align with conserved regions [190]. The structural resolution and R factor of templates are also important to take into account as the quality of a target model is dependent on them.

2.1.1 GPCRdb database

GPCRdb server [191, 192] is used for a wide variety of GPCR communities, with over 1800 monthly users. It provides reference data, dynamic visualization of data, statistics, and web server analysis tools. Currently, there are 988 GPCR receptors, 450 GPCR-G protein complexes, and specifically, Class A receptors are 766 <https://gpcrdb.org/structure/statistics>. There are also 52 5-Hydroxytryptamine or Serotonin receptors in their respective conformations (Table 1), and 29 Aminergic receptors (class A) complexes with G_s protein but all are in an active conformation (Table 2).

Table 1 Experimentally solved Serotonin receptors with active (A), intermediate (IM), and inactive (IA) conformations via GPCRdb

Serotonin receptor	PDB ID active/inactive	Resolution	Signal protein-- subtype
5HT4R	7XT8/(A)	3.1	Gs
	7XT9/(A)	3.2	Gs
5HT6R	7XTB/(A)	3.3	Gs
5HT7R	7XTC/(A)	3.2	Gs
5HT1F	7EXD/(A)	3.4	Gi/o-- α 1
5HT1D	7E32/(A)	2.9	Gi/o-- α 1
5HT1A	7E2X/(A)	3.0	Gi/o-- α 1
	7E2Y/(A)	3.0	Gi/o-- α 1
	7E2Z/(A)	3.1	Gi/o-- α 1
5HT1E	7E33/(A)	2.9	Gi/o-- α 1
5HT5A	7X5H/(A)	3.1	Gi/o-- α 1
	7UM5/(A)	2.7	Gi/o-- α O
	7UM4/(IA)	2.8	Gi/o
	7UM6/(A)	2.8	Gi/o-- α O
	7UM7/(A)	2.8	Gi/o-- α O
5HT2A	7WC7/(IA)	2.6	Gq/11-- α q
	7WC4/(IA)	3.2	
	7WC8/(IA)	2.5	
	7WC6/(IA)	2.6	
	7WC5/(IA)	3.2	
	7WC9/(IA)	2.5	
	7VOE/(IA)	2.9	
	7VOD/(IA)	3.3	
	7RAN/(A)	3.5	
	6WGT/(IA)	3.4	
	6WH4/(IA)	3.4	
	6A93/(IA)	3.0	
	6A94/(IA)	2.9	
	6WHA/(A)	3.4	

5HT2B	6DS0/(IM)	3.2	Beta Gq/11-- α q
	6DRY/(IM)	2.9	
	6DRX/(IM)	3.1	
	6DRZ/(IM)	3.1	
	5TVN/(IM)	2.9	
	4NC3/(IM)	2.8	
	4IB4/(IM)	2.7	
	5TUD/(A)	3.0	
	7SRS/(A)	3.3	
	7SRR/(A)	2.9	
5HT2C	6BQG/(A)	3.0	Gq/11— α q Gq/11— α q Gq/11— α q Gq/11-- α q
	6BQH/(IA)	2.7	
	8DPF/(A)	2.8	
	8DPG/(A)	3.6	
	8DPH/(A)	3.2	
	8DPI/(A)	3.4	
5HT1B	7C61/(IA)	3.0	Gi/o-- α o
	5V54/(IA)	3.9	
	4IAQ/(IA)	2.8	
	4IAR/(IA)	2.7	
	6G79/(A)	3.8	

The GPCRdb sequence analysis tool pipeline regularly updates the templates and models to reflect the updates of the database. This tool is developed using Python in the Django web framework and utilizes various tools from the Biopython library [193]. The GPCRdb server utilizes the integration of different manually annotated resources, including GPCR structures from Protein Data Bank with defined helix domains, loop regions, preferred chains, and structure-based sequence alignment with generic BW numbering [132]. It also has a position-specific rotamer library [194].

2.1.2 Main template selection via GPCRdb

The 3D structure of the inactive state of 5HT7R (I-5HT7R) was not experimentally solved. To investigate the interaction interface of I-5HT7R-Gs protein complex, it is important to construct

a 3D model of I-5HT7R based on available templates. The sequence of human 5HT7R isoform D was retrieved from the UniProt database (UniProtKB: P34969 <https://www.uniprot.org/uniprot/P34969>). In GPCRdb, there is at least one (the most complete) demonstrative template is annotated to define aligned transmembrane segments (TM1-TM7), intracellular loops (ICL1-ICL3), extracellular loops (ECL1-ECL3), or to construct any distorted or missing region in the structure of GPCR. The sequence alignment of 5HT7R and other 5-Hydroxytryptamine or serotonin receptors was performed via GPCRdb BLAST (GPCRdb alignment) [164, 195, 196]. A target model's (I-5HT7R) main template is selected based on several factors: i) class (class A Rhodopsin ---Aminergic receptors-- 5-Hydroxytryptamine receptors—5HT7R), ii) state (inactive), iii) sequence-structure selection (full sequence) and iv) select receptors (5-Hydroxytryptamine receptors). The template conformations are decided based on the inward and outward movement of TM5 and TM6 respectively, towards intracellular sites (G protein binding sites). As a result of BLAST, sequence alignment was obtained and a Multiple sequence viewer [197] was used to visualize the selected sequences and manually refine the alignment of 5HT7R.

Table 2 Aminergic receptors from Class A complex with Gs protein (data from GPCRdb)

Receptors	Method	PDB	Resolution	State	Signal Protein
5-Hydroxytryptamine	cryo-EM	7XT9	3.2	Active	Gs
5-Hydroxytryptamine	cryo-EM	7XT8	3.1	Active	Gs
5-Hydroxytryptamine	cryo-EM	7XTB	3.3	Active	Gs
5-Hydroxytryptamine	cryo-EM	7XTC	3.2	Active	Gs
Adrenoceptors	cryo-EM	7DHI	3.3	Active	Gs
Adrenoceptors	cryo-EM	7DHR	3.8	Active	Gs
Adrenoceptors	cryo-EM	7BZ2	3.8	Active	Gs
Adrenoceptors	cryo-EM	6NI3	3.8	Active	Gs
Adrenoceptors	X-ray	6E67	3.7	Active	Gs
Adrenoceptors	X-ray	3SN6	3.2	Active	Gs
Dopamine	cryo-EM	7X2C	3.2	Active	Gs
Dopamine	cryo-EM	7X2F	3	Active	Gs
Dopamine	cryo-EM	7F1O	3.1	Active	Gs
Dopamine	cryo-EM	7X2D	3.3	Active	Gs

Dopamine	cryo-EM	7F0T	3.1	Active	Gs
Dopamine	cryo-EM	7F24	4.2	Active	Gs
Dopamine	cryo-EM	7F1Z	3.5	Active	Gs
Dopamine	cryo-EM	7F23	3.6	Active	Gs
Dopamine	X-ray	7JOZ	3.8	Active	Gs
Dopamine	cryo-EM	7CKX	3.5	Active	Gs
Dopamine	cryo-EM	7CKZ	3.1	Active	Gs
Dopamine	cryo-EM	7LJC	3	Active	Gs
Dopamine	cryo-EM	7CKW	3.2	Active	Gs
Dopamine	cryo-EM	7CKY	3.2	Active	Gs
Dopamine	cryo-EM	7CRH	3.3	Active	Gs
Dopamine	cryo-EM	7LJD	3.2	Active	Gs
Dopamine	cryo-EM	7JV5	3	Active	Gs
Dopamine	cryo-EM	7JVQ	3	Active	Gs
Dopamine	cryo-EM	7JVP	2.9	Active	Gs

After selecting templates for the Homology modeling of I-5HT7R, the subsequent step is to perform a Multiple sequence alignment (MSA) of template sequences and target sequence. We used serotonin receptors in their inactive state with sequence identity >30%. We chose two serotonin receptors as a template 5HT2A and 5HT1B with different PDB structures. Among all serotonin receptors, only 5HT2A and 5HT1B have PDB structures in their inactive state and with good resolution. We have to be very careful about checking a few points for the amendments of sequence alignments for example the gaps within the region representing the secondary structural elements, the position of proline, cysteine residues in alignment, loop regions of TM helices, and the alignment of conserved regions [190]. Alignment was done manually in multiple sequence viewer by keeping in mind the above-mentioned points (Table 3).

After completing the sequence alignment, the subsequent step involves constructing the initial model of I-5HT7R. There are different methods for building models which differ in the modeling technique of backbone structure [198].

For example, the fragment-based modeling technique first identifies non-gapped regions in the alignment and subsequently constructs the backbone structure for those regions. In some cases,

a consensus backbone structure is prepared first based on the structure of all given templates and then from these backbone fragments libraries, the torsional angles are derived before modeling the target sequence using the consensus structure. Afterward, side chain modeling and loop modeling are performed [199, 200].

Table 3 Serotonin receptor: Sequence identity/similarity with full sequence, C/N termini, and alignments. MSA with full sequence and MSA after cutting with 5HT7R values

Serotonin Receptor	Signal protein	Full Sequence identity/similarity	Sequence identity/similarity			MSA identity%/similarity %	
			with C-termini	with N-termini	after cutting sequence		after cutting
5HT7R	G _s ¹						
5HT4R	G _s ¹	25/37	29/43	28/41	34/49	33/49	39/60
5HT2A	G _{αq} ²	22/37	25/42	24/41	28/47	23/42	28/48
5HT1F	G _{αi/o} ³	24/36	27/41	28/42	33/50	35/53	37/54
5HT1B	G _{αi/o} ³	24/36	28/40	28/42	34/48	33/49	36/51
5HT5A	G _{i/o} ¹	22/36	26/41	27/43	31/50	31/50	33/52
5HT1D	G _{αi/o} ³	23/35	27/40	28/41	33/49	33/49	35/50
5HT2B	G _{q/11} ⁴	19/35	21/38	21/39	25/43	20/38	26/46
5HT1A	G _{αi/o} ³	22/34	24/38	25/40	29/45	32/51	35/54
5HT1E	G _{αi/o} ³	24/34	28/40	28/40	34/48	35/52	37/53
5HT2C	G _{q/11} ⁵	19/34	21/38	21/37	25/43	21/39	26/46
5HT6R	G _{αs} ¹	21/33	24/37	25/38	29/44	25/39	30/47

¹ <https://www.sciencedirect.com/topics/biochemistry-genetics-and-molecular-biology/5-ht4-receptor>

² <https://www.sciencedirect.com/science/article/pii/S0092867420310667?via%3Dihub>

³ <https://www.nature.com/articles/s41422-021-00527-4>

⁴ <https://www.nature.com/articles/s41594-018-0116-7>

⁵ https://en.wikipedia.org/wiki/5-HT2C_receptor

2.1.3 3D structural modeling of the 5HT7R inactive state

There were three approaches used for the generation of an inactive state of 5HT7R (I-5HT7R). These approaches include the utilization of experimental structure of active state 5HT7R (PDB ID: 7XTC), *ab initio* modeling, and template-based modeling.

2.1.4 Template-based modeling:

Template-based modeling was used for those regions where conformational changes are involved such as G77^{1.28}-L123^{2.46}, A325^{6.33}-V338^{6.46}, and N380^{7.49}-Q402^{8.61}. The regions from 1-76 (N-terminus) and 403-479 (C-terminus) were already cut during sequence alignment because we had no available templates for these regions. The selected templates in their inactive conformation 5HT2A and 5HT1B showed the highest sequence identity (30 % and 37% respectively). All PDB structures of 5HT1B were like each other, thus, we chose the structure with the highest resolution (PDB ID: 4IAQ, 2.8Å). From the templates of 5HT2A, we chose PDB ID: 7WC4, 3.20 Å structure, as it has a small α -helix in ICL2, and the rest of the structure was like other PDB structures of 5HT2A. The “automodel” class [201] of MODELLER Program was used for the modeling of I-5HT7R based on the above-mentioned templates and resultant 20 models were made [202]. The final model was selected based on normalized DOPE scores generated for each model. DOPE score is simply a sum of interaction between pairs of atoms and it can be decomposed into scores for each residue and can be plotted as ‘an energy profile in MODELLER [176].

According to a recently published paper, the inactive serotonin receptors have a salt bridge between TM3-TM6, and this ionic lock prevents the activation of 5HT receptors. This ionic lock position is R180^{3.50} and E322^{6.30}. For the activation of class A GPCRs, the breakdown of this ionic lock is necessary [159].

2.1.5 *Ab initio* modeling

Ab initio modeling via MODELLER[202] Program was used for the region of I-5HT7R, where the template information was not available. The word *ab initio* means “from the beginning”. This modeling method assumes that all the information related to protein structure is consisting in its amino acid sequences, and the globular protein will fold into a shape where the lowest free energy is possible. With *ab initio* modeling, multiple possible conformations of the

interested region are generated, followed by the calculation that which conformation has the lowest energy state which is favored by nature [176].

For the *ab initio* modeling, the ICL3 region 275-324 and a few residues of ECL3 (354-358) were chosen. The MODELLER class “LoopModel” was used for the modeling of ICL3 of 5HT7R. We have performed loop refinement with both slow and fast algorithms and built one hundred models for slow and fast algorithms protocol. We have selected the conformation of ICL3 with minimum clashes with downstream partner G_s protein and 1-palmitoyl-2-oleoyl-sn-glycero-3-phosphocholine (POPC) membrane. For the modeling of ECL2, the formation of a disulfide bridge between Cys354 and Cys358 was forced during the modeling of this region similar to other receptors.

2.1.6 Active state 5HT7R --Experimental Structure

We have taken regions from the experimental structure of 5HT7R, which is not compromised by inactive conformation. These regions are from residue 124-273, 339-353, 359-379. In Schrodinger Program [197], the protein splicing tool [203] was used for combining these regions of *ab initio* modeling (275-324, 354-358), experimental structure (124-273, 339-353, 359-379), and template-based modeling (77-123, 325-338, 380-402). the final model was minimized using the “minimize Biologics” [204] tool of Schrodinger. We then manually changed the rotameric state of R380^{3.50} (similar to 6WH4) to ensure the formation of the ionic lock with E322^{6.30}.

In general, Once the model is constructed, it is important to check the quality of the model. For this purpose, several online tools are available to check the quality of generated model by examining the deviation of bond lengths, angles, dihedral or torsional angles in the target structure to that of known 3D structure. Some online tool names are Procheck [205], WHATIF [206], ProSa [207], Anolea [208].

2.1.7 Refinement of the GDP-bound G_s protein

For the modeling of inactive conformation of G_s protein, we considered the crystal structures of GDP-bound G_s protein (PDB IDs: 6EG8 and 6AU6). There were missing residues from 1-8 and 73-86 in 6EG8 and from 1-37, and 71-84 in 6AU6 in the G_s subunit structures, which were modeled with the “automodel” class of MODELLER, and ten models were built. The

Starting 1-8 residues of α N Helix of G_s protein were ignored in the chosen model. The other subunits of G_s protein such as $G\beta_1$ and $G\gamma_2$ were taken from the PDB structure of 6EG8.

2.1.8 Refinement of the 5HT7R- G_s complex (active state)

The crystal structure of the active state 5HT7R- G_s complex (PDB ID: 7XTC) was recently experimentally solved and deposited in Protein Data Bank [196]. There were missing residues that were not crystalized in the active state of 5HT7R such as residues from 280-323 (ICL3) and 355-359 (a small region of ECL3). These residues were taken into account from the I-5HT7R and incorporated into the active state of 5HT7R.

The active state G_s protein included some mutations in its PDB structure such as G226A, T284D, K274D, S54N, E268A, I285T, N271K, and R280K. We reverted these residues into their wild type by using “Build” tool [204] in Schrodinger. There were also missing residues in $G\alpha_s$ subunit such as residues from 63-208 and 253-259. For the modeling of these regions, we used dopamine and glucagon receptors as templates (PDB IDs: 7JOZ and 6X18, respectively) as they have a complete region for this $G\alpha_s$ helix. We used “automodel” class of MODELLER for the modeling and ten models were generated and selected the best model based on DOPE score. It was also carefully investigated that there is no steric clash of this $G\alpha$ domain with other regions of G_s protein as well as with ICL3 of 5HR7R and POPC membrane.

2.1.9 Modeling of 5HT7R- G_s preassembled complex

For the modeling of the preassembled complex (I-5HT7R- G_s protein), we followed the approach of a recently published article by Mafi et al. [159]. We separately superimposed the inactive state of 5HT7R, and inactive $G\alpha_s$, $G\beta_1$ and $G\gamma_2$ to their corresponding protein chains in the active state conformation 5HT7R- G_s complex. This alignment of the inactive state complex to the active state complex has a structural alignment score of 0.229 and RMSD value of 2.3Å.

2.1.10 Protein preparation of preassembly and coupling complexes

A Protein preparation wizard of Schrodinger maestro version 12.9.123 MMshare version 5.5.123 was used for the final preparation of the preassembled complex and active state complex [203, 209] [197]. All the steps of protein preparation were taken into account such as adding hydrogens atoms, and disulfide bonds created [210]. Proper protonation states were

assigned to His, Glu, and Asp using Interactive Optimizer. At the end minimization of the prepared complexes was also performed using OPLS4 Force Field [211].

2.2 Molecular Dynamics (MD) simulations

The initial application of MD simulation methods was used by Alder and Wainwright in 1957 to study the liquid system [212], and the second application was used by Rahman and Stillinger [213]. MD simulation is a versatile approach to investigate the structure, function, and dynamics of macromolecular systems including the DNA, proteins, enzymes, RNA, organic and inorganic molecules at atomic level resolution [214]. After the 20th century, computers with heavy computational power were able to solve problems numerically. The initial simulation utilizing the Monte Carlo method was performed by Metropolis using Monte Carlo method [215]. The next simulation was reported for a hard-sphere system [216], later on, this technique was employed to study liquid argon [217] and crystalline copper [218]. Since then, the MD simulation was laid out step by step [217] [219, 220] and applications were offered to polyatomic systems such as hydrocarbons [221], proteins [222], and to water molecules [213]. Moreover, during that time, McCammon performed MD simulation of a protein system and he found that a protein is not a rigid structure but also a fluid-like material in which atoms are in a continuous state of motion [223]. X-ray crystallography or nuclear magnetic resonance (NMR) provide us with the static structure or a snapshot of a molecule that alone is not enough to explain the dynamic mechanism of a system [171].

MD simulation provides detailed information about the dynamics of macromolecules considering water molecules and eventual ligands. MD simulation has been widely used to investigate ion channels, membrane proteins, binding sites of drugs, protein-protein interaction, protein-ligand interaction [224], free-energy landscape, and orthosteric [225] and allosteric pathways occurring in the human body [226].

2.2.1 Classical Molecular Dynamics simulation

Newton's equation of motion is used to track a set of particles under investigation to study their time evolution during the classical molecular dynamics simulation [227]. In MD simulation, atoms are represented as spheres or balls and their covalent bonds are modeled as harmonic spring which connects these balls. Before starting the simulation, the initial set of coordinates of the investigated system is taken into account. Then Newton's equation of motion (Equation

1) is applied to the particles of the system, allowing for the calculation of new positions and momentum of the particles. This process is repeated iteratively for a defined period of time, which is determined based on thermodynamics properties.

$$F = ma \quad (\text{eq. 1})$$

In this way, the trajectories are recorded by repeating the above-mentioned procedure which evolves during the time, and this is the advantage of MD over MC simulation [214]. There are molecular mechanics force fields that play a vital role in MD simulation as these forces hold the particles together and also calculate their potential energies [228].

2.2.2 Force fields

A force field is defined as an atomic parameter and a set of equations that play a role to define all types of interactions between atoms of the system [227]. The following equations illustrated the potential energies, their corresponding derivatives, and the force of any particle i at a given time as:

$$F_i = \nabla V_i \quad (\text{eq. 2})$$

Here F is the force and V is its potential energy. There are types of interactions present in a particle of a system: bonded interactions and non-bonded interactions and their potential energies are described as follows:

$$V_{system} = V_{bonded} + V_{nonbonded} \quad (\text{eq. 3})$$

2.2.3 Bonded interactions

Four types of bonded interactions exist between particles within the system such as bond angle, bond stretching, dihedral (or torsion) angle, and improper dihedral angle [228].

For the bonded interaction, bonds are treated as spring characterized by a specific force constant K_b , energy, and bond length equilibrium that is necessary to compress or stretch that bond as illustrated in Hooke's law:

$$V_{bond} = \sum^{bonds} K_b (b - b_0)^2 \quad (\text{eq. 4})$$

In the above equation, b represents bond length at a given time, b_0 is for the equilibrium bond length and K_b represents the force constant for the stiffness of the bond.

For the angle bending from its equilibrium position (θ_0) between triplet atoms is treated harmonically and their potential energy (V_{angle}) can be shown as follows:

$$V_{angle} = \sum^{angles} K_\theta (\theta - \theta_0)^2 \quad (\text{eq. 5})$$

In the above equation, θ is the angle at a given time, θ_0 is the angle at the equilibrium angle and K_θ is the stiffness of the bond angle.

The energy required to rotate that bond is obtained from dihedral or torsional ($V_{torsion}$) interaction potential as follows:

$$V_{torsion} = \sum^{torsions} K_x (1 + \cos(n_x - \Delta)) \quad (\text{eq. 6})$$

In the above equation, x represents the dihedral, n is for the multiplicity, K_x is the barrier height parameter, and Δ is the phase. For the periodic rotation, the Cosine value is considered. The improper dihedral energy or angle is a four-body interaction between particles of the system and its used to represent the out-of-plane geometry or to maintain planarity or chirality. The torsional angle potential energy or proper dihedral angle is calculated on polyatomic particles of four consecutive atoms, here are three bonds present in atom 1 and atom 4. The improper dihedral interaction refers to a structural arrangement where 3 atoms surround a 4th central atom. This potential energy can also be modeled using harmonic potential energy as follows:

$$V_{impropers} = \sum^{impropers} K_\varphi (\varphi - \varphi_0)^2 \quad (\text{eq. 7})$$

In the above equation, the φ_0 represents the equilibrium angle and K_φ is for force constant.

2.2.4 Non-bonded interactions

Non-bonded atoms don't form a covalent bond and their interaction with each other is known as non-bonded interaction. It consists of Coulomb interaction and Van der Waals interaction. The Van der Waals interaction includes attractive forces and repulsive forces and is known as Lennard-Jones interaction as follows:

$$V_{vdW} = \sum_{ij}^{nonbonded} 4\epsilon_{ij} \left(\left(\frac{\sigma}{r} \right)^{12} - \left(\frac{\sigma}{r} \right)^6 \right) \quad (\text{eq. 8})$$

In the given equation, i and j are the atoms involved in the interaction, ϵ_{ij} represents the potential minimum for interaction between these two atoms (ij), r_{ij} is the distance between atom i,j , and σ_{ij} is the separation distance when atoms are at zero energy. The second term in the given equation correspond to attractive forces between atoms i,j and the first term denote the repulsive forces between atoms. Once the atoms begin to approach each other, the role of the -6 term (model dispersion) becomes more pronounced and since this term is negative, thus, the energy becomes more and more attractive. When the atoms reach to energy minimum position (where the atoms can't come closer to each other anymore), the repulsive forces started dominating and increasing energy, thus, the term 12 starts dominating. The values of attractive σ^6 and repulsive σ^{12} term parameters are dependent on atom types [228].

Coulomb's Law describes the electrostatic interaction (V_E) energy between particles of the system. The following term describes the distance between atoms of interaction and the effect of atomic charges. As we know, opposite charges attract each other and the same or similar charges repel each other. This electrostatic interaction energy is calculated with the following equation:

$$V_E = \frac{q_i q_j}{4\pi \epsilon_0 r_{ij}^2} \quad (\text{eq. 9})$$

In the given equation, r_{ij} represents the distance between atom i and j , q_i , and q_j represent the charges on the atom, ϵ_0 represent the permittivity in the vacuum and π is the constant.

There are four most popular force fields for MD simulations of macromolecules such as OPLS [229, 230], CHARMM gui [231, 232], and AMBER force field [233-235], GROMOS [235].

These force fields use the same functional form for bonded interaction and non-bonded interaction, but their calculating methods are different for each force field including the use of combination rule for Lennard-Jones potential, improper dihedral, and different ways of calculation for 1-4 non-bonded interaction. These force fields are optimized to do simulations on the data generated via thermodynamics, crystallography, quantum mechanics, and spectroscopy. The force field can also utilize subsets of the target data to optimize its parameters. As a result, the optimized parameter values may differ slightly depending on the specific subset of data used for optimization [228].

In MD simulation we can parameterize new molecules by using GAFF (General Amber Force Field) force field. GAFF is an extension of amber force field which provides a robust set of parameters for organic molecules. There are a wide range of atom types, angle bending, non-bonded interactions, bond stretching as well as interaction types of electrostatic interactions and van der Waals interactions. In MD simulations, by assigning an appropriate force field by GAFF, one can study the molecular behavior, energies of molecule and the structural changes in it.

2.2.5 Integration algorithms for MD

There are various numerical integration algorithms used to solve the Newton's equation of motion such as leap-Frog algorithm [236], Verlet algorithm [217], Velocity Verlet algorithm [237]. Taylor series expansion is used for the calculation of acceleration, velocity, and the position of the particle under these mentioned algorithms.

Verlet algorithm is the most common algorithm in MD simulation. The leap-frog, and Velocity Verlet are based on the Verlet algorithm. For this thesis work, these algorithms are being used as these are already implemented in GROMACS tools. In Verlet algorithm, the new position of an atom is calculated by using:

- 1) acceleration and position of a particle at time t
- 2) position of particle at a previous time $t-\Delta t$ as shown in the following equation:

$$r(t + \Delta t) = 2r(t) - r(t - \Delta t) + (\Delta t)^2 a(t)$$

(eq. 10)

In the above-mentioned equation, t represents the time, r position, a acceleration and Δt for time step. $r(t - \Delta t)$ represents the position from a previous step but it is not self-explanatory, and it requires additional methods to calculate the position from a previous step.

The Verlet algorithm also doesn't calculate velocity with position simultaneously as it needs the next position to calculate velocity for the next step.

Whereas, in the Velocity Verlet algorithm the velocity, acceleration, and position for the next step ($t + \Delta t$), are calculated concurrently as shown in the following equation:

$$r(t + \Delta t) = r(t) + v(t) \Delta t + \frac{1}{2} a(t) (\Delta t)^2 \quad (\text{eq. 11})$$

$$v(t + \Delta t) = v(t) + \frac{1}{2} (a(t) + a(t + \Delta t)) \cdot (\Delta t) \quad (\text{eq. 12})$$

In the above-mentioned equations, it is demonstrated that the position in the next step relies on the velocity, acceleration, and position in the current step. The velocity in the next step is determined by taking the acceleration and velocity in the current step as well as the acceleration at the next step.

The leap-frog algorithm follows the principle of "frog step", where the velocity for the next half-time is calculated based on the previous half-step velocity and the acceleration at the current time. By using this approach, the next half velocity and current position at the time t , the position at the next step ($t + \Delta t$) can be calculated.

$$v\left(t + \frac{1}{2} \Delta t\right) = v\left(t - \frac{1}{2} \Delta t\right) + \Delta t \cdot a(t) \quad (\text{eq. 13})$$

$$r(t + \Delta t) = r(t) + \Delta t \cdot v\left(t + \frac{1}{2} \Delta t\right) \quad (\text{eq. 14})$$

in the leapfrog algorithm, the position and the velocity are not determined simultaneously, but rather they alternate with each other by time step. The concepts of time and the time step are important for accurately simulating the studied system. The " t " represents the current time in

the simulation. It is a variable that denoted the time at which velocity and the position of the particles are being calculated and updated. Whereas the time step is indicated as Δt . It represents the interval at which the simulation progresses. It defines the resolution of the simulation and affects the efficiency and accuracy of this algorithm. The advantage of this algorithm is that we only store the values of $v(t - 1/2(\Delta t))$ and $r(t)$ and the rest of the parameters can be calculated based on these two parameters. We can't calculate velocities and positions at the same time as the potential energies and kinetic energies cannot be accessible at the same time. Thus, directly calculating the total energy for a given time isn't possible [214].

A periodic Boundary condition (PBC) is an important technique in MD simulations that allows a simulated system to behave as if it were infinitely large. The primary principle of using this technique is to eliminate the influence of the surface which is a characteristic of any finite system of matter. By doing this, the internal structure of the system can be accurately governed by bulk forces rather than surface effects such as surface tension. This is particularly important when studying the system where the surface forces dominate. The concept of PBC is showed in Figure 9, in which the blue color box denotes the system being simulated. The surrounding boxes are the exact replicas which duplicate every detail of the particles present within the simulated cell. Even the velocities of the particles are identical (represented as arrows). However, when an atom exits the simulated cell, it is immediately restored by another atom with the same velocity, entering from the opposite side of the cell. This process ensures the constant total number of atoms within the cell. Moreover, as the system is now free from surface boundaries, thus, no atom experiences any surface forces. This efficiently removes the influence of surface effects.

In Figure 9, the cutoff radius (r_{cut}) is also shown which is employed when determining the forces between two atoms. It is shown in the figure 9 that an atom in the simulation cell can interact with its counterpart in the neighboring cell, which is an image of one of the atoms within the simulated cell. This interaction is only possible when the distance between them is within the cutoff radius. Whereas the equivalent atom present within the simulated cell is disregarded as it is beyond the cutoff radius. In other cases, the interaction arises solely from an atom within the simulated cell itself. Therefore, the calculated interaction always considers the closed image, following the principle of minimum image convention. It is important to note that the cutoff radius ensures that an atom can only interact with a single image of any given atom and the value of cutoff can't exceed half the width of the cell. The minimum-image convention is used to determine the shortest distance between particles that account for the

periodicity of the system and it prevents the artificial truncation or distortion of long-range interactions. The PBC and the minimum-image convention techniques are essential to eliminate edge effect, conserve energy and to accurately represent the behavior of simulated system in MD simulations.

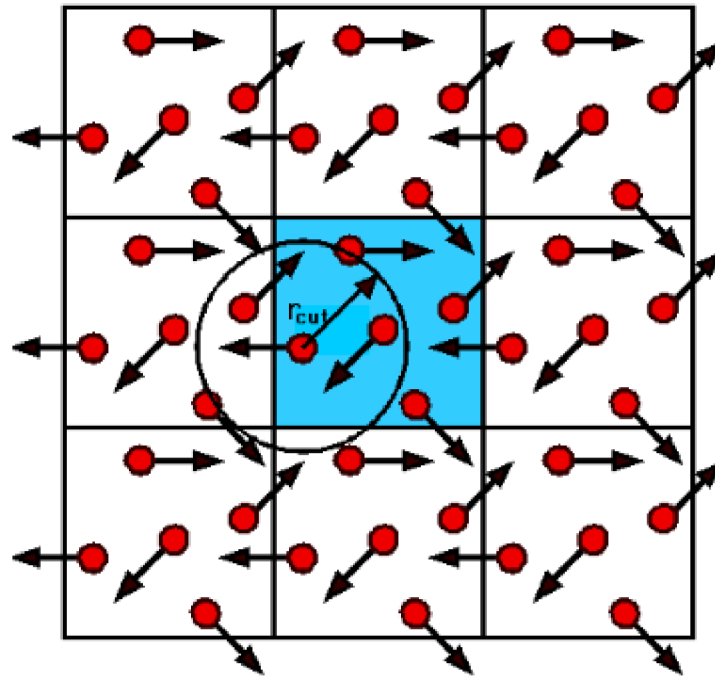


Figure 9 Periodic Boundary Conditions (PBC)

2.2.6 Energy minimization

The structures we obtained from X-ray crystallography, or any other experimental or theoretical method need structural amendments such as atoms can be overlapped, distorted bonds or angles, or occupied an unfavorable position. These structures without modification are not stable and they have higher energy. If we start MD simulation with this structure, it might crash at some time due to abnormal interactions or higher force involvement. In this situation, energy minimization is utilized to resolve potential clashes from biomolecules [214, 238].

There are various algorithms involved that help to refine the structure of proteins to find the best coordinates with minimum potential energy. The arrangement of atomic coordinates within the system determines the potential energy of the investigated system. When a system has N number of particles, the potential energy function for that system will have $3N$ variables. Therefore, finding a global minimum is challenging due to the nonlinearity of the optimization. Various algorithms including Newton-Raphson, Conjugate Gradient, [238], and Steepest

Descent Algorithm [239] are employed in molecular modeling, based on the level of derivative orders required. The first-order derivative methods are Steepest Descent and Conjugate Gradient. These methods utilize the gradient of potential energies to determine the subsequent point, and ultimately, follow a path towards the minimum energy point over the potential energy surface.

The Steepest Descent method aims to minimize potential energies by directly calculating the forces acting on an atom and adjusting their coordinates accordingly. Therefore, this method makes more sense. In this method, the coordinates are initially altered using a randomly defined step value, and the potential energies of newly coordinated structure are calculated based on new forces that arises due to altered coordinates. The new step size is adjusted, either it increases or decreases accordingly, and this process is repeated iteratively. This method is highly vigorous and used to identify the closest local minima. However, Due to the irregular nature of the potential energy surface, which contains multiple local minima, it is not feasible to find global minima. The Steepest Descent method is useful for removing small clashes in the system which require small structural adjustments of biomolecules.

The second-order derivative method, known as Newton-Raphson method, suggested that the potential energy surface exhibits a quadratic to variable behavior in the system within the vicinity of energy minima. This method is effective for small molecules, but not well-suited for macromolecules as in this system, the potential energy surface is not well quadratic, and it also has various local minima. In certain cases, it is advisable to employed Steepest Descent initially and subsequently transition to the other method (Newton-Raphson method) [214, 240].

2.2.7 Equilibration and production of MD

Equilibration is an important step in MD simulation that aims to bring the system to a stable and representative state before running the actual production of simulation. During this process, the system undergoes relaxation and reaches thermodynamic equilibrium by redistributing the energies and adjusting the internal interactions. After energy minimization, the system gradually couple or stepwise increase the desired temperature and pressure. This can be achieved by utilizing thermostats or barostat which are employed to regulate the temperature and pressure of the system. This gradual adjustment allows the system to adopt the desired thermodynamic conditions and stabilize over time. The equilibration is often performed by two

ensembles such as NVT and NPT to regulate the temperature and pressure of the system. The NVT ensemble is known as the canonical ensemble, that is utilized to maintain a constant number of particles (N), volume (V) and the temperature (T) during MD simulation. In NVT, the system exchanges the energy with the heat bath to keep the temperature constant. There are different algorithms such as Nose-Hoover thermostat, Langevin dynamics and the velocity rescaling, that are used to control and maintain the desired temperature of simulation. The NPT ensemble is called as isothermal-isobaric ensemble, and it maintains a constant number of particles (N), pressure (P), and the temperature (T) during simulation. In addition to energy exchange with a heat bath, the system also exchanges the volume with a pressure bath to maintain a constant pressure. There are various algorithms such as Berendsen Barostat or the Parrinello-Rahman method are employed to control and adjust the volume of the system and thereby controlling the pressure. Proper equilibration is crucial for better sampling of the system and to more meaningful analysis of the system's dynamics, thermodynamics, and structural properties during the subsequent production run.

During the production step of MD simulation, the biomolecular system evolves over a period of time, and it captures the dynamics of the system. There are some important considerations for running the MD simulation and defining its condition. The first important condition is equilibration. Equilibration is an essential step that makes sure that the system has undergone to an adequate equilibration phase. The second condition is time length that defines the length, which determines the duration production run, and it depends on the specific research objectives and the timescale of the phenomenon being investigated.

It should be long enough to allow the system to evolve the relevant conformational changes, dynamics, and transition. The long production run allows better statistics, and it enhances the reliability of the results. The next important condition is the temperature and pressure that established during equilibration are typically maintained. Sampling frequencies such as positions, energies, velocities that defined the properties of the system should be determined. These frequencies should be chosen wisely to keep in mind the computational resources and storage requirements. The careful consideration of the above-mentioned factors ensures the meaningful results of MD simulation. Upon completion of the production run, the trajectories are extracted to analyze the relevant information such as thermodynamic properties, kinetic behavior and to investigate the structural properties.

2.2.8 MD simulation of PETase-BHET

For the MD simulation of PETase, the wild-type *Ideonella sakaiensis* PETase enzyme with the PDB:5XJH code was utilized [241]. The MD simulation was performed via GROMACS program [242] and there were three simulation systems were prepared such as cholinium phosphate (choline phosphate) $[\text{Ch}]_3[\text{PO}_4]$, 1-ethyl-3-methylimidazolium acetate $[\text{C2MIM}][\text{Ac}]$, and 1-butyl-3-methylimidazolium acetate $[\text{C4MIM}][\text{Ac}]$ with three different concentrations (for each system) such as 20%, 30% and 40%. We have found that $[\text{Ch}]_3[\text{PO}_4]$ have shown high solubilization capacity and an effective depolymer [36]. To prepare the initial structures of PETase-BHET with ionic liquids, PACKMOL [243] was employed. To establish a control condition, PETase was also simulated independently in a pure aqueous medium. General amber force field GAFF [244] was employed for the parametrization of ligand (BHET) and ionic liquids. Amber force field has consistently demonstrated its ability to accurately predict the transport and thermodynamic properties of ionic liquids [245-247]. Each simulation system was enclosed within a cubic box with a dimension of 12 nm using a PACKMOL program package [243]. Next the system was rendered inert by introducing the Na^+/Cl^- ions according to requirement. The system was initially brought to equilibrium in NVT for 500 ps at the temperature 300K. Following the NVT equilibrium, the system underwent additional equilibrium with NPT ensemble. The temperature and pressure were maintained at 300K and 1bar by weak coupling bath using the Berendsen method [248]. The Van der Waals forces for the system were calculated using Lennard-Jones potential with the 10 Å cut-off distance. For the long range electrostatic interactions, particle mesh Ewald method [249] was employed. All simulations for each of three different systems were run for 150 ns, with the time step 2 fs and saved trajectory every 10 ps. The analysis after the simulation were also performed using the GROMACS program package [250, 251]. VMD [252] was used for the visualization of data, and for the graphical imaging preparation xmgrace program [253] was used.

2.2.9 MD simulation of GPCR-Gs protein

Homolwat [254] webserver <https://alf06.uab.es/homolwat/> [255] was utilized for the addition of conserved water molecules and GPCRmd protocol [256] was employed to prepare the system. The orientation of the prepared system within the membrane was derived from a crystalline structure of serotonin ID (5HT1D), that is deposited in the Orientations of Proteins in Membranes (OPM) database [257]. Then Two complexes are superimposed to OPM reference structure. The prepared system is then embedded into POPC membrane by using

HTMD program [258]. TIP3P water molecules were incorporated in the system using VMD Solvate Plugin 1.5. Furthermore, the system was neutralized by introducing Na⁺/Cl⁻ ions according to need. All the N- and C-terminus chains (GPCR, G α , G β , G γ) were capped with ACE and CT3, with the exception of G α helix 5 (L394^{H5.26}), which remained negatively charged.

The protocol mentioned above was used for the system preparation of I-5HT7R with the full length of ICL3 without its downstream partner, G_s protein. As the force field, CHARMM36 [259, 260] and CGenFF [261, 262] were used for protein, lipid, TIP3P water model, Guanosine-5'-diphosphate (GDP), and nucleic acid were used in our work. 5-Carboxamidotryptamine (5CT) ligand parameters and topology in 7XTC were obtained from ParamChem (<https://cgenff.umaryland.edu/>).

Table 4 System details of MD simulation for GPCR-Gs protein

Sim #	System	GPCR State	Size	Replicas	Length	Total MD Sampling
1	5-HT7R-5CT-Gs	Active-Full AGO	Total=273350	3	500ns (3)	1.5 μ s
2	Preassembled complex 5-HT7R-Gs-GDP	Inactive-APO	Total=287296	3	500ns (3)	1.5 μ s

ACEMD program [263] based on OpenMM [264], was used for MD simulation with periodic boundary conditions (PBC) for both equilibrium and production simulation. The system was equilibrated through the Conjugate gradient minimization to address clashes brought by system preparation. Subsequently, both systems were equilibrated NPT and the temperature was maintained at 310 K. We run three different replicas for each equilibrated system for 500 ns MD (Table 4).

2.3 Analysis of MD Simulations

2.3.1 RMSD

Root Mean Square Deviation (RMSD) serves as a measure of an average deviation of atoms over the simulation in comparison to crystallographic structure or the first frame of the simulation. The RMSD is utilized to quantify the displacement of backbone atoms of proteins relative to their initial structure. It is represented with respect to time, and it allows us to observe changes in the protein's structural conformations throughout the simulation time. When the RMSD curve becomes relatively stable, it shows that the protein has reached equilibrium. Thus, RMSD plot provides valuable insights into the stability and structural dynamics of the protein during MD simulation.

The presence and arrangement of secondary structure of the system including the alpha helices and the beta sheets are vital for overall folding and stability. It influences the RMSD value as well as it correlates the beta factor. A well-defined secondary structure exhibits the lower value of RMSD due to constrained atomic positions and interactions within these regions. Whereas the regions with high beta factors demonstrated the increased atomic motion and the flexibility and are likely to have a higher value of RMSD. The beta factor gives insight into the local flexibility within the beta sheets, with higher value of it, indicating the greater structural deviation and higher value of RMSD. By taken into account the secondary structure, RMSD value and the beta factor, one can obtain comprehensive information about protein dynamics, stability, and flexibility. These factors offer valuable insight into protein folding, function and the effect of structural changes or protein behavior.

$$RMSD = \sqrt{\frac{1}{N} \sum_N (r_i(t_0) - r_i(t))^2}$$

(eq. 15)

Here N expresses the number of atoms, r represents the position of atom i, and t represents the time.

2.3.2 RMSF calculations

The root means square fluctuation (RMSF) quantifies the fluctuation of residues or atoms of protein in relation to the average structure of the simulation. To determine the RMSF, the

positions of residues or the atoms in the trajectory are aligned and the deviation of individual residues or atoms from their reference or average positions are computed. The RMSF of residues is plotted against residue number and represents which residue of the protein is fluctuating more during the MD simulation.

$$RMSF = \sqrt{\frac{1}{T} \sum_T (r(t) - \bar{r})^2}$$

(eq. 16)

Here r represents the position of residues, T represents the total time of simulation and \bar{r} represents the average position.

2.3.3 SASA

Solvent Accessible Surface Area (SASA) quantifies the extend of the protein's surface area that is accessible to solvent molecules. SASA provides valuable information about the exposure of the protein's surface to the surrounding solvent molecules. To calculate the SASA values, we considered the position of both the protein residues and the surrounding solvent molecules. The common method is to use the probe sphere that represents the solvent molecules. This sphere rolled over the molecular surface of the protein and the portion of the protein that is accessible to the solvent is measured. This surface area is quantified as the SASA value in the plot.

2.3.4 Radius of Gyration

The radius of gyration (R_g) quantifies the overall compactness of a protein over the course of simulation time. The R_g quantifies the spatial distribution of particles of proteins and provides information about their shape and conformational properties. It is used to study the folding or unfolding of protein or nucleic acid or polymer during the MD simulation time.

2.3.5 Hydrogen Bond

The hydrogen bond is an important intermolecular or intramolecular interaction of biomolecules and solvents that shows the structural stability of the studied system. This bonding occurs by following the specific conditions. One of the primary conditions is the

existence of electronegative atoms including oxygen, fluorine, nitrogen, which exhibit a strong affinity for electrons. These atoms are commonly found in a molecule capable of forming hydrogen bonds. The second requirement is the presence of a hydrogen atom that forms a covalent bond with an atom possessing high electronegativity. This hydrogen atom acquires a partial positive charge. proximity is an important factor for hydrogen bonding. Subsequently, the distance between hydrogen atom and the electronegative atom is typically $\leq 3.5 \text{ \AA}$ and the angle should be $\leq 30^\circ$. The hydrogen atom and the electronegative atom must be linearly or nearly linear aligned configuration. This alignment facilitate an ideal electrostatic interaction between the partial positive charge on the hydrogen and the partial negative charge on the electronegative atom. During MD simulation, the analysis of a particular hydrogen bond provides information about the dynamics and properties of that bond. It also helps us to understand protein folding, enzymatic reaction, ligand binding, and other biomolecular processes.

2.3.6 Radial distribution function (RDF)

The radial distribution function (RDF) quantifies the probability of locating of a particle at a specific distance as “r” from a reference particle. It is used to measure the distribution of certain molecules around a particular atom or molecule. The RDF is also used to investigate different types of interactions such as molecular correlation, solute-solvent interactions, and intermolecular forces. It gives information about the arrangement of particles, the presence of local ordering, and the effect of temperature or pressure.

$$g(r) = \frac{1}{\rho N} \left\langle \sum_i \sum_j \delta[r - r_{ij}] \right\rangle$$

(eq. 17)

3. Results and discussions

3.1 MD simulation of PETase_PET ionic interaction

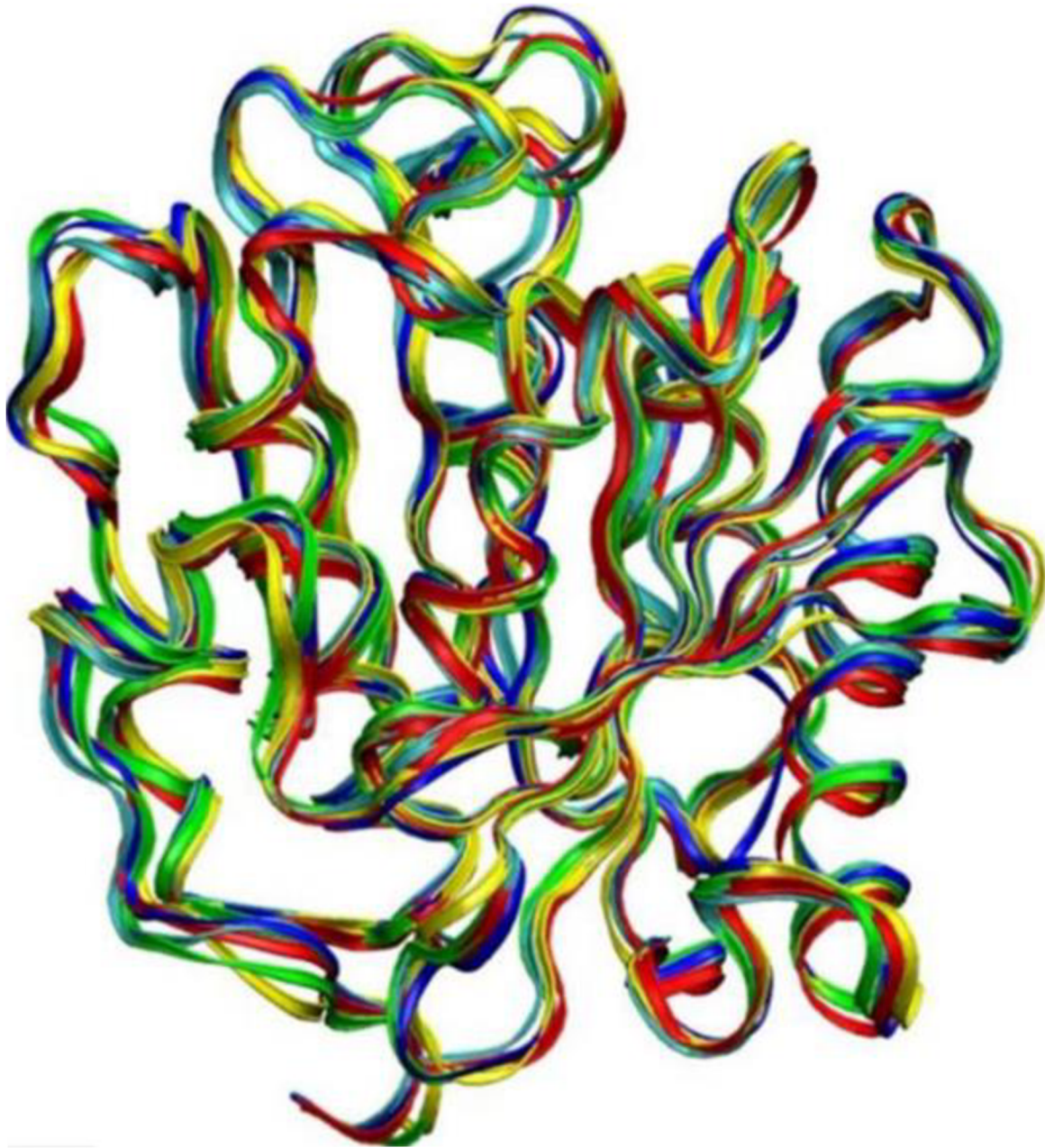


Figure 10 superimposed PETase backbone structure with different solvents (40%). Blue color depicted the Wild-type, red color is for water simulation, simulation with [Ch]₃[PO₄], [C₄MIM][Ac] and [C₂MIM][Ac] are shown in yellow, green, and light blue, respectively.

3.1.1 MD simulations

Our investigation aimed to analyze the impact of non-aqueous solvents such as [Ch]₃[PO₄], [C₄MIM][Ac] and [C₂MIM][Ac] on the structure of PETase and its ligand BHET with three different concentrations such as 20% 30% and 40%. PETase with substrate (intermediate) polymer consisting of the two BHET units. Running long MD simulation time can benefit in

various ways. Firstly, it allows extensive structural state sampling and a wide range of interactions. Secondly, it helps in the analysis of solvent effects by providing information about solvation, PETase-BHET interaction and the stability of PETase. Lastly, the long simulations assist in validation and comparison of results across different ionic liquids and water with different concentrations. Therefore, we performed 150ns long MD simulation of the above-mentioned protein complex system with three different non-aqueous solvents $[\text{Ch}]_3[\text{PO}_4]$, $[\text{C4MIM}][\text{Ac}]$, $[\text{C2MIM}][\text{Ac}]$ and with the water at three different concentrations 20% 30% and 40%. We have also performed MD simulation of the PETase-2BHET complex in pure water as the control system and compared other MD simulations results with it. The PETase backbone structures after 150ns of MD simulations in the aqueous solvents of studied ionic liquids ($[\text{Ch}]_3[\text{PO}_4]$, $[\text{C4MIM}][\text{Ac}]$ and $[\text{C2MIM}][\text{Ac}]$) as well as the water have been superimposed and results depicted on Figure 10. We have found no significant difference in the backbone structure of PETase (Figure 10).

3.1.2 RMSD plot

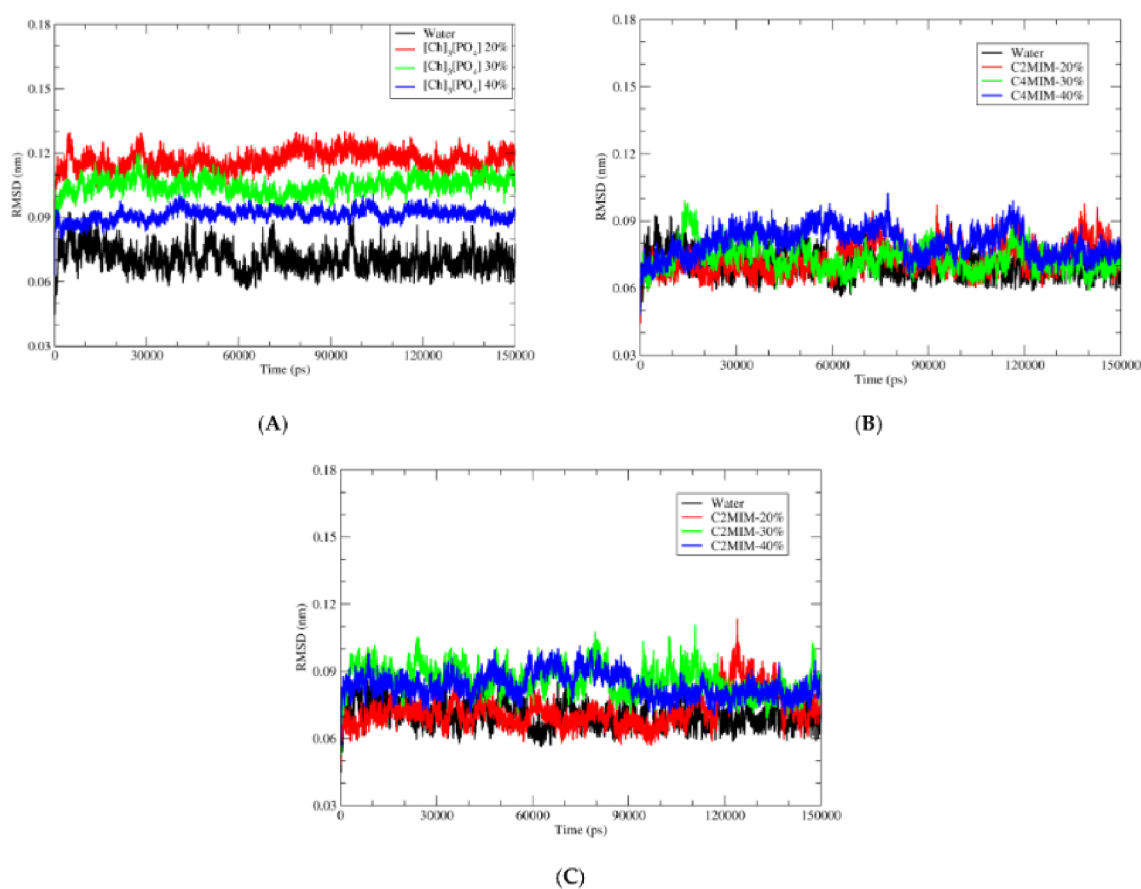


Figure 11 Root mean square deviation (RMSD) of Ca atoms of wild type of PETase with water and three different ionic liquids solutions.

The RMSD calculation of the PETase provides the quantitative measurement of the degree of stability of the system during MD simulation. Figure 11 displays the RMSD values of PETase in both water and in other ionic liquids environment. We have found that the structure of PETase in water is stable during the MD simulation and stays closer to crystal structure in comparison with the MD simulations in the other ionic liquids. The rmsd values of PETase in water are observed to be lower than the values of PETase in the ionic liquids. It indicates a better agreement between PETase structure and the crystal structure, suggesting that the PETase maintains its shape when surrounded by water molecules.

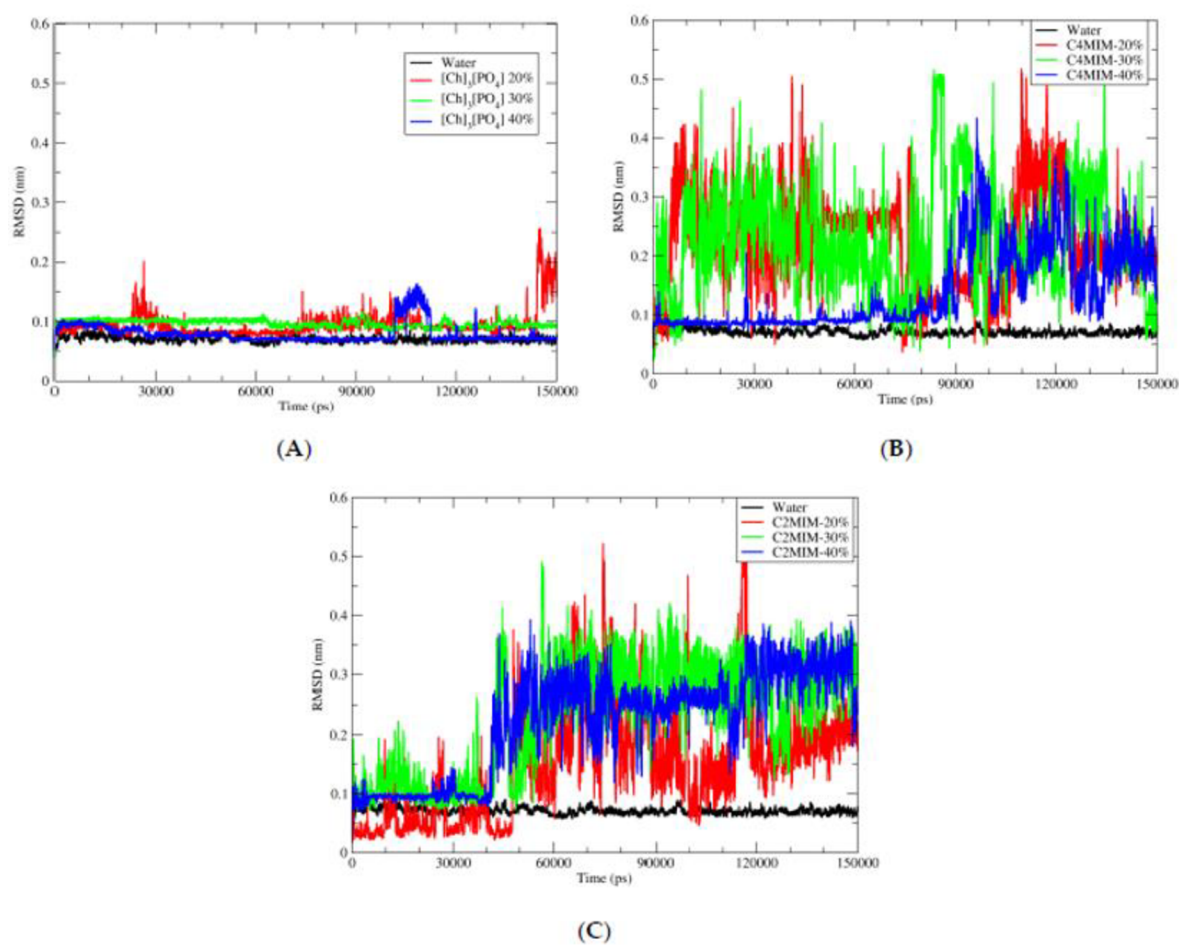


Figure 12 Root mean square deviation (RMSD) of BHET with respect to PETase in water and three different ionic liquids solutions

Moreover, we also found that the fluctuation of RMSD values of PETase decreases by increasing the concentration of ionic liquids from 20% to 40%. Which indicates that the structure is more stable with less thermal fluctuation. Furthermore, the results depicted in Figure 11 illustrate that the impact of ionic liquid on the structure of PETase is more pronounced when using $[\text{Ch}]_3[\text{PO}_4]$ (Figure 11 A) compared to the other ionic liquids, namely

[C4MIM][Ac] and [C2MIM][Ac]. It is also demonstrated that when other ionic liquids are present, there is not significant deviation of backbone structure (Figure 11 B, C). However, even the RMSD value of overall PETase structure does not exhibit a significant deviation from its initial structure. This suggests that the selected ionic liquid [Ch]₃[PO₄], would not cause significant structural alterations to the enzyme. Consequently, the system remains suitable for conducting further studies on the reaction mechanism of BHET hydrolysis.

Apart from the overall protein structure it is crucial to investigate the active site of PETase, which performs a vital role for the breakdown of BHET using catalytic triad.

For this purpose, we also computed the rmsd of BHET. The position of three catalytic triad amino acids (Ser-131, His-208 and Asp-17) with respect to BHAT, which help in the hydrolysis of BHET via SN-2 reaction mechanism are important to maintain. In the presence of studied solvents, the position of BHET is expected to remain stable during the MD simulation. The analysis revealed that the structure of BHET in the presence of [Ch]₃[PO₄] (Figure 12 A) and water was not deviating much from its initial structure with respect to PETase. Whereas, the same stability of BHET molecule was not found in other studied ionic liquids [C4MIM][Ac] or [C2MIM][Ac] (Figure 12 B, C respectively).

The trajectory analysis of BHET showed that after 40 ns of simulation, the BHET molecule exhibit a noticeable displacement from its catalytic residue SER-131 and it started to undergo bending due to non-bonded interaction of BHET rings. The stability of BHET with water and [Ch]₃[PO₄] during entire MD simulation time indicated that there was not significant deviation of position and geometry of BHET within PETase. Moreover, when concentration of ionic liquid reduced from 40% to 20%, the instability of BHET increased for [C2MIM][Ac] and [C4MIM][Ac] (Figure 12 B, C). This instability of BHET was due to bending of BHET during the MD simulation and this bending might be a reason of electrostatic interaction between two sites of BHET.

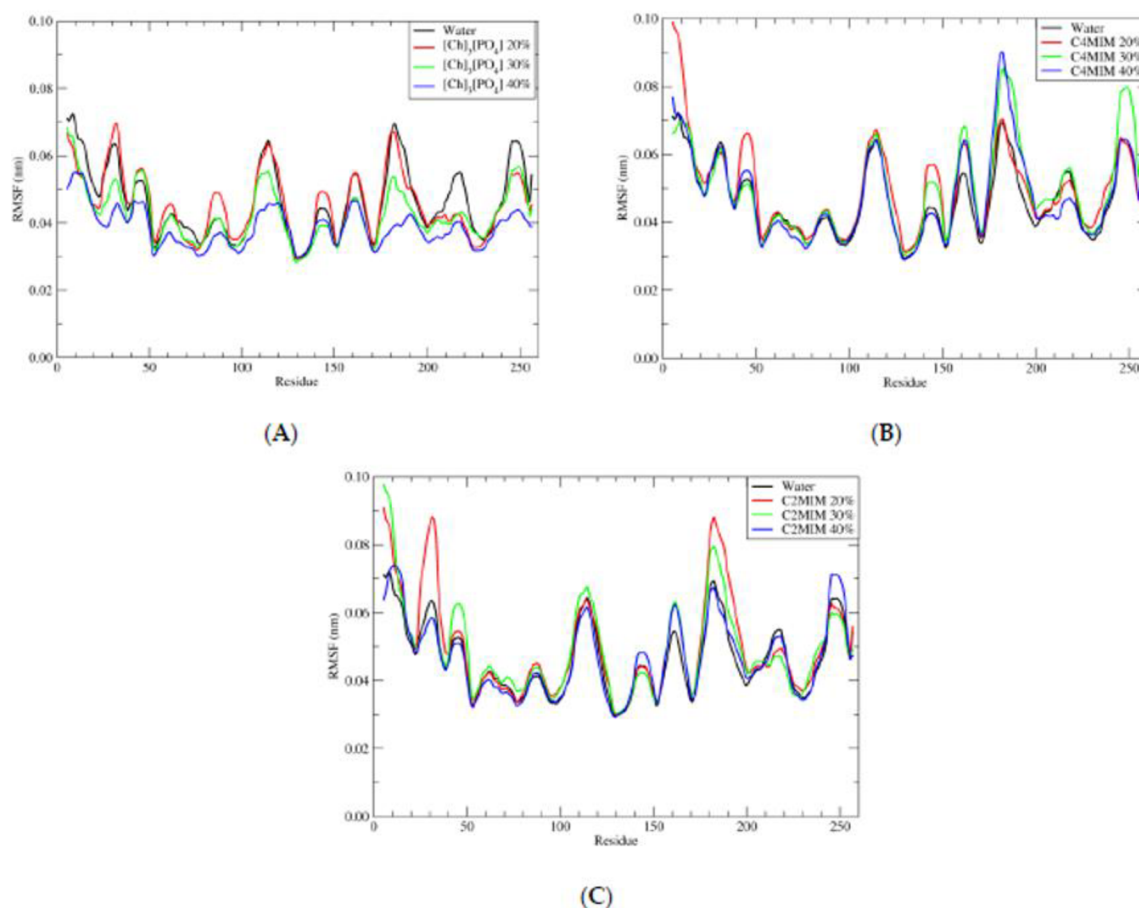


Figure 13 Root mean square fluctuation (RMSF) of wild-type of PETase with water and ionic liquid solutions in the presence of ligand BHET.

3.1.3 Root Mean square Fluctuation (RMSF)

After the rmsd analysis, the structural stability of each protein residue was investigated with RMSF and plotted in Figure 13. The analysis showed that rmsf value of PETase in 40% of $[\text{Ch}]_3[\text{PO}_4]$ is lower compared to water (Figure 13 A) which aligned with the lower fluctuation of RMSD value (Figure 11 A). There were some residues at position 100-120 and 170-180, which were fluctuating more. Asn-183 exhibits the greatest instability as indicated by its highest RMSF value. This residue also demonstrates the highest RMSF value among other ionic liquids like $[\text{C4MIM}][\text{Ac}]$ and $[\text{C2MIM}][\text{Ac}]$.

3.1.3 Hydrogen bonds

The stability of proteins is also influenced by its interaction with the solvent. The solvent interactions have the potential to enhance or disrupt the stability of amino acids within a protein. The hydrogen bond interactions play a crucial role in determining the overall stability of the protein structure. Thus, the quantity of hydrogen bonds within the protein serves as a

validation of its structural stability. Upon analyzing the quantity of H-bonds between water and the PETase, we have observed that at elevated concentration of IL, leads to a reduction of hydrogen bonds. This phenomenon could be attributed to the larger size of cations and anions present in aqueous solutions of ionic liquids when compared to pure water. During the MD simulation of PETase in 40% of [Ch]₃[PO₄], a significant H-bond interaction between the PO₄³⁻ and residue Asn-183 has been found. One H-bond was found between hydrogen of Asn-183 and the oxygen of phosphate group and the distance was between 1.8 Å to 3 Å. Nevertheless, it was not stable enough during the MD simulation time. Whereas, there were not any hydrogen bonds found between [C4MIM][Ac], [C2MIM][Ac] and Asn-183 as they don't have reasonable entity for its bond formation. Thus, it produced the higher value of RMSF with these ionic liquids (Figure 13 B, C).

3.1.4 Radial distribution function

The radial distribution function (RDF) is a statistical analysis that quantifies the possibility of finding a particle at a specific distance from a reference particle. The surface of PETase has hydrophobic patches and it was interesting to find interaction between this hydrophobic surface and the (CH₃)₃N⁺ group of cholinium cation, and the rings of imidazolium [C4MIM], and [C2MIM] of ionic liquids.

We were expecting that there would be a high probability density of methyl group from cholinium cation surrounding the methyl groups of hydrophobic amino acids of PETase. It was found that Ala-123 from the surface of PETase, exhibited a high density of methyl group from the cholinium cation. It was also found that in the higher concentration of cholinium phosphate (40%), the RDF value for this density around Ala-123 was higher. The density of rings of [C4MIM], and [C2MIM] around Ala-123 were less than it was expected. Thus, the RDF analysis also shows that [Ch]₃[PO₄] has a more noticeable effect on the stability of hydrophobic surface.

The further details of this research project are described in **Paper 1**

3.2 5HT7R Modeling Discussion

3.2.1 Active and inactive states of 5HT7R

In the GPCR-G protein interaction project, we aim to characterize the interaction interface between 5HT7R and the G_s protein in the active (5HT7R) and inactive states (I-5HT7R) when

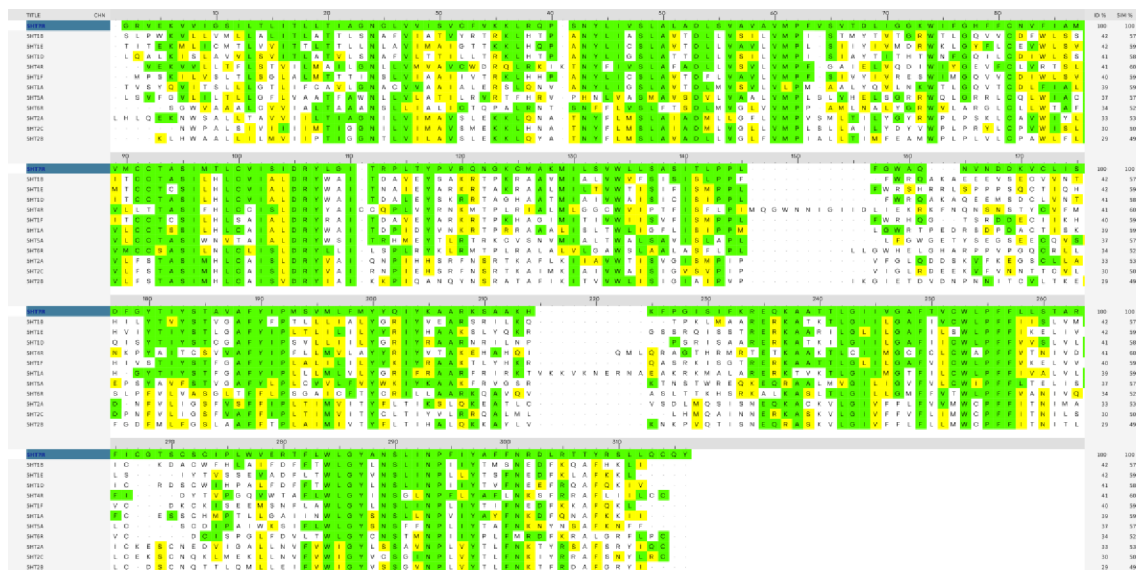


Figure 15 Multiple sequence alignment (MSA) of 5HT7R and all serotonin receptors (5HT4R, 5HT2A, 5HT1F, 5HT1B, 5HT5A, 5HT1D, 5HT2B, 5HT1A, 5HT1E, 5HT2C, and 5HT6R). Green and Yellow colors are for identical residues (green) and similar residues (yellow).

The 5-hydroxytryptamine (5HT) receptors are divided into seven types of serotonin receptors such as 5HT1R (1A, 1B,1C,1D,1E, and 1F), the 5HT2R (2A, 2B, and 2C), 5HT3R, 5HT4R, 5HT5R, 5HT6R, and 5-HT7R [154] (Figure 14). There is one 5HT receptor like 5HT3R, which functions as a ligand-gated ion channel. Rest of the serotonin receptors belong to the superfamily of GPCRs. The coupling of 5HT receptors with a downstream partner is different for different receptors such as 5HT1R, 5HT5R couple with $G_{i/o}$ [265], the 5HT2R couple with $G_{q/11}$ and 5HT4R, 5HT6R, and 5HT7R couple with G_s protein [155, 159, 266]. The 5HT7R shares with other serotonin GPCRs a sequence identity ranging from 29 to 42%, with 5HT2A and 5HT1B being the most similar to 5HT7R (Figure 15). Among all serotonin receptors, the 5HT5A, 5HT2A, 5HT2C, and 5HT1B have their crystal structures in their inactive conformation. The 5HT5A inactive structure with PDB ID: 7UM4 has incomplete crystal structure, and the 5HT2C doesn't have a very good sequence identity and similarity with the 5HT7R sequence. Thus, for the modeling of 5HT7R, we considered 5HT1B and 5HT2A serotonin receptors with sequence identity 42% and 33% (Figure 15). The 5HT2A and 5HT1B have multiple structures available (Table 1), we selected the structure with good resolution and more crystalize for homology modeling. There were regions in 5HT7R which were affected by conformational changes such as G77^{1.28}-L123^{2.46} (TM1-ICL1-TM2), A325^{6.33}-V338^{6.46} (TM6), N380^{7.49}- Q402^{8.61} (TM7-H8) (Figure 16 B) and Multiple Template-based modeling was used for these regions. We also used 'ab initio' method for the modeling of the region where no structural information was available. The presence of Cysteine residue increases the

stability of GPCR protein as it helps to build disulfide bonds. Disulfide bonds are important for protein stability, trafficking, and functionality [267]. Interestingly, the ECL3 of 5HT7R consists of three Cys residues such as C354, C358, and C360, and these three Cys residues are unique features as compared to all other serotonin receptors (Figure 17). In the experimental structures of other serotonin receptors, it has been observed that the two Cys residues form a disulfide bond. In the available serotonin experimental structures (Figure 17), the two cysteine residues form a disulfide bond. The ECL3 of 5HT7R is also the longest among the serotonin family. The missing ECL3 region 354-358 was then modeled constraining, the first two cysteine residues, C354 and C358, to form a disulfide bond and included in both the active and inactive structures of 5-HT7R (Figure 16 A, B).

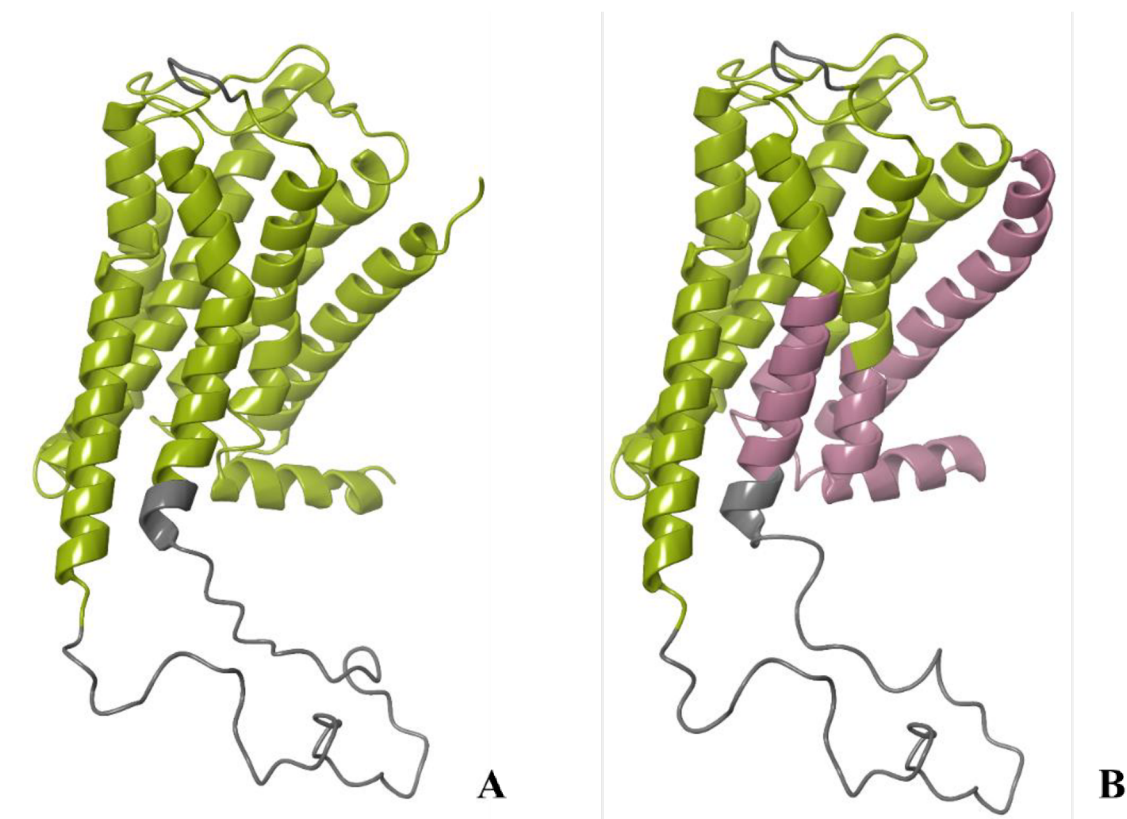


Figure 16 Modeling of 5HT7R in the A) active and B) inactive state. The region from the active structure is shown in green, those modeled from templates are shown in purple and the *ab initio* regions are demonstrated in gray.

The ICL3 was not resolved in the experimental structure of 5HT7R and in other serotonin receptors. Thus, for the modeling of ICL3, ‘*ab initio*’ method was used. The selected residues of ICL3 were 275-324. We modeled and used the same ICL3 confirmation for the sake of similarity.

3.2.2 Preassembled and active state complexes between 5HT7R and the G_s protein

The preassembled complex is formed between inactive GDP-bound G_s protein and an inactive I-5HT7R. The phenomenon of preassembly complex formation was also illustrated in a recent publication [268]. It was mentioned that the G protein coupling geometry in the apo 5HT1A-G_i protein [268] complex resembled that of liganded GPCRs in their active state conformation. Thus, we followed the phenomenon to adopt similar geometry and orientation as of Xu's publication.

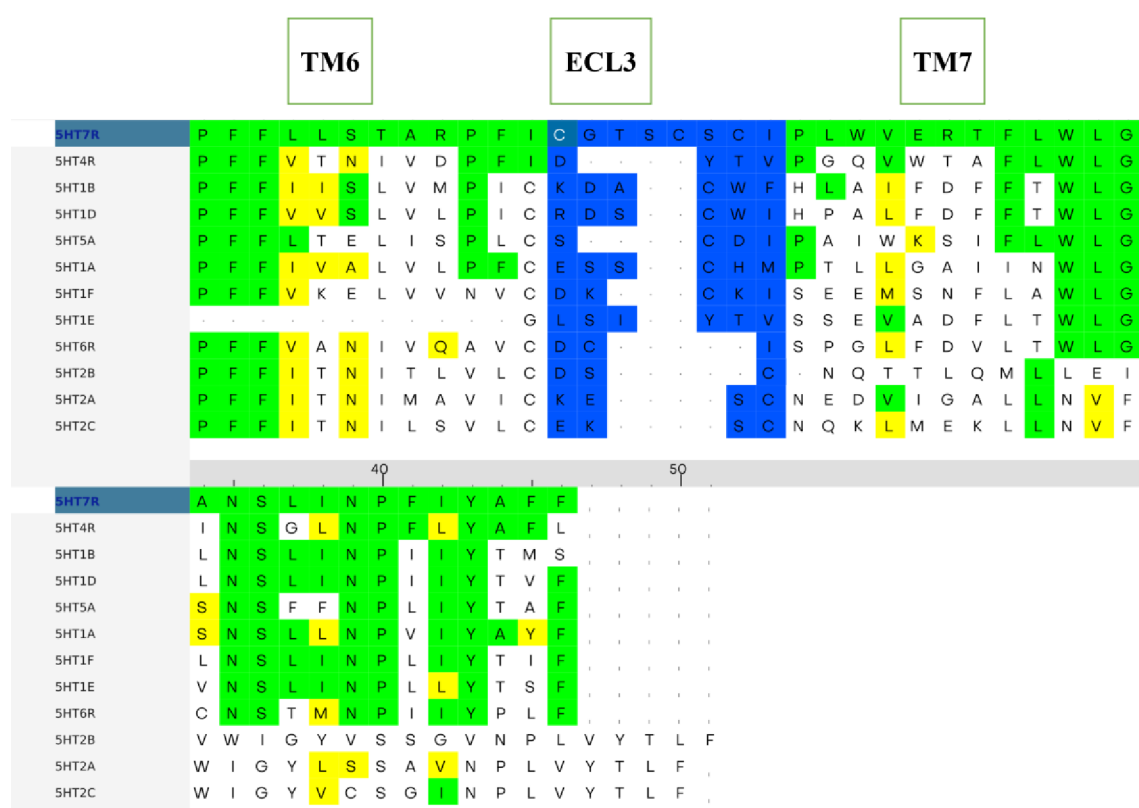


Figure 17 Sequence of other serotonin receptors with 5HT7R, illustrating only TM6, ECL3 and TM7. The green color shows identical residues, yellow color shows similar residues and blue color shows ECL3 residues

3.2.3 Molecular Dynamics simulations of active and preassembly complexes

After building models in the active and inactive conformations, we investigated the complexes in their motion during MD simulations. For this purpose, we run 3 replicas (R1, R2, and R3) of each complex (active and preassembly complex) for 500 ns of simulation. After MD simulations certain analysis was performed like RMSD to access the stability of the complexes during MD simulation.

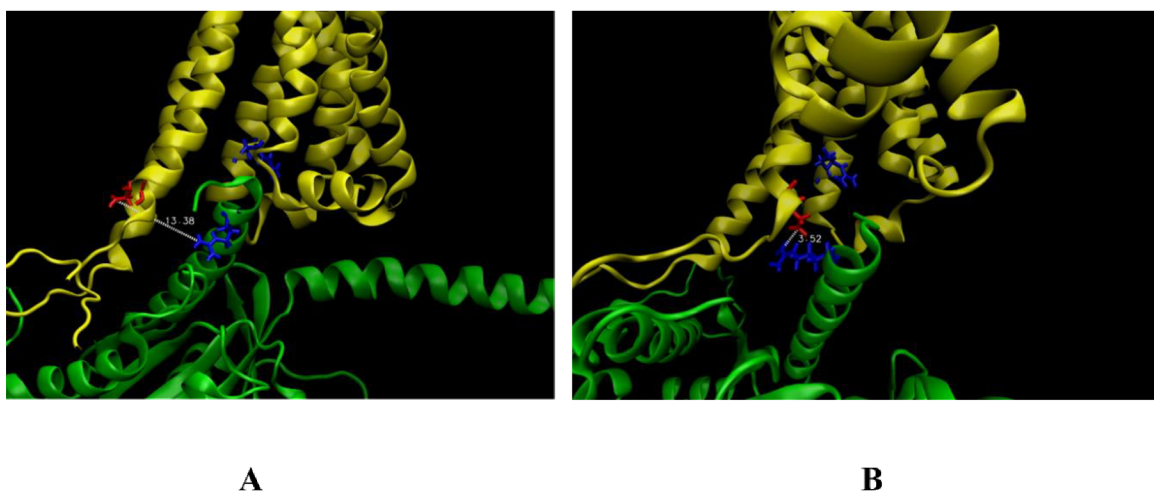


Figure 18 Ionic lock TM6 (322), H5 (389) A) active, B) preassembly complex after md simulation. The yellow color is for inactive 5HT7R, and the green color cartoon represents G_s protein.

The RMSD analysis found that the 5HT7R was quite stable in the active and preassembly complexes and among the G_s protein, only the $G\text{-}\gamma$ protein of preassembly complex was unstable for a period of simulation such as 310-360 ns of time. The rest of the complexes in their three replicas were stable for 500 ns simulation time.

Similarly, RMSF analysis was also performed to investigate the fluctuation of each residue of the active and preassembly complexes. The active (5HT7R) and preassembly (I-5HT7R) GPCR were quite stable during MD simulation but only ICL3 and other loop regions were fluctuating a bit.

3.2.4 Interaction interfaces for the active and inactive complexes before and after MD simulation

Electrostatic interaction is a very important factor between 5HT7R and G_s protein as it is the driving force between them. Thus, the active state complex is stabilized by the electrostatic interaction between 5HT7R and G_s protein. The H5 helix or the C-terminal of $G\alpha_s$ forms a negative charge surface, and that is complemented by the positive charge surface of 5HT7R. This indicates that electrostatic interactions serve as the driving force for the 5-HT7R- G_s coupling in the active state conformation.

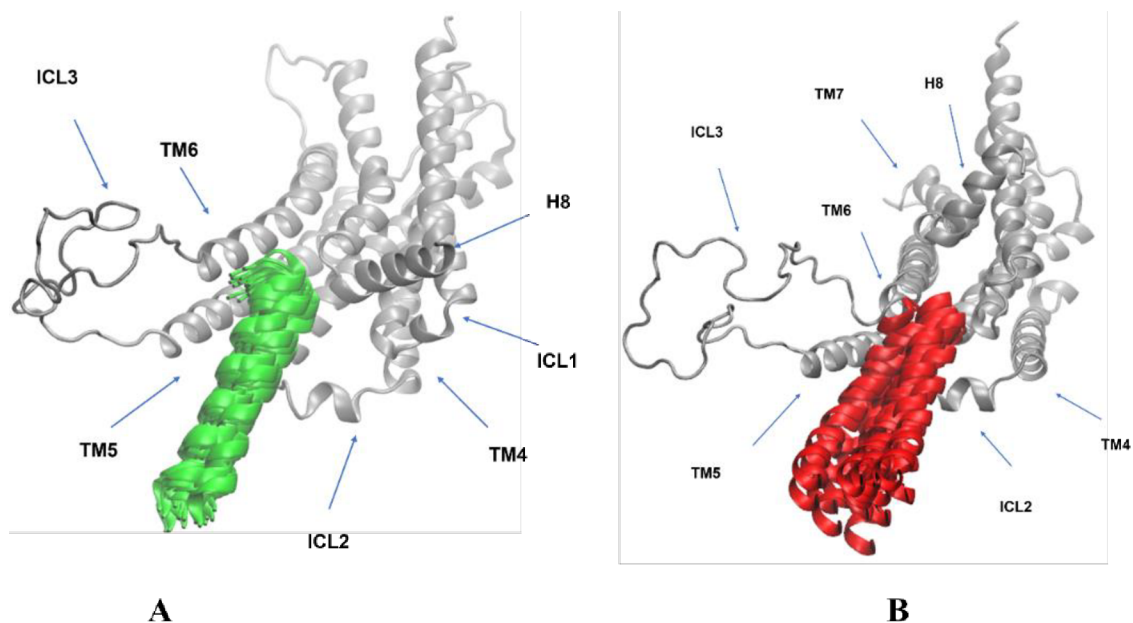


Figure 19 The interaction of the A) active and B) preassembly 5HT7 receptor with the $\alpha 5$ helix of the Gs protein during MD simulation.

Instead, in the preassembled complex, TM6 of the 5HT7R, it is tight to TM3 through the ionic lock formed between R180^{3.50} and E322^{6.30} (Figure 18). Therefore, the G protein binding interface is occluded by TM6, hiding key electrostatic interactions. The breakdown of this ionic lock is important for changing conformation from preassembly state complex to an active state complex. During MD simulation of the preassembly complex, it was found that E322^{6.30} residue is interacting with G α protein (Figure 18 B), and for the active state complex, these interacting residues were far from each other (Figure 18 A). Interestingly, the different extension and rotation of Gs $\alpha 5$ helix highlights other important electrostatic contacts with various regions of 5HT7R in an active and inactive conformation (Figure 19 A, B). The side-chain side-chain interactions of an active state complex and a preassembly complex after the MD simulation of 3 replicas were also investigated and shown in Figure 20 A, B.

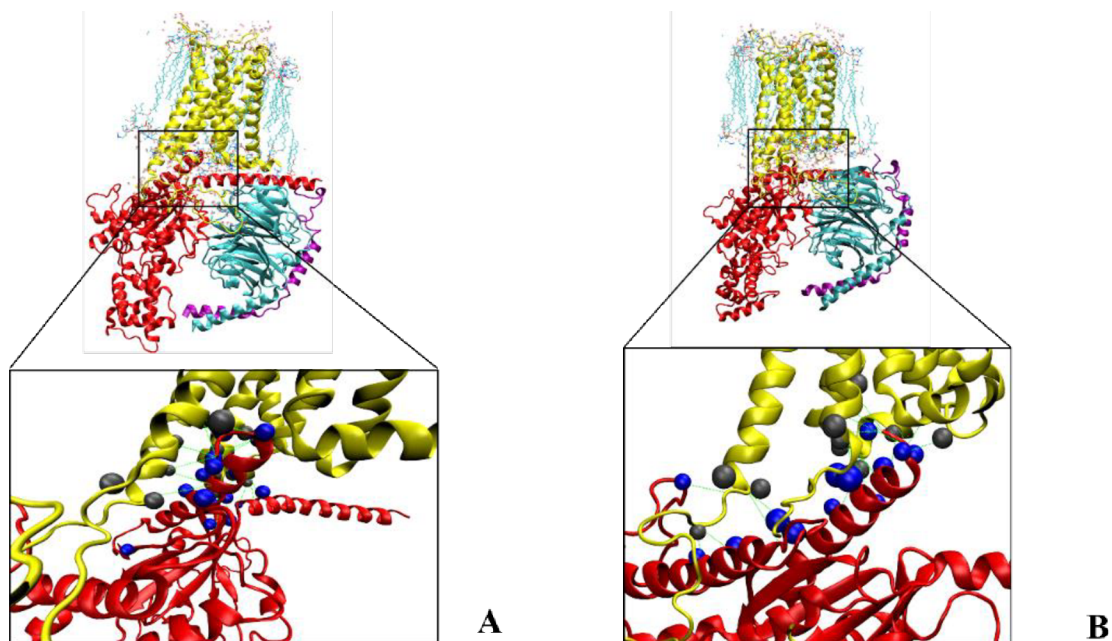


Figure 20 The sidechain-to-sidechain intermolecular contacts between A) active and B) preassembly complexes after MD simulation. The yellow color cartoon is for 5HT7R, and the red color represents the G α proteins.

We have also calculated the percentage contact analysis for the unique interaction of static active 5HT7R and G α protein in Figure 21 A, B.



Figure 21 A: unique interaction with the percentage of GPCR:G protein contacts specific to the static active structure of 5HT7R-Gs protein, B: unique interaction with the percentage of GPCR:G protein contacts specific to the static active structure Gs protein with 5HT7R.



Figure 22 A: unique interaction in static preassembly complex % of 5HT7R interactions with Gs protein, B: The pie chart displays the % of GPCR:G protein contacts specific to the static structure Gs protein interactions with 5HT7R.

The pie chart shows the percentage of each region (transmembranes or loops) of active 5HT7R that is involved in the interaction of G α protein. The plot shows that TM5 has major interacting residues with G α protein (Figure 21 A). Whereas, from the G α protein, the major interacting region is H5 helix that is involved in the static active complex formation Figure 21 B.

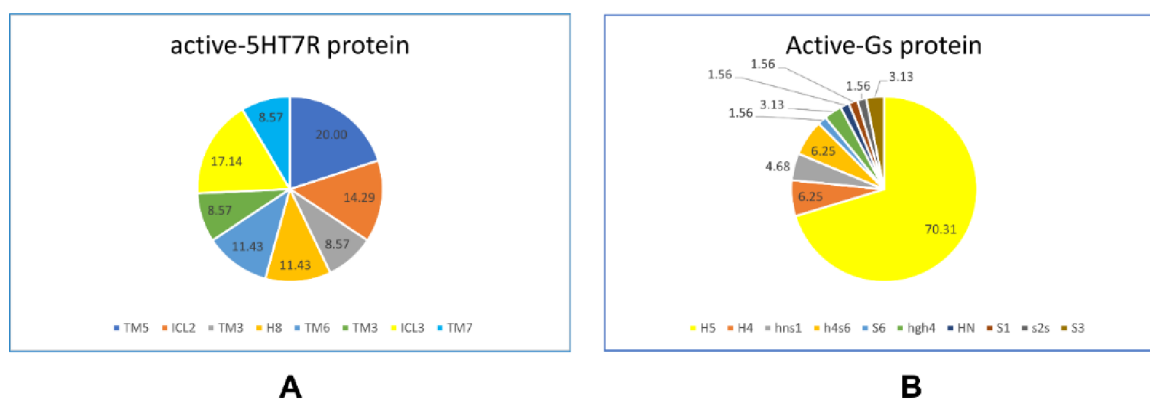


Figure 23 A: unique interaction % of active complex 5HT7R-Gs protein after MD. B: the pie chart displays % of GPCR:G protein contacts specific to Gs protein with 5HT7R

For the formation of static preassembly complex, the major residues with a higher percentage are from ICL2 (Figure 22 A, B). The second major interacting region is TM5 which is involved in the interaction with part of G α protein Figure 22 A. Like G α protein of static active state complex, in the preassembled complex formation, the major interacting region is H5 helix of Gs protein (Figure 22 B).



Figure 24 A: unique Interactions % of preassembly complex 5HT7R-Gs protein after MD. B: The pie chart displays the % of GPCR:G protein contacts specific to the structure Gs protein interactions with 5HT7R.

We also plotted specific interaction contact percentages for active state complex after MD simulation in Figure 23 A, B. The TM5 maintained the highest number of percentage interactions with $G\alpha_s$ protein after the MD simulation. Thus, it is suggested that TM5 played a major binding role for active state complex formation (Figure 23 A). Similarly, the H5 helix of $G\alpha_s$ protein also showed the highest percentage of specific contacts with 5HT7R (Figure 23 B).

The pie chart is also plotted for the preassembly complex after the MD simulation. It shows that the ICL2 maintained a major percentage of interaction with $G\alpha_s$ protein Figure 24 A, likewise, the H5 helix of $G\alpha_s$ protein also been observed for the interaction with 5HT7R Figure 24 B.

The further details of this research project are described in **Paper 2**.

4. Conclusion

The presence of solvents such as ionic liquids can have an impact on the interaction between biomolecular structure and the water molecules. These ionic liquids have the potential ability to change the flexibility, stability, and functionality of biomolecular systems via binding with the structure of a protein or the ligand or by altering the water network. During my Ph.D. work, I used molecular dynamics simulations to investigate how particular ionic liquids and their aqueous solutions influence the structural properties of the protein (enzyme) by providing valuable insight into its interactions, stability, and flexibility.

I have also studied in detail the role of ionic liquid for drug discovery. The detailed discussion is in paper 3 (book chapter). Ionic liquid-based drug materials can be used for cancer therapy gene delivery and antimicrobial treatments. Different techniques such as nanoparticles, liposomes, and nano-emulsions are used for the fabrication of ionic liquid-based nanomaterials for drug delivery.

The focus of my first research work was on the plastic degrading enzymes, particularly at PETase (PET degrading enzyme) for its wide implication on the environmental science and recycling of the plastics. Particularly I was analyzing the possible ionic liquids as co-solvent candidates for the stability, structural properties and function of the PETase as the ionic liquids can increase the solubility of the PET. In this research work, that has been already published, the MD simulations were employed to study the interaction pattern between the aqueous solution of ionic liquids, water, and the PETase enzyme. The stability of the enzyme site along its ligand bis (hydroxyethyl) terephthalate (BHET) in the presence of ionic liquid solution has been also inspected. Three particular ionic liquids such as cholinium phosphate $[\text{Ch}]_3[\text{PO}_4]$, 1-butyl-3-methyl-imidazolium acetate $[\text{C4MIM}][\text{Ac}]$, and 1-ethyl-3-methyl-imidazolium acetate $[\text{C2MIM}][\text{Ac}]$ were considered during our study. According to MD analysis, along with hydrophobic surface interactions, it was found that only $[\text{Ch}]_3[\text{PO}_4]$ exhibited a minimal impact on the structure of PETase and BHET ligand. The suitability of a water solution containing $[\text{Ch}]_3[\text{PO}_4]$ as a solvent for BHET hydrolysis is evident from its beneficial effects on the reaction process. These findings are promising for the future investigation of $[\text{Ch}]_3[\text{PO}_4]$ for the biodegradation of PET.

In the other research work, computational modeling was employed to explore the protein-protein interaction. The 5-hydroxytryptamine 7 receptor (5HT7R) belongs to class A G protein-coupled receptor (GPCR) involved in various functions, including circadian rhythm, thermoregulation, memory, learning, and sleep cycle regulations. It was found that this receptor

can pre-associate with the Gs protein in its inactive state prior to activation. During this work, we used the homology modeling technique to model the inactive state of 5HT7R and also run the long MD simulation to investigate the interface of inactive 5HT7R and Gs protein in the preassembly complex and compared it with the active state complex of 5HT7R with Gs protein. After MD simulation analysis, it was found that the binding interface of active and inactive complexes has some common interacting residues, whereas most of the interacting residues are different. This interface investigation of the preassembly complex is of vital importance for future research of the class A GPCR-downstream complexes.

5. References

1. Ritchie, H., *Where does the plastic in our oceans come from*. Our World Data, 2021. **1**.
2. Geyer, R., J.R. Jambeck, and K.L. Law, *Production, use, and fate of all plastics ever made*. Science advances, 2017. **3**(7): p. e1700782.
3. Barnes, S.J., *Understanding plastics pollution: The role of economic development and technological research*. Environmental pollution, 2019. **249**: p. 812-821.
4. Neufeld, L., et al. *The new plastics economy: rethinking the future of plastics*. in *World Economic Forum*. 2016.
5. programme, U.e. *New Plastics Economy Global Commitment 2018*; Available from: https://www.unep.org/interactives/beat-plastic-pollution/?gclid=CjwKCAiA3KefBhByEiwAi2LDHD8Yh-Mgykq2PKIXOKLhmYi57srfWjoXljkI9szCjndDr1XbzCmsJhoCbZEqAvD_BwE.
6. Willis, S., *A primer for daily life* 2005: Routledge.
7. Webb, H.K., et al., *Plastic degradation and its environmental implications with special reference to poly (ethylene terephthalate)*. Polymers, 2012. **5**(1): p. 1-18.
8. Walker, T., et al., *Marine debris surveys at Bird Island, South Georgia 1990–1995*. Marine pollution bulletin, 1997. **34**(1): p. 61-65.
9. do Sul, J.A.I. and M.F. Costa, *Marine debris review for Latin America and the wider Caribbean region: from the 1970s until now, and where do we go from here?* Marine pollution bulletin, 2007. **54**(8): p. 1087-1104.
10. Auta, H.S., C. Emenike, and S.H. Fauziah, *Distribution and importance of microplastics in the marine environment: a review of the sources, fate, effects, and potential solutions*. Environment international, 2017. **102**: p. 165-176.
11. Derraik, J.G., *The pollution of the marine environment by plastic debris: a review*. Marine pollution bulletin, 2002. **44**(9): p. 842-852.
12. Pemberton, D., N. Brothers, and R. Kirkwood, *Entanglement of Australian fur seals in man-made debris in Tasmanian waters*. Wildlife Research, 1992. **19**(2): p. 151-159.
13. Ross, P.S. and C. Morales-Caselles, *Out of sight, but no longer out of mind: microplastics as a global pollutant*. Integrated Environmental Assessment and Management, 2015. **11**(4): p. 721-722.
14. Rochman, C.M., et al., *Early warning signs of endocrine disruption in adult fish from the ingestion of polyethylene with and without sorbed chemical pollutants from the marine environment*. Science of the total environment, 2014. **493**: p. 656-661.
15. Lee, K.-W., et al., *Size-dependent effects of micro polystyrene particles in the marine copepod *Tigriopus japonicus**. Environmental science & technology, 2013. **47**(19): p. 11278-11283.
16. Mato, Y., et al., *Plastic resin pellets as a transport medium for toxic chemicals in the marine environment*. Environmental science & technology, 2001. **35**(2): p. 318-324.
17. Rios, L.M., C. Moore, and P.R. Jones, *Persistent organic pollutants carried by synthetic polymers in the ocean environment*. Marine pollution bulletin, 2007. **54**(8): p. 1230-1237.
18. Hirai, H., et al., *Organic micropollutants in marine plastics debris from the open ocean and remote and urban beaches*. Marine pollution bulletin, 2011. **62**(8): p. 1683-1692.
19. Schecter, A., et al., *Perfluorinated compounds, polychlorinated biphenyls, and organochlorine pesticide contamination in composite food samples from Dallas, Texas, USA*. Environmental health perspectives, 2010. **118**(6): p. 796-802.
20. Trudel, D., et al., *Total consumer exposure to polybrominated diphenyl ethers in North America and Europe*. Environmental science & technology, 2011. **45**(6): p. 2391-2397.
21. Chung, S., et al., *Effects of grilling and roasting on the levels of polycyclic aromatic hydrocarbons in beef and pork*. Food Chemistry, 2011. **129**(4): p. 1420-1426.

22. Zhou, Q., Y. Gao, and G. Xie, *Determination of bisphenol A, 4-n-nonylphenol, and 4-tert-octylphenol by temperature-controlled ionic liquid dispersive liquid-phase microextraction combined with high performance liquid chromatography-fluorescence detector*. *Talanta*, 2011. **85**(3): p. 1598-1602.
23. Boscolo, A., " *Throwaway Living*": A Study of American Perceptions of Disposability Surrounding Single-Use Products, 2017.
24. Yamada-Onodera, K., et al., *Degradation of polyethylene by a fungus, Penicillium simplicissimum* YK. *Polymer Degradation and Stability*, 2001. **72**(2): p. 323-327.
25. Zheng, Y., E.K. Yanful, and A.S. Bassi, *A review of plastic waste biodegradation*. *Critical reviews in biotechnology*, 2005. **25**(4): p. 243-250.
26. Marqués-Calvo, M.S., et al., *Enzymatic and microbial biodegradability of poly (ethylene terephthalate) copolymers containing nitrated units*. *Polymer Degradation and Stability*, 2006. **91**(4): p. 663-671.
27. Koutny, M., J. Lemaire, and A.-M. Delort, *Biodegradation of polyethylene films with prooxidant additives*. *Chemosphere*, 2006. **64**(8): p. 1243-1252.
28. Andrady, A.L., *Microplastics in the marine environment*. *Marine pollution bulletin*, 2011. **62**(8): p. 1596-1605.
29. Raquez, J.M., et al., *Oxidative degradations of oxodegradable LDPE enhanced with thermoplastic pea starch: Thermo-mechanical properties, morphology, and UV-ageing studies*. *Journal of Applied Polymer Science*, 2011. **122**(1): p. 489-496.
30. Weiner, S. and P.M. Dove, *An overview of biomineralization processes and the problem of the vital effect*. *Reviews in mineralogy and geochemistry*, 2003. **54**(1): p. 1-29.
31. Li, X., et al., *Biomineralization on polymer-coated multi-walled carbon nanotubes with different surface functional groups*. *Colloids and Surfaces B: Biointerfaces*, 2014. **123**: p. 753-761.
32. Raaman, N., et al., *Biodegradation of plastic by Aspergillus spp. isolated from polythene polluted sites around Chennai*. *J. Acad. Indus. Res*, 2012. **1**(6): p. 313-316.
33. Li, Y., et al., *The effect of mechanical loads on the degradation of aliphatic biodegradable polyesters*. *Regenerative Biomaterials*, 2017. **4**(3): p. 179-190.
34. L. D. Poulikakos , C.P., Hofkoc, F. Gschösser d, A. Cannone Falchetoe, M. Buena, M. Arraigadaa, J. Sousaf and R.R.g. , C. Petit h, M. Loizidoub, M.N. Partl, *Polyethylene Terephthalate*, in *Resources, Conservation and Recycling*2017, Elsevier. p. 32-44.
35. Benyathiar, P., et al., *Polyethylene Terephthalate (PET) Bottle-to-Bottle Recycling for the Beverage Industry: A Review*. *Polymers*, 2022. **14**(12): p. 2366.
36. Sun, J., et al., *Solubilization and Upgrading of High Polyethylene Terephthalate Loadings in a Low-Costing Bifunctional Ionic Liquid*. *ChemSusChem*, 2018. **11**(4): p. 781-792.
37. 2021; Available from: <https://www.coherentmarketinsights.com/market-insight/pet-packaging-market-5290>.
38. Koshti, R., L. Mehta, and N. Samarth, *Biological recycling of polyethylene terephthalate: a mini-review*. *Journal of Polymers and the Environment*, 2018. **26**: p. 3520-3529.
39. Samperi, F., et al., *Thermal degradation of poly (ethylene terephthalate) at the processing temperature*. *Polymer Degradation and Stability*, 2004. **83**(1): p. 3-10.
40. Francis, R., *Recycling of polymers: methods, characterization and applications*2016: John Wiley & Sons.
41. Karayannidis, G.P. and D.S. Achilias, *Chemical recycling of poly (ethylene terephthalate)*. *Macromolecular Materials and Engineering*, 2007. **292**(2): p. 128-146.
42. Paszun, D. and T. Szychaj, *Chemical recycling of poly (ethylene terephthalate)*. *Industrial & engineering chemistry research*, 1997. **36**(4): p. 1373-1383.
43. Long, T.E. and J. Scheirs, *Modern polyesters: chemistry and technology of polyesters and copolyesters*2005: John Wiley & Sons.

44. Kurokawa, H., et al., *Methanolysis of polyethylene terephthalate (PET) in the presence of aluminium tiisopropoxide catalyst to form dimethyl terephthalate and ethylene glycol*. *Polymer Degradation and Stability*, 2003. **79**(3): p. 529-533.
45. Chen, J.W. and L.W. Chen, *The glycolysis of poly (ethylene terephthalate)*. *Journal of Applied Polymer Science*, 1999. **73**(1): p. 35-40.
46. Xi, G., M. Lu, and C. Sun, *Study on depolymerization of waste polyethylene terephthalate into monomer of bis (2-hydroxyethyl terephthalate)*. *Polymer Degradation and Stability*, 2005. **87**(1): p. 117-120.
47. Firas, A. and P. Dumitru, *Recycling of PET*. *Eur Polym J*, 2005. **41**(7): p. 1453-1477.
48. Wang, H., et al., *Fe-containing magnetic ionic liquid as an effective catalyst for the glycolysis of poly (ethylene terephthalate)*. *Catalysis Communications*, 2010. **11**(8): p. 763-767.
49. Baliga, S. and W.T. Wong, *Depolymerization of poly (ethylene terephthalate) recycled from post-consumer soft-drink bottles*. *Journal of Polymer Science Part A: Polymer Chemistry*, 1989. **27**(6): p. 2071-2082.
50. Ghaemy, M. and K. Mossaddegh, *Depolymerisation of poly (ethylene terephthalate) fibre wastes using ethylene glycol*. *Polymer Degradation and Stability*, 2005. **90**(3): p. 570-576.
51. Yoshioka, T., et al., *Effects of metal oxides on the pyrolysis of poly (ethylene terephthalate)*. *Journal of analytical and applied pyrolysis*, 2005. **73**(1): p. 139-144.
52. Nakkabi, A., et al., *Biodegradation of poly (ethylene terephthalate) by Bacillus Subtilis*. *Int J Recent Adv Multidiscip Res*, 2015. **2**(12): p. 1060-1062.
53. Gross, R.A. and B. Kalra, *Biodegradable polymers for the environment*. *science*, 2002. **297**(5582): p. 803-807.
54. Kale, S.K., et al., *Microbial degradation of plastic: a review*. *Journal of Biochemical Technology*, 2015. **6**(2): p. 952-961.
55. Müller, R.J., et al., *Enzymatic degradation of poly (ethylene terephthalate): rapid hydrolyse using a hydrolase from T. fusca*. *Macromolecular rapid communications*, 2005. **26**(17): p. 1400-1405.
56. Furukawa, M., et al., *Efficient degradation of poly (ethylene terephthalate) with Thermobifida fusca cutinase exhibiting improved catalytic activity generated using mutagenesis and additive-based approaches*. *Scientific reports*, 2019. **9**(1): p. 16038.
57. Kanelli, M., et al., *Surface modification of poly (ethylene terephthalate)(PET) fibers by a cutinase from Fusarium oxysporum*. *Process biochemistry*, 2015. **50**(11): p. 1885-1892.
58. Acero, E., et al., *Wei 383 R, Zimmermann W, Zinn M, Cavaco-Paulo A, Freddi G, Schwab H, Guebitz G. 2011. 384 Enzymatic surface hydrolysis of PET: Effect of structural diversity on kinetic properties of 385 cutinases from Thermobifida*. *Macromolecules*. **44**: p. 4632-4640.
59. Dimarogona, M., et al., *Structural and functional studies of a Fusarium oxysporum cutinase with polyethylene terephthalate modification potential*. *Biochimica et Biophysica Acta (BBA)-General Subjects*, 2015. **1850**(11): p. 2308-2317.
60. Chen, C.C., et al., *Structural studies reveal the molecular mechanism of PET ase*. *The FEBS Journal*, 2018. **285**(20): p. 3717-3723.
61. Song, M.R., et al. *Experimental study of seismic performance on three-story prestressed fabricated concrete frame*. in *Advanced Materials Research*. 2011. Trans Tech Publ.
62. Wang, X., et al., *Preparation of a PET-hydrolyzing lipase from Aspergillus oryzae by the addition of bis (2-hydroxyethyl) terephthalate to the culture medium and enzymatic modification of PET fabrics*. *Engineering in life sciences*, 2008. **8**(3): p. 268-276.
63. Vickers, N.J., *Animal communication: when i'm calling you, will you answer too?* *Current biology*, 2017. **27**(14): p. R713-R715.
64. de Castro, A.M., et al., *Screening of commercial enzymes for poly (ethylene terephthalate)(PET) hydrolysis and synergy studies on different substrate sources*. *Journal of Industrial Microbiology and Biotechnology*, 2017. **44**(6): p. 835-844.

65. Stauch, B., S.J. Fisher, and M. Cianci, *Open and closed states of Candida antarctica lipase B: Protonation and the mechanism of interfacial activation*. Journal of lipid research, 2015. **56**(12): p. 2348-2358.
66. Zhang, H., et al., *The Bacteroidetes Aequorivita sp. and Kaistella jeonii produce promiscuous esterases with PET-hydrolyzing activity*. Frontiers in microbiology, 2022. **12**: p. 3874.
67. Loch, T.P. and M. Faisal, *Emerging flavobacterial infections in fish: a review*. Journal of advanced research, 2015. **6**(3): p. 283-300.
68. Foley, M.H., D.W. Cockburn, and N.M. Koropatkin, *The Sus operon: a model system for starch uptake by the human gut Bacteroidetes*. Cellular and Molecular Life Sciences, 2016. **73**: p. 2603-2617.
69. Dodd, D., R.I. Mackie, and I.K. Cann, *Xylan degradation, a metabolic property shared by rumen and human colonic Bacteroidetes*. Molecular microbiology, 2011. **79**(2): p. 292-304.
70. Thomas, F., et al., *Environmental and gut bacteroidetes: the food connection*. Frontiers in microbiology, 2011. **2**: p. 93.
71. Ribitsch, D., et al., *Hydrolysis of polyethyleneterephthalate by p-nitrobenzylesterase from Bacillus subtilis*. Biotechnology progress, 2011. **27**(4): p. 951-960.
72. Kawai, F., et al., *A novel Ca²⁺-activated, thermostabilized polyesterase capable of hydrolyzing polyethylene terephthalate from Saccharomonospora viridis AHK190*. Applied microbiology and biotechnology, 2014. **98**: p. 10053-10064.
73. Maurya, A., A. Bhattacharya, and S.K. Khare, *Enzymatic remediation of polyethylene terephthalate (PET)-based polymers for effective management of plastic wastes: an overview*. Frontiers in Bioengineering and Biotechnology, 2020. **8**: p. 602325.
74. Ribitsch, D., et al., *Characterization of a new cutinase from Thermobifida alba for PET-surface hydrolysis*. Biocatalysis and Biotransformation, 2012. **30**(1): p. 2-9.
75. Verger, R., *'Interfacial activation' of lipases: facts and artifacts*. Trends in Biotechnology, 1997. **15**(1): p. 32-38.
76. Bornscheuer, U.T., *Feeding on plastic*. science, 2016. **351**(6278): p. 1154-1155.
77. Yoshida, S., et al., *A bacterium that degrades and assimilates poly (ethylene terephthalate)*. science, 2016. **351**(6278): p. 1196-1199.
78. Carr, C.M., D.J. Clarke, and A.D. Dobson, *Microbial polyethylene terephthalate hydrolases: current and future perspectives*. Frontiers in microbiology, 2020. **11**: p. 571265.
79. Kawai, F., T. Kawabata, and M. Oda, *Current state and perspectives related to the polyethylene terephthalate hydrolases available for biorecycling*. ACS Sustainable Chemistry & Engineering, 2020. **8**(24): p. 8894-8908.
80. Taniguchi, I., et al., *Biodegradation of PET: current status and application aspects*. Acs Catalysis, 2019. **9**(5): p. 4089-4105.
81. Austin, H.P., et al., *Characterization and engineering of a plastic-degrading aromatic polyesterase*. Proceedings of the National Academy of Sciences, 2018. **115**(19): p. E4350-E4357.
82. Hachisuka, S.-i., T. Nishii, and S. Yoshida, *Development of a targeted gene disruption system in the poly (ethylene terephthalate)-degrading bacterium Ideonella sakaiensis and its applications to PETase and MHETase genes*. Applied and environmental microbiology, 2021. **87**(18): p. e00020-21.
83. Khabiri, M., et al., *Interaction of organic solvents with protein structures at protein-solvent interface*. Journal of molecular modeling, 2013. **19**: p. 4701-4711.
84. Fetzner, S. and F. Lingens, *Bacterial dehalogenases: biochemistry, genetics, and biotechnological applications*. Microbiol. Mol. Biol. Rev., 1994. **58**(4): p. 641-685.
85. Damborský, J., et al., *Structure-specificity relationships for haloalkane dehalogenases*. Environmental toxicology and chemistry, 2001. **20**(12): p. 2681-2689.

86. Stucki, G. and M. Thueer, *Experiences of a large-scale application of 1, 2-dichloroethane degrading microorganisms for groundwater treatment*. Environmental science & technology, 1995. **29**(9): p. 2339-2345.
87. Samak, N.A., et al., *Recent advances in biocatalysts engineering for polyethylene terephthalate plastic waste green recycling*. Environment international, 2020. **145**: p. 106144.
88. Al-Sabagh, A., et al., *Greener routes for recycling of polyethylene terephthalate*. Egyptian Journal of Petroleum, 2016. **25**(1): p. 53-64.
89. Moniruzzaman, M., et al., *Recent advances of enzymatic reactions in ionic liquids*. Biochemical Engineering Journal, 2010. **48**(3): p. 295-314.
90. Roosen, C., P. Müller, and L. Greiner, *Ionic liquids in biotechnology: applications and perspectives for biotransformations*. Applied microbiology and biotechnology, 2008. **81**: p. 607-614.
91. Constatinescu, D., C. Herrmann, and H. Weingärtner, *Patterns of protein unfolding and protein aggregation in ionic liquids*. Physical Chemistry Chemical Physics, 2010. **12**(8): p. 1756-1763.
92. Olivier-Bourbigou, H., L. Magna, and D. Morvan, *Ionic liquids and catalysis: Recent progress from knowledge to applications*. Applied Catalysis A: General, 2010. **373**(1-2): p. 1-56.
93. Suojiang, Z., *Encyclopedia of Ionic Liquids: living edition*, 2020, Springer.
94. Hadad, C., E. Husson, and A.N. van Nhien, *Encyclopedia of Ionic Liquids: Conversion of Chitin in Ionic Liquids*, 2020, Springer Singapore.
95. Akdogan, Y., M.J. Junk, and D. Hinderberger, *Effect of ionic liquids on the solution structure of human serum albumin*. Biomacromolecules, 2011. **12**(4): p. 1072-1079.
96. Halle, B., *Protein hydration dynamics in solution: a critical survey*. Philosophical Transactions of the Royal Society of London. Series B: Biological Sciences, 2004. **359**(1448): p. 1207-1224.
97. Bubalo, M.C., et al., *Toxicity mechanisms of ionic liquids*. Arhiv za higijenu rada i toksikologiju, 2017. **68**(3): p. 171-179.
98. Klähn, M., et al., *On the different roles of anions and cations in the solvation of enzymes in ionic liquids*. Physical Chemistry Chemical Physics, 2011. **13**(4): p. 1649-1662.
99. Gorke, J., F. Sreinc, and R. Kazlauskas, *Toward advanced ionic liquids. Polar, enzyme-friendly solvents for biocatalysis*. Biotechnology and Bioprocess Engineering, 2010. **15**: p. 40-53.
100. Wang, H., G. Gurau, and R.D. Rogers, *Ionic liquid processing of cellulose*. Chemical Society Reviews, 2012. **41**(4): p. 1519-1537.
101. Xu, A. and F. Wang, *Carboxylate ionic liquid solvent systems from 2006 to 2020: Thermal properties and application in cellulose processing*. Green Chemistry, 2020. **22**(22): p. 7622-7664.
102. Wang, H., et al., *Degradation of poly (ethylene terephthalate) using ionic liquids*. Green Chemistry, 2009. **11**(10): p. 1568-1575.
103. Tournier, V., et al., *An engineered PET depolymerase to break down and recycle plastic bottles*. Nature, 2020. **580**(7802): p. 216-219.
104. Marrucho, I., L. Branco, and L. Rebelo, *Ionic liquids in pharmaceutical applications*. Annual review of chemical and biomolecular engineering, 2014. **5**: p. 527-546.
105. Patel, D.D. and J.M. Lee, *Applications of ionic liquids*. The Chemical Record, 2012. **12**(3): p. 329-355.
106. Page, T.A., et al., *Dynamics of loop 1 of domain I in human serum albumin when dissolved in ionic liquids*. The Journal of Physical Chemistry B, 2009. **113**(38): p. 12825-12830.
107. Todd, A.D., et al., *Reactive compatibilization of poly (ethylene terephthalate) and high-density polyethylene using amino-telechelic polyethylene*. Macromolecules, 2016. **49**(23): p. 8988-8994.
108. Shi, H., et al., *Synthesis and hydrophobic properties of F & Si containing poly (ethylene terephthalate)*. RSC Advances, 2016. **6**(108): p. 106540-106546.
109. Swatloski, R.P., et al., *Dissolution of cellose with ionic liquids*. Journal of the American chemical society, 2002. **124**(18): p. 4974-4975.

110. Silva, C.V.G., et al., *PET glycolysis optimization using ionic liquid [Bmin] ZnCl₃ as catalyst and kinetic evaluation*. *Polímeros*, 2018. **28**(5): p. 450-459.
111. Yue, Q., et al., *Glycolysis of poly (ethylene terephthalate)(PET) using basic ionic liquids as catalysts*. *Polymer Degradation and Stability*, 2011. **96**(4): p. 399-403.
112. Yue, Q., et al., *The glycolysis of poly (ethylene terephthalate) waste: Lewis acidic ionic liquids as high efficient catalysts*. *Polymers*, 2013. **5**(4): p. 1258-1271.
113. Wang, Y., et al., *Zinc-catalyzed ester bond cleavage: Chemical degradation of polyethylene terephthalate*. *Journal of Cleaner Production*, 2019. **208**: p. 1469-1475.
114. Di Pizio, A., M. Behrens, and D. Krautwurst, *Beyond the flavour: the potential druggability of chemosensory G protein-coupled receptors*. *International Journal of Molecular Sciences*, 2019. **20**(6): p. 1402.
115. Roth, B.L. and W.K. Kroeze, *Integrated approaches for genome-wide interrogation of the druggable non-olfactory G protein-coupled receptor superfamily*. *Journal of Biological Chemistry*, 2015. **290**(32): p. 19471-19477.
116. Sriram, K. and P.A. Insel, *G protein-coupled receptors as targets for approved drugs: how many targets and how many drugs?* *Molecular pharmacology*, 2018. **93**(4): p. 251-258.
117. Harmar, A.J., *Family-B G-protein-coupled receptors*. *Genome biology*, 2001. **2**(12): p. 1-10.
118. Do, H.N., et al., *Unique features of different classes of G-protein-coupled receptors revealed from sequence coevolutionary and structural analysis*. *Proteins: Structure, Function, and Bioinformatics*, 2022. **90**(2): p. 601-614.
119. Davies, M.N., et al., *GPCRTree: online hierarchical classification of GPCR function*. *BMC Res Notes*, 2008. **1**: p. 67.
120. Pandy-Szekeres, G., et al., *GPCRdb in 2018: adding GPCR structure models and ligands*. *Nucleic Acids Res*, 2018. **46**(D1): p. D440-D446.
121. Harding, S.D., et al., *The IUPHAR/BPS Guide to PHARMACOLOGY in 2018: updates and expansion to encompass the new guide to IMMUNOPHARMACOLOGY*. *Nucleic Acids Res*, 2018. **46**(D1): p. D1091-D1106.
122. Fredriksson, R., et al., *The G-protein-coupled receptors in the human genome form five main families. Phylogenetic analysis, paralogon groups, and fingerprints*. *Molecular pharmacology*, 2003. **63**(6): p. 1256-1272.
123. Yang, J., et al., *G protein-coupled receptor kinases: Crucial regulators of blood pressure*. *Journal of the American Heart Association*, 2016. **5**(7): p. e003519.
124. Bar-Shavit, R., et al., *G protein-coupled receptors in cancer*. *International Journal of Molecular Sciences*, 2016. **17**(8): p. 1320.
125. Chien, E.Y., et al., *Structure of the human dopamine D₃ receptor in complex with a D₂/D₃ selective antagonist*. *science*, 2010. **330**(6007): p. 1091-1095.
126. Schwartz, T.W., et al., *Molecular mechanism of action of non-peptide ligands for peptide receptors*. *Curr Pharm Design*, 1995. **1**: p. 325-342.
127. Schwartz, T.W., *Locating ligand-binding sites in 7TM receptors by protein engineering*. *Current Opinion in Biotechnology*, 1994. **5**(4): p. 434-444.
128. Oliveira, L., A.C.d.M. Paiva, and G. Vriend, *A common motif in G-protein-coupled seven transmembrane helix receptors*. *Journal of Computer-Aided Molecular Design*, 1993. **7**(6): p. 649-658.
129. Baldwin, J.M., *The probable arrangement of the helices in G protein-coupled receptors*. *The EMBO journal*, 1993. **12**(4): p. 1693-1703.
130. Baldwin, J.M., G.F. Schertler, and V.M. Unger, *An alpha-carbon template for the transmembrane helices in the rhodopsin family of G-protein-coupled receptors*. *Journal of molecular biology*, 1997. **272**(1): p. 144-164.
131. Ballesteros, J.A. and H. Weinstein, *[19] Integrated methods for the construction of three-dimensional models and computational probing of structure-function relations in G protein-coupled receptors*, in *Methods in neurosciences* 1995, Elsevier. p. 366-428.

132. Isberg, V., et al., *Generic GPCR residue numbers—aligning topology maps while minding the gaps*. Trends in pharmacological sciences, 2015. **36**(1): p. 22-31.
133. Wootten, D., et al., *Polar transmembrane interactions drive formation of ligand-specific and signal pathway-biased family BG protein-coupled receptor conformations*. Proceedings of the National Academy of Sciences, 2013. **110**(13): p. 5211-5216.
134. Hollenstein, K., et al., *Insights into the structure of class B GPCRs*. Trends in pharmacological sciences, 2014. **35**(1): p. 12-22.
135. Pin, J.-P., T. Galvez, and L. Prézeau, *Evolution, structure, and activation mechanism of family 3/C G-protein-coupled receptors*. Pharmacology & therapeutics, 2003. **98**(3): p. 325-354.
136. Doré, A.S., et al., *Structure of class C GPCR metabotropic glutamate receptor 5 transmembrane domain*. Nature, 2014. **511**(7511): p. 557-562.
137. Wang, C., et al., *Structural basis for Smoothed receptor modulation and chemoresistance to anticancer drugs*. Nature communications, 2014. **5**(1): p. 1-11.
138. Unal, H. and S.S. Karnik, *Domain coupling in GPCRs: the engine for induced conformational changes*. Trends in pharmacological sciences, 2012. **33**(2): p. 79-88.
139. Carpenter, E.P., et al., *Overcoming the challenges of membrane protein crystallography*. Current opinion in structural biology, 2008. **18**(5): p. 581-586.
140. Zhao, J., et al., *G protein-coupled receptors (GPCRs) in Alzheimer's disease: a focus on BACE1 related GPCRs*. Frontiers in aging neuroscience, 2016. **8**: p. 58.
141. Weis, W.I. and B.K. Kobilka, *The molecular basis of G protein-coupled receptor activation*. Annual review of biochemistry, 2018. **87**: p. 897-919.
142. Liu, X., et al., *Structural insights into the process of GPCR-G protein complex formation*. Cell, 2019. **177**(5): p. 1243-1251. e12.
143. Offermanns, S., *G-proteins as transducers in transmembrane signalling*. Progress in biophysics and molecular biology, 2003. **83**(2): p. 101-130.
144. Suzuki, N., N. Hajicek, and T. Kozasa, *Regulation and physiological functions of G12/13-mediated signaling pathways*. Neurosignals, 2009. **17**(1): p. 55-70.
145. Hakak, Y., et al., *Global analysis of G-protein-coupled receptor signaling in human tissues*. FEBS letters, 2003. **550**(1-3): p. 11-17.
146. Hein, P. and M. Bünemann, *Coupling mode of receptors and G proteins*. Naunyn-Schmiedeberg's archives of pharmacology, 2009. **379**(5): p. 435-443.
147. Andressen, K.W., et al., *Related GPCRs couple differently to Gs: preassociation between G protein and 5-HT7 serotonin receptor reveals movement of Gas upon receptor activation*. The FASEB Journal, 2018. **32**(2): p. 1059-1069.
148. Nobles, M., A. Benians, and A. Tinker, *Heterotrimeric G proteins precouple with G protein-coupled receptors in living cells*. Proceedings of the National Academy of Sciences, 2005. **102**(51): p. 18706-18711.
149. Galés, C., et al., *Probing the activation-promoted structural rearrangements in preassembled receptor-G protein complexes*. Nature structural & molecular biology, 2006. **13**(9): p. 778-786.
150. Damian, M., et al., *Ghrelin receptor conformational dynamics regulate the transition from a preassembled to an active receptor: Gq complex*. Proceedings of the National Academy of Sciences, 2015. **112**(5): p. 1601-1606.
151. Qin, K., et al., *Inactive-state preassembly of Gq-coupled receptors and Gq heterotrimers*. Nature chemical biology, 2011. **7**(10): p. 740-747.
152. Ayoub, M.A., et al., *Differential association modes of the thrombin receptor PAR1 with Gail, Ga12, and β -arrestin 1*. The FASEB Journal, 2010. **24**(9): p. 3522-3535.
153. Kilander, M.B., et al., *Disheveled regulates precoupling of heterotrimeric G proteins to Frizzled 6*. The FASEB Journal, 2014. **28**(5): p. 2293-2305.
154. Giulietti, M., et al., *How much do we know about the coupling of G-proteins to serotonin receptors?* Molecular Brain, 2014. **7**(1): p. 1-15.

155. Ulsund, A.H., et al., *Preassociation between the 5-HT7 serotonin receptor and G protein Gs: molecular determinants and association with low potency activation of adenylyl cyclase*. The FASEB Journal, 2019. **33**(3): p. 3870-3886.
156. Hauser, S.R., et al., *The 5-HT7 receptor as a potential target for treating drug and alcohol abuse*. Frontiers in neuroscience, 2015. **8**: p. 448.
157. Zlojutro, M., et al., *Genome-wide association study of theta band event-related oscillations identifies serotonin receptor gene HTR7 influencing risk of alcohol dependence*. American Journal of Medical Genetics Part B: Neuropsychiatric Genetics, 2011. **156**(1): p. 44-58.
158. García-Nafría, J. and C.G. Tate, *Structure determination of GPCRs: cryo-EM compared with X-ray crystallography*. Biochemical Society Transactions, 2021. **49**(5): p. 2345-2355.
159. Mafi, A., S.-K. Kim, and W.A. Goddard III, *The mechanism for ligand activation of the GPCR–G protein complex*. Proceedings of the National Academy of Sciences, 2022. **119**(18): p. e2110085119.
160. Ayoub, M.A., A. Al-Senaidy, and J.-P. Pin, *Receptor-G protein interaction studied by bioluminescence resonance energy transfer: lessons from protease-activated receptor 1*. Frontiers in endocrinology, 2012. **3**: p. 82.
161. Jang, S., et al., *Evolution of the Kondo lattice electronic structure above the transport coherence temperature*. Proceedings of the National Academy of Sciences, 2020. **117**(38): p. 23467-23476.
162. Anderson, S.D., et al., *Modeling Angiotensin II-mediated activation of the Angiotensin II Type 1 Receptor*. The FASEB Journal, 2018. **32**: p. 555.16-555.16.
163. Huang, S., et al., *GPCRs steer Gi and Gs selectivity via TM5-TM6 switches as revealed by structures of serotonin receptors*. Molecular Cell, 2022.
164. Kooistra, A.J., et al., *GPCRdb in 2021: integrating GPCR sequence, structure and function*. Nucleic Acids Research, 2021. **49**(D1): p. D335-D343.
165. Ballante, F., et al., *Structure-Based Virtual Screening for Ligands of G Protein–Coupled Receptors: What Can Molecular Docking Do for You?* Pharmacological Reviews, 2021. **73**(4): p. 527-565.
166. Bender, B.J., B. Marlow, and J. Meiler, *Improving homology modeling from low-sequence identity templates in Rosetta: A case study in GPCRs*. PLoS computational biology, 2020. **16**(10): p. e1007597.
167. Di Pizio, A., et al., *Ligand binding modes from low resolution GPCR models and mutagenesis: chicken bitter taste receptor as a test-case*. Scientific reports, 2017. **7**(1): p. 1-11.
168. Lodh, A., K. Thool, and I. Samajdar, *X-ray diffraction for the determination of residual stress of crystalline material: An overview*. Transactions of the Indian Institute of Metals, 2022. **75**(4): p. 983-995.
169. Rawson, S., et al., *The changing landscape of membrane protein structural biology through developments in electron microscopy*. Molecular membrane biology, 2016. **33**(1-2): p. 12-22.
170. Hu, Y., et al., *NMR-based methods for protein analysis*. Analytical chemistry, 2021. **93**(4): p. 1866-1879.
171. Shi, Y., *A glimpse of structural biology through X-ray crystallography*. Cell, 2014. **159**(5): p. 995-1014.
172. Baase, W.A., et al., *Lessons from the lysozyme of phage T4*. Protein science, 2010. **19**(4): p. 631-641.
173. Walz, T. and N. Grigorieff, *Electron crystallography of two-dimensional crystals of membrane proteins*. Journal of structural biology, 1998. **121**(2): p. 142-161.
174. Blakeley, M.P., et al., *Neutron crystallography: opportunities, challenges, and limitations*. Current opinion in structural biology, 2008. **18**(5): p. 593-600.
175. Krieger, E., S.B. Nabuurs, and G. Vriend, *Homology modeling*. Structural bioinformatics, 2003. **44**: p. 509-523.

176. Brown, H.P., *Homology-based Structural Prediction of the Binding Interface Between the Tick-Borne Encephalitis Virus Restriction Factor TRIM79 and the Flavivirus Non-structural 5 Protein*, 2016, University of Toledo.
177. Richardson, J.S., *The anatomy and taxonomy of protein structure*. Advances in protein chemistry, 1981. **34**: p. 167-339.
178. Chothia, C. and A.M. Lesk, *The relation between the divergence of sequence and structure in proteins*. The EMBO journal, 1986. **5**(4): p. 823-826.
179. Zhang, C. and C. DeLisi, *Estimating the number of protein folds*. Journal of molecular biology, 1998. **284**(5): p. 1301-1305.
180. *blast* Available from: <https://blast.ncbi.nlm.nih.gov/Blast.cgi?PAGE=Proteins>.
181. Altschul, S.F., et al., *Basic local alignment search tool*. Journal of molecular biology, 1990. **215**(3): p. 403-410.
182. Altschul, S.F., et al., *Gapped BLAST and PSI-BLAST: a new generation of protein database search programs*. Nucleic Acids Research, 1997. **25**(17): p. 3389-3402.
183. *uniprot*. Available from: <https://www.uniprot.org/blast>.
184. Pundir, S., et al., *UniProt tools*. Current protocols in bioinformatics, 2016. **53**(1): p. 1.29. 1-1.29. 15.
185. *gpcrdb*. Available from: <https://gpcrdb.org/similaritysearch/referenceselection>.
186. Munk, C., et al., *GPCRdb: the G protein-coupled receptor database—an introduction*. British journal of pharmacology, 2016. **173**(14): p. 2195-2207.
187. *ncbi*. Available from: <https://www.ebi.ac.uk/Tools/sss/ncbiblast/nucleotide.html>.
188. Johnson, M., et al., *NCBI BLAST: a better web interface*. Nucleic Acids Research, 2008. **36**(suppl_2): p. W5-W9.
189. Chung, S.Y. and S. Subbiah. *How similar must a template protein be for homology modeling by side-chain packing methods*. in *Pac Symp Biocomput*. 1996. Citeseer.
190. Lushington, G.H., *Comparative modeling of proteins*. Molecular Modeling of Proteins, 2015: p. 309-330.
191. Isberg, V., et al., *GPCRdb: an information system for G protein-coupled receptors*. Nucleic Acids Research, 2016. **44**(D1): p. D356-D364.
192. Isberg, V., et al., *GPCRDB: an information system for G protein-coupled receptors*. Nucleic Acids Research, 2014. **42**(D1): p. D422-D425.
193. Cock, P.J., et al., *Biopython: freely available Python tools for computational molecular biology and bioinformatics*. Bioinformatics, 2009. **25**(11): p. 1422-1423.
194. Fidom, K., et al., *A new crystal structure fragment-based pharmacophore method for G protein-coupled receptors*. Methods, 2015. **71**: p. 104-112.
195. Pándy-Szekeres, G., et al., *The G protein database, GproteinDb*. Nucleic Acids Research, 2022. **50**(D1): p. D518-D525.
196. PDB. *PDB*. 2022; Available from: <https://www.rcsb.org/structure/7XTC>.
197. Schrodinger, *Maestro Schrodinger*, in *Schrodinger2021-3*, Maestro, Schrödinger LLC. New York, NY.
198. Lushington, G.H., *Comparative modeling of proteins*. Molecular Modeling of Proteins, 2008: p. 199-212.
199. Sternberg, M.J., *Protein structure prediction: A practical approach: a practical approach* 1996: Oxford University Press, USA.
200. Sutcliffe, M.J., et al., *Knowledge based modelling of homologous proteins, Part I: Three-dimensional frameworks derived from the simultaneous superposition of multiple structures*. Protein Engineering, Design and Selection, 1987. **1**(5): p. 377-384.
201. Sgro, J.-Y., *MODELLER-I-Introduction*. 2017.
202. Webb, B. and A. Sali, *Comparative protein structure modeling using MODELLER*. Current protocols in bioinformatics, 2016. **54**(1): p. 5.6. 1-5.6. 37.

203. Madhavi Sastry, G., et al., *Protein and ligand preparation: parameters, protocols, and influence on virtual screening enrichments*. Journal of Computer-Aided Molecular Design, 2013. **27**: p. 221-234.
204. Jacobson, M.P., et al., *A hierarchical approach to all-atom protein loop prediction*. Proteins: Structure, Function, and Bioinformatics, 2004. **55**(2): p. 351-367.
205. Laskowski, R.A., et al., *PROCHECK: a program to check the stereochemical quality of protein structures*. Journal of applied crystallography, 1993. **26**(2): p. 283-291.
206. Vriend, G., *WHAT IF: a molecular modeling and drug design program*. Journal of molecular graphics, 1990. **8**(1): p. 52-56.
207. Wiederstein, M. and M.J. Sippl, *ProSA-web: interactive web service for the recognition of errors in three-dimensional structures of proteins*. Nucleic Acids Research, 2007. **35**(suppl_2): p. W407-W410.
208. Benkert, P., M. Künzli, and T. Schwede, *QMEAN server for protein model quality estimation*. Nucleic Acids Research, 2009. **37**(suppl_2): p. W510-W514.
209. Madhavi Sastry, G., et al., *Protein and ligand preparation: parameters, protocols, and influence on virtual screening enrichments*. Journal of Computer-Aided Molecular Design, 2013. **27**(3): p. 221-234.
210. Greenwood, J.R., et al., *Towards the comprehensive, rapid, and accurate prediction of the favorable tautomeric states of drug-like molecules in aqueous solution*. Journal of Computer-Aided Molecular Design, 2010. **24**(6): p. 591-604.
211. Lu, C., et al., *OPLS4: Improving force field accuracy on challenging regimes of chemical space*. Journal of chemical theory and computation, 2021. **17**(7): p. 4291-4300.
212. Popova, E., B. Okrugin, and I. Neelov, *Molecular dynamics simulation of interaction of short lysine brush and oppositely charged Semax peptides*. Natural Science, 2016. **8**(12): p. 499-510.
213. Rahman, A. and F.H. Stillinger, *Molecular dynamics study of liquid water*. The Journal of Chemical Physics, 1971. **55**(7): p. 3336-3359.
214. Adcock, S.A. and J.A. McCammon, *Molecular dynamics: survey of methods for simulating the activity of proteins*. Chemical reviews, 2006. **106**(5): p. 1589-1615.
215. Metropolis, N., et al., *Equation of state calculations by fast computing machines*. The Journal of Chemical Physics, 1953. **21**(6): p. 1087-1092.
216. Alder, B.J. and T.E. Wainwright, *Studies in molecular dynamics. I. General method*. The Journal of Chemical Physics, 1959. **31**(2): p. 459-466.
217. Verlet, L., *Computer" experiments" on classical fluids. I. Thermodynamical properties of Lennard-Jones molecules*. Physical Review, 1967. **159**(1): p. 98.
218. Gibson, J., et al., *Dynamics of radiation damage*. Physical Review, 1960. **120**(4): p. 1229.
219. Verlet, L., *Computer" experiments" on classical fluids. II. Equilibrium correlation functions*. Physical Review, 1968. **165**(1): p. 201.
220. Tildesley, D.J. and M.P. Allen, *Computer simulation of liquids* 1987: Clarendon Oxford.
221. Ryckaert, J.-P. and A. Bellemans, *Molecular dynamics of liquid n-butane near its boiling point*. Chemical Physics Letters, 1975. **30**(1): p. 123-125.
222. McCammon, J.A., B.R. Gelin, and M. Karplus, *Dynamics of folded proteins*. Nature, 1977. **267**(5612): p. 585-590.
223. Karplus, M. and J.A. McCammon, *Molecular dynamics simulations of biomolecules*. Nature structural biology, 2002. **9**(9): p. 646-652.
224. Zara, Z., et al., *Surface Interaction of Ionic Liquids: Stabilization of Polyethylene Terephthalate-Degrading Enzymes in Solution*. Molecules, 2022. **27**(1): p. 119.
225. Nicoli, A., et al., *Modeling the Orthosteric Binding Site of the G Protein-Coupled Odorant Receptor OR5K1*. bioRxiv, 2022: p. 2022.06. 01.494157.
226. Zhuravlev, P.I. and G.A. Papoian, *Protein functional landscapes, dynamics, allostery: a tortuous path towards a universal theoretical framework*. Quarterly reviews of biophysics, 2010. **43**(3): p. 295-332.

227. Lindahl, E., *Molecular dynamics simulations*. Molecular Modeling of Proteins, 2015: p. 3-26.
228. Guvench, O. and A.D. MacKerell, *Comparison of protein force fields for molecular dynamics simulations*. Molecular Modeling of Proteins, 2008: p. 63-88.
229. Oostenbrink, C., et al., *A biomolecular force field based on the free enthalpy of hydration and solvation: the GROMOS force-field parameter sets 53A5 and 53A6*. Journal of computational chemistry, 2004. **25**(13): p. 1656-1676.
230. Jorgensen, W.L., D.S. Maxwell, and J. Tirado-Rives, *Development and testing of the OPLS all-atom force field on conformational energetics and properties of organic liquids*. Journal of the American Chemical Society, 1996. **118**(45): p. 11225-11236.
231. MacKerell Jr, A.D., et al., *All-atom empirical potential for molecular modeling and dynamics studies of proteins*. The Journal of Physical Chemistry B, 1998. **102**(18): p. 3586-3616.
232. Mackerell Jr, A.D., M. Feig, and C.L. Brooks III, *Extending the treatment of backbone energetics in protein force fields: Limitations of gas-phase quantum mechanics in reproducing protein conformational distributions in molecular dynamics simulations*. Journal of computational chemistry, 2004. **25**(11): p. 1400-1415.
233. Cornell, W.D., et al., *A second generation force field for the simulation of proteins, nucleic acids, and organic molecules*. Journal of the American Chemical Society, 1995. **117**(19): p. 5179-5197.
234. Duan, Y., et al., *A point-charge force field for molecular mechanics simulations of proteins based on condensed-phase quantum mechanical calculations*. Journal of computational chemistry, 2003. **24**(16): p. 1999-2012.
235. Lindorff-Larsen, K., et al., *Improved side-chain torsion potentials for the Amber ff99SB protein force field*. Proteins: Structure, Function, and Bioinformatics, 2010. **78**(8): p. 1950-1958.
236. Van Gunsteren, W.F. and H.J. Berendsen, *A leap-frog algorithm for stochastic dynamics*. Molecular Simulation, 1988. **1**(3): p. 173-185.
237. Swope, W.C., et al., *A computer simulation method for the calculation of equilibrium constants for the formation of physical clusters of molecules: Application to small water clusters*. The Journal of Chemical Physics, 1982. **76**(1): p. 637-649.
238. Leach, A.R., *Molecular modelling: principles and applications* 2001: Pearson education.
239. Allwright, J., *Conjugate gradient versus steepest descent*. Journal of Optimization Theory and Applications, 1976. **20**: p. 129-134.
240. McCammon, J.A. and S.C. Harvey, *Dynamics of proteins and nucleic acids* 1988: Cambridge University Press.
241. Joo, S., et al., *Structural insight into molecular mechanism of poly (ethylene terephthalate) degradation*. Nature communications, 2018. **9**(1): p. 382.
242. Pronk, S., et al., *GROMACS 4.5: a high-throughput and highly parallel open source molecular simulation toolkit*. Bioinformatics, 2013. **29**(7): p. 845-854.
243. Martínez, L., et al., *PACKMOL: A package for building initial configurations for molecular dynamics simulations*. Journal of computational chemistry, 2009. **30**(13): p. 2157-2164.
244. Dickson, C.J., et al., *Lipid14: the amber lipid force field*. Journal of chemical theory and computation, 2014. **10**(2): p. 865-879.
245. Sprenger, K., V.W. Jaeger, and J. Pfaendtner, *The general AMBER force field (GAFF) can accurately predict thermodynamic and transport properties of many ionic liquids*. The Journal of Physical Chemistry B, 2015. **119**(18): p. 5882-5895.
246. Shaposhnikova, A., et al., *Stabilization of Haloalkane Dehalogenase Structure by Interfacial Interaction with Ionic Liquids*. Crystals, 2021. **11**(9): p. 1052.
247. D'Oronzo, E., et al., *Activation/inactivation role of ionic liquids on formate dehydrogenase from Pseudomonas sp. 101 and its mutated thermostable form*. ChemCatChem, 2018. **10**(15): p. 3247-3259.

248. Ryckaert, J.-P., G. Ciccotti, and H.J. Berendsen, *Numerical integration of the cartesian equations of motion of a system with constraints: molecular dynamics of n-alkanes*. Journal of computational physics, 1977. **23**(3): p. 327-341.
249. Essmann, U., et al., *A smooth particle mesh Ewald method*. The Journal of Chemical Physics, 1995. **103**(19): p. 8577-8593.
250. Berendsen, H.J., D. van der Spoel, and R. van Drunen, *GROMACS: A message-passing parallel molecular dynamics implementation*. Computer physics communications, 1995. **91**(1-3): p. 43-56.
251. Van Der Spoel, D., et al., *GROMACS: fast, flexible, and free*. Journal of computational chemistry, 2005. **26**(16): p. 1701-1718.
252. Humphrey, W., A. Dalke, and K. Schulten, *VMD: visual molecular dynamics*. Journal of molecular graphics, 1996. **14**(1): p. 33-38.
253. Turner, P., *XMGRACE, Version 5.1. 19*. Center for Coastal and Land-Margin Research, Oregon Graduate Institute of Science and Technology, Beaverton, OR, 2005. **2**.
254. Mayol, E., et al., *HomolWat: a web server tool to incorporate 'homologous' water molecules into GPCR structures*. Nucleic Acids Research, 2020. **48**(W1): p. W54-W59.
255. Olivella García, M., *HomolWat: a web server tool to incorporate «homologous» water molecules into GPCR structures*. Nucleic Acids Research, 2020, vol. 48, núm. 1, p. 54-59, 2020.
256. Rodríguez-Espigares, I., et al., *GPCRmd uncovers the dynamics of the 3D-GPCRome*. Nature Methods, 2020. **17**(8): p. 777-787.
257. Lomize, M.A., et al., *OPM: orientations of proteins in membranes database*. Bioinformatics, 2006. **22**(5): p. 623-625.
258. Doerr, S., et al., *HTMD: high-throughput molecular dynamics for molecular discovery*. Journal of chemical theory and computation, 2016. **12**(4): p. 1845-1852.
259. Huang, J. and A.D. MacKerell Jr, *CHARMM36 all-atom additive protein force field: Validation based on comparison to NMR data*. Journal of computational chemistry, 2013. **34**(25): p. 2135-2145.
260. Huang, J., et al., *CHARMM36m: an improved force field for folded and intrinsically disordered proteins*. Nature Methods, 2017. **14**(1): p. 71-73.
261. Vanommeslaeghe, K. and A.D. MacKerell Jr, *Automation of the CHARMM General Force Field (CGenFF) I: bond perception and atom typing*. Journal of chemical information and modeling, 2012. **52**(12): p. 3144-3154.
262. Vanommeslaeghe, K., E.P. Raman, and A.D. MacKerell Jr, *Automation of the CHARMM General Force Field (CGenFF) II: assignment of bonded parameters and partial atomic charges*. Journal of chemical information and modeling, 2012. **52**(12): p. 3155-3168.
263. Harvey, M.J., G. Giupponi, and G.D. Fabritiis, *ACEMD: accelerating biomolecular dynamics in the microsecond time scale*. Journal of chemical theory and computation, 2009. **5**(6): p. 1632-1639.
264. Eastman, P., et al., *OpenMM 7: Rapid development of high performance algorithms for molecular dynamics*. PLoS computational biology, 2017. **13**(7): p. e1005659.
265. Tan, Y., et al., *Structural insights into the ligand binding and Gi coupling of serotonin receptor 5-HT5A*. Cell Discovery, 2022. **8**(1): p. 50.
266. Hauser, A.S., et al., *Common coupling map advances GPCR-G protein selectivity*. Elife, 2022. **11**: p. e74107.
267. Naranjo, A.N., et al., *Conserved disulfide bond is not essential for the adenosine A2A receptor: Extracellular cysteines influence receptor distribution within the cell and ligand-binding recognition*. Biochimica Et Biophysica Acta (BBA)-Biomembranes, 2015. **1848**(2): p. 603-614.
268. Xu, P., et al., *Structural insights into the lipid and ligand regulation of serotonin receptors*. Nature, 2021. **592**(7854): p. 469-473.

PAPER 1

Surface Interaction of Ionic Liquids: Stabilization of Polyethylene Terephthalate-Degrading Enzymes in Solution

Zeenat Zara, Deepti Mishra, Saurabh Kumar Pandey, Eva Csefalvay, Fatemeh Fadaei, Babak Minofar, and David Reha

Article

Surface Interaction of Ionic Liquids: Stabilization of Polyethylene Terephthalate-Degrading Enzymes in Solution

Zeenat Zara^{1,2}, Deepti Mishra², Saurabh Kumar Pandey^{2,3} , Eva Csefalvay², Fatemeh Fadaei^{1,2}, Babak Minofar^{2,*} and David Řeha^{2,*} 

¹ Faculty of Science, University of South Bohemia in Ceske Budejovice, Branišovská 1760, 370 05 České Budějovice, Czech Republic; zeenaz00@prf.jcu.cz (Z.Z.); fadaei@nh.cas.cz (F.F.)

² Laboratory of Structural Biology and Bioinformatics, Institute of Microbiology of the Czech Academy of Sciences, Zamek 136, 373 33 Nove Hradky, Czech Republic; deepti.bioinfo@gmail.com (D.M.); saurabhkpandey@gmail.com (S.K.P.); csefalvay@nh.cas.cz (E.C.)

³ Institute of Photonics and Electronics of the Czech Academy of Sciences, Chaberská 1014/57, 182 00 Praha 8-Kobylisy, Czech Republic

* Correspondence: minofar@nh.cas.cz (B.M.); reha@nh.cas.cz (D.Ř.)

Abstract: The effect of aqueous solutions of selected ionic liquids solutions on *Ideonella sakaiensis* PETase with bis(2-hydroxyethyl) terephthalate (BHET) substrate were studied by means of molecular dynamics simulations in order to identify the possible effect of ionic liquids on the structure and dynamics of enzymatic Polyethylene terephthalate (PET) hydrolysis. The use of specific ionic liquids can potentially enhance the enzymatic hydrolyses of PET where these ionic liquids are known to partially dissolve PET. The aqueous solution of cholinium phosphate were found to have the smallest effect of the structure of PETase, and its interaction with (BHET) as substrate was comparable to that with the pure water. Thus, the cholinium phosphate was identified as possible candidate as ionic liquid co-solvent to study the enzymatic hydrolyses of PET.

Keywords: molecular dynamics (MD) simulations; PETase; BHET; PET; ionic liquids (ILs)



Citation: Zara, Z.; Mishra, D.; Pandey, S.K.; Csefalvay, E.; Fadaei, F.; Minofar, B.; Řeha, D. Surface Interaction of Ionic Liquids: Stabilization of Polyethylene Terephthalate-Degrading Enzymes in Solution. *Molecules* **2022**, *27*, 119. <https://doi.org/10.3390/molecules27010119>

Academic Editor: Angelo Nacci

Received: 30 November 2021

Accepted: 22 December 2021

Published: 26 December 2021

Publisher's Note: MDPI stays neutral with regard to jurisdictional claims in published maps and institutional affiliations.



Copyright: © 2021 by the authors. Licensee MDPI, Basel, Switzerland. This article is an open access article distributed under the terms and conditions of the Creative Commons Attribution (CC BY) license (<https://creativecommons.org/licenses/by/4.0/>).

1. Introduction

Due to the major concern on the global environmental crisis, research on how to recycle synthetic polymers has been promoted extensively for the last two decades. Among various synthetic polymers, the polyethylene terephthalate (PET), with its simple synthesis, robustness, and durability, led to a drastic increase in its industrial production; therefore, by the year 2020, production has reached more than 70 million metric tons [1–3]. Different chemical degradation approaches, e.g., hydrolysis, ammonolysis, aminolysis, methanolysis, and glycolysis have been introduced to recycle and remove the plastics. Nevertheless, these techniques need high temperatures and produce other environmental pollutants as byproducts.

The high solubility of PET in solvents, as the first step of recycling, is difficult; therefore, finding proper solvents for recycling and degrading is challenging. There are few solvents that were commonly used for PET solubilization, such as dichloroacetic acid [4,5] trifluoroacetic acid [6], phenol/1,1,2,2-tetrachloroethane solution [7], and chlorophenol [8]. Nonetheless, these solvents are not only costly but also toxic; therefore, it is desirable to use pretreated PET to avoid any secondary pollution in the environment.

The hydrophobic nature and crystallinity of PET are two major issues on dissolution and recycling of PET; therefore, finding environmentally friendly solvents is needed. Herein, ionic liquids (ILs) can be used to overcome this problem, as some ILs can partially change the crystalline structure of PET to an amorphous structure [9,10]. Moreover, as an alternative to traditionally used volatile organic compounds, many ionic liquids are environmentally friendly and some of them can enhance the stability and catalytic activity of certain enzymes [11,12]. ILs in general have unique features, such as strong solvent

power for dissolution of organic and inorganic compounds, thermal stability, non-volatility, electrochemical stability, and low flammability [13,14]. Ionic liquids can be mixed with water at various concentrations, forming so-called hydrated ionic liquids, and hence, water and ILs act as co-solvents in the solution [15–21]. At the present time, ionic liquids have attracted enormous research interest due to their specific advantages and variability, which can be achieved by optimization of the choice of cation and anion combinations, influencing thermal stability, non-volatility, and many other properties [22,23]. Ionic liquids can be used for degradation of complex polymers, as was shown for cellulose, which can be utilized by ILs [24,25]. Degradation of PET in the presence of several ILs has been reported experimentally, and the results show that ILs have increased the degradation ability of PET [4,7]. The advantage of using ILs as a co-solvent over conventional catalysts, such as metal acetates, to recycle PET is that the purification of the glycolysis products is simpler. The mechanism of action of ILs is based on the changes of the highly crystalline structure of PET film into an amorphous structure (lost crystalline structure), which can be easily attacked by PETase during catalytic degradation.

One of the methods for disposal of plastic waste is biodegradation of plastic materials by enzymes [26]. Development of these environmentally friendly methods is desirable. In the case of PET, the terephthalic (TPA) moiety present in PET is hydrophobic, which makes it resistant to the bio-degradation process. In view of this, industries are focusing more on synthesizing bio-based—rather than oil-based—polymers. Herein, microorganisms play important roles in the clean-up of pollutants released by humans within the ecosystem. The process of enzymatic hydrolysis of PET films was first reported by Müller et al. (2005). The hydrolytic enzyme was purified from the culture supernatant of *T. fusca* [27]. Recently, the bacterial strain *Ideonella sakaiensis* was discovered and shown to grow on low-crystallinity PET films while using PET as a carbon source [28–33]. The enzyme, known as PETase, showed much higher depolymerization activity against PET films at the mesophilic temperature, unlike thermophilic PET-degrading enzymes tested to date. PETase works with a two-step process of degradation, at the first step, it degrades the PET into Mono-(2-hydroxyethyl) terephthalate (MHET) and then the different enzyme MHETase degrades the MHET into TPA and ethylene glycol [34]. The unique feature of PETase from *Ideonella sakaiensis* is the fact that it degrades PET film at room temperature, unlike other hydrolases, which function only at high temperatures [35,36]. This confirms the unique structural and sequence features of *Ideonella sakaiensis* PETase. Additionally, experiments reveal that *Ideonella sakaiensis* PETase exhibits the highest activity among the other thermophilic PET degrading enzymes [4,37].

Here, we report molecular dynamics (MD) simulations of *Ideonella sakaiensis* PETase with various ionic liquids in order to understand the effect of aqueous solutions of ILs on the structure of PETase and the catalytic/active site of PETase in the presence of ILs. For MD simulations, the wild-type of *Ideonella sakaiensis* PETase with ligand (bis(2-hydroxyethyl) terephthalate (BHET)) have been simulated in pure water and in different concentrations of three different ionic liquids, which were used as a solvent for dissolution of PET.

2. Results and Discussion

2.1. Root Mean Square Deviation (RMSD)

In order to investigate the effect of non-aqueous solvent on the complex structure of *Ideonella sakaiensis* PETase with ligand (BHET), we performed here MD simulations with three different ionic liquids (Figure 1) in three different concentrations (20%, 30%, 40%) by mass.

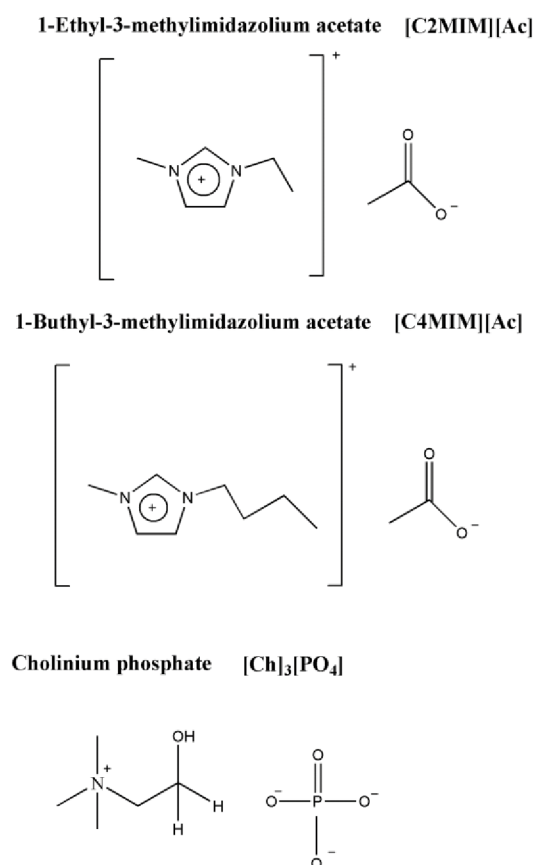


Figure 1. Chemical structures of 1-Ethyl-3-methylimidazolium acetate [C2MIM][Ac], 1-Butyl-3-methylimidazolium acetate [C4MIM][Ac] and Cholinium phosphate [Ch]₃[PO₄].

The comparison of the wild-type *Ideonella sakaiensis* PETase structures in different solvents after 150 ns of MD simulation is shown in Figure 2, where the PETase backbone in different solvents was superimposed.

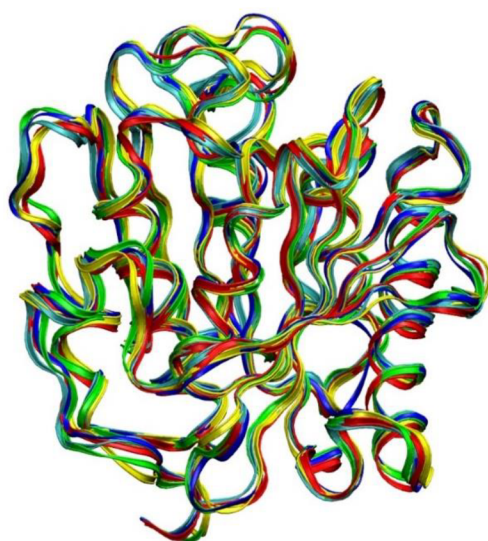


Figure 2. PETase backbone structure is superimposed with different solvents. The wild-type crystal structure is in blue. MD simulation for 150 ns with water as a solvent is in red. Simulation with [Ch]₃[PO₄], [C4MIM][Ac] and [C2MIM][Ac] is represented in yellow, green, and light blue, respectively.

Simulation of the PETase complex with the ligand in water was kept as a control. Calculating the root mean square deviation (RMSD) of proteins permits the quantification of the degree of stability of the enzyme during the MD simulations. Here, in Figure 3 we have shown RMSD of backbone atoms of PETase in three different ionic liquids and in water.

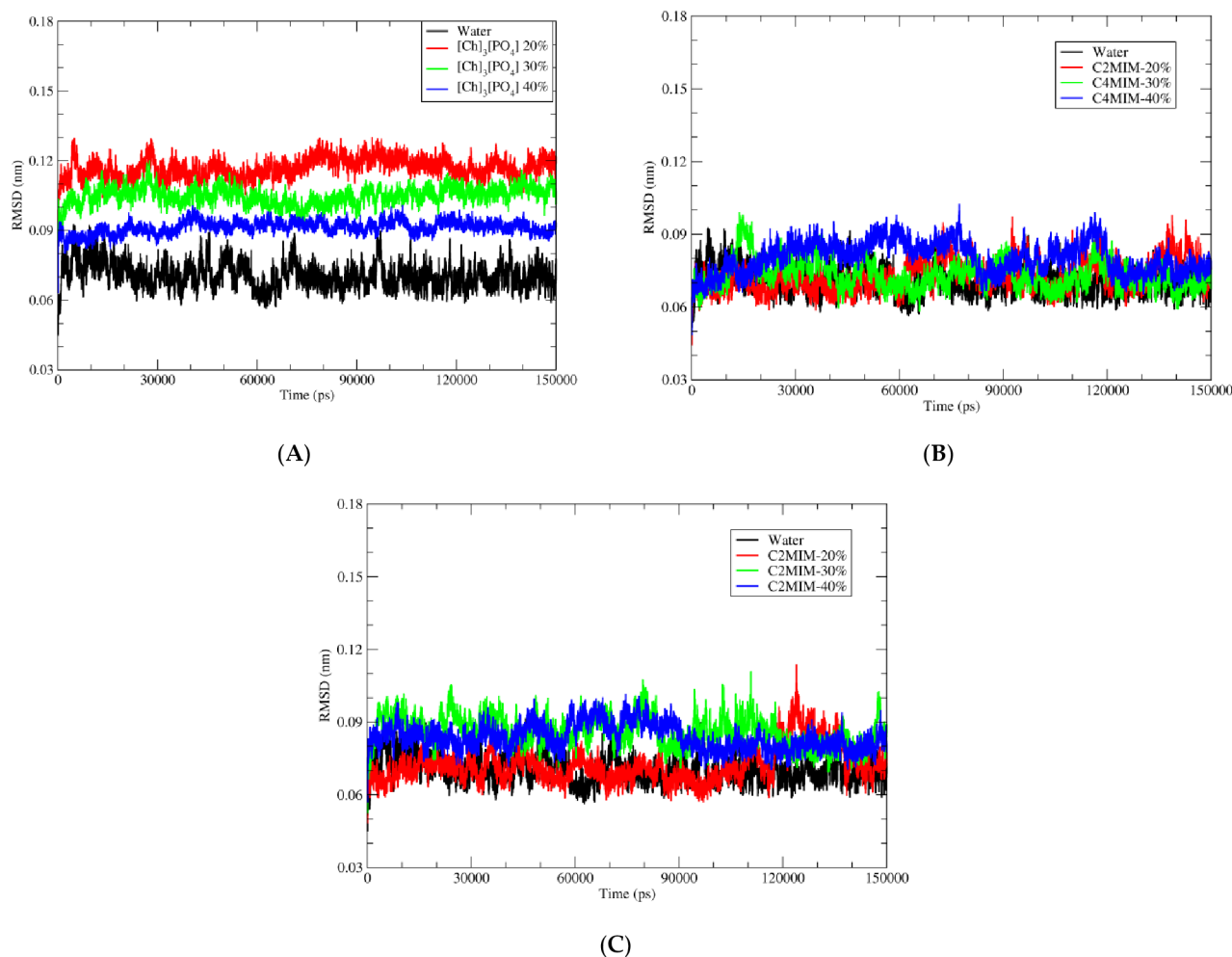


Figure 3. Root mean square deviation (RMSD) of C α atoms of wild type of PETase with water and three different ionic liquids solutions. (A) Pure water in black; 20% of [Ch]₃[PO₄] in red; 30% of [Ch]₃[PO₄] in green and 40% of [Ch]₃[PO₄] in blue. (B) Pure water in black; 20% of [C4MIM][Ac] in red; 30% of [C4MIM][Ac] in green and 40% of [C4MIM][Ac] in blue. (C) Pure water in black; 20% of [C2MIM][Ac] in red; 30% of [C2MIM][Ac] in green and 40% of [C2MIM][Ac] in blue.

As depicted in Figure 3, RMSD values for PETase in water is lower than in ionic liquids during MD simulation of all systems, indicating that PETase structure in water is closer to the crystal structure than the structures in ionic liquids. On the other hand, the fluctuation of RMSD decreases with increased concentration of ILs, indicating more stable structures with less thermal fluctuations. Figure 3A shows the deviation of backbone atoms with respect to the reference structure (PDB code 5XJH) when inserted in water and in [Ch]₃[PO₄] ionic liquid with 3 different percentages: 40%, 30%, and 20%. We observed that the overall structure of PETase is not deviating much from its starting structure which implies that the chosen ionic liquids [Ch]₃[PO₄] would not significantly alter the enzyme structure and it is suitable for further studies on the reaction mechanism of BHET hydrolysis. We further investigate two other ionic liquids, [C4MIM][Ac] and [C2MIM][Ac]. In both [C4MIM][Ac] and [C2MIM][Ac] ionic liquids, we have not observed significant deviation of backbone

atom of PETase with the addition of these ILs. The RMSD graphs for [C4MIM][Ac] and [C2MIM][Ac] is shown in Figure 3B,C, respectively.

2.2. Ligand RMSD

Analysis in the previous section showed that the enzyme structure is quite stable and not deviated much from the crystal structure after immersing into three different ionic liquid solutions. Now, the next main step is to see the reaction site of PETase, where catalytic triad (facilitating the BHET hydrolysis) is present on the active site of the enzyme. The ligand BHET is surrounded by three catalytic amino acids, which will help BHET hydrolysis through SN-2 reaction mechanism. For this purpose, the position of the BHET ligand should be stable during MD simulations in the presence of different solvents. Therefore, we have plotted the RMSD of BHET atoms during the simulation in order to identify the stability of BHET atoms. The RMSD of the ligand, with respect to the PETase, was calculated during the simulation time of 150 ns. Here, as depicted in Figure 4A, the BHET atoms are not deviating much from their starting structure in the presence of $[\text{Ch}]_3[\text{PO}_4]$.

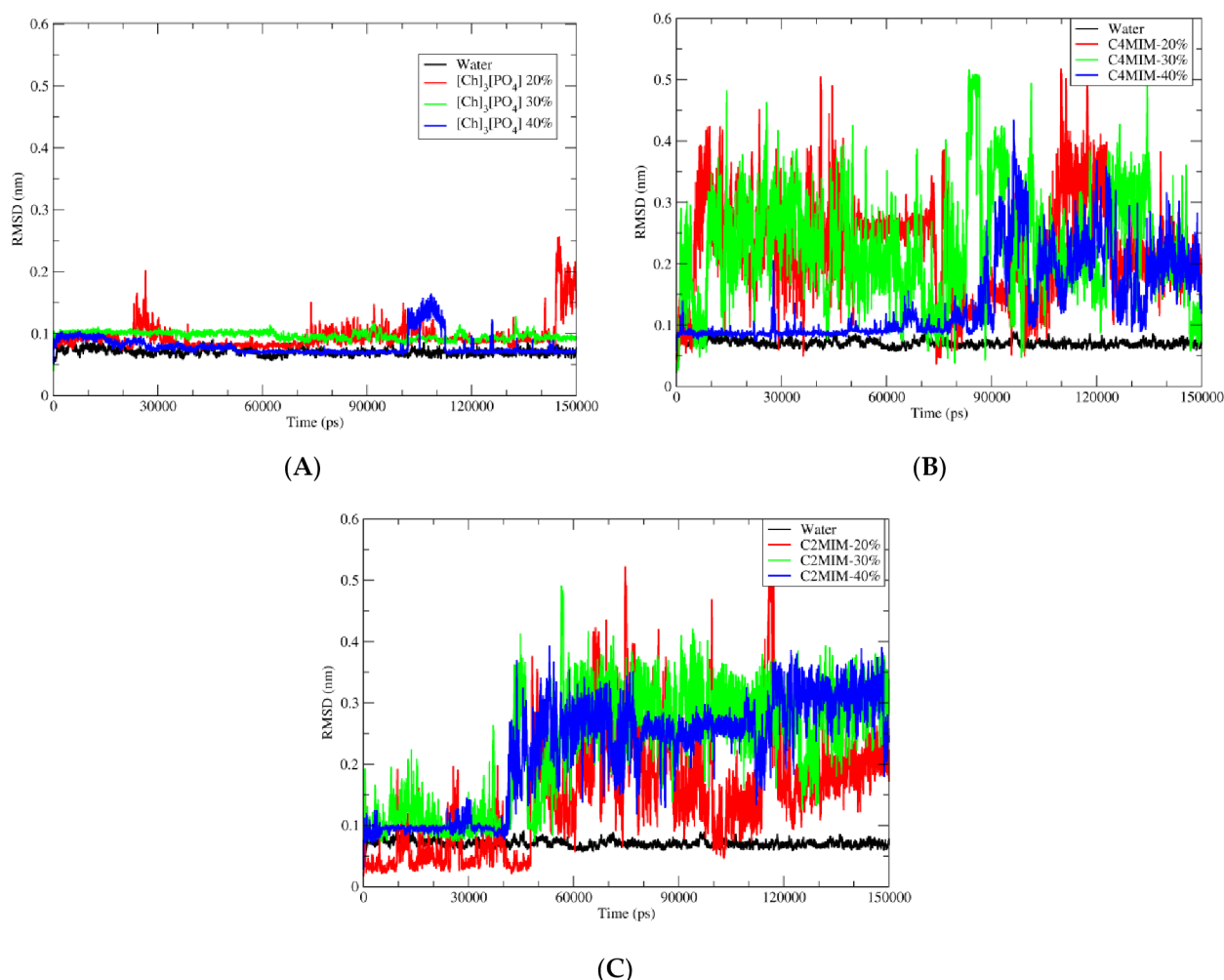


Figure 4. Root mean square deviation (RMSD) of BHET with respect to PETase in water and three different ionic liquids solutions. (A) Pure water in black; 20% of $[\text{Ch}]_3[\text{PO}_4]$ in red; 30% of $[\text{Ch}]_3[\text{PO}_4]$ in green and 40% of $[\text{Ch}]_3[\text{PO}_4]$ in blue. (B) Pure water in black; 20% of [C4MIM][Ac] in red; 30% of [C4MIM][Ac] in green and 40% of [C4MIM][Ac] in blue. (C) Pure water in black; 20% of [C2MIM][Ac] in red; 30% of [C2MIM][Ac] in green and 40% of [C2MIM][Ac] in blue.

As shown in graph Figure 4A, the ligand is quite stable in pure aqueous media and in the presence of $[\text{Ch}]_3[\text{PO}_4]$ ionic liquid. However, the same stability trend has not

been observed in the case of [C4MIM][Ac] or [C2MIM][Ac] ionic liquids, as shown in Figure 4B,C, respectively. A detailed inspection of the trajectory revealed that after 40 ns, the BHET molecule starts moving away from catalytic triad residue ser-131 and the BHET molecule starts bending from the central carbonyl carbon due to non-bonding interaction between two sites of BHET rings. The same trend of instability of BHET was observed for [C4MIM][Ac] after 40 ns of MD simulation, whereas the stabilization in the presence of [Ch]₃[PO₄] and pure water for the entire simulation indicated no significant deviation of the geometry and position of BHET molecule within PETase. Furthermore, when the concentration of ionic liquids decreased to 30% and 20%, the instability of BHET increased for [C2MIM][Ac] and [C4MIM][Ac]. Again, the molecule started to bend from the carbonyl carbon and this might be due to electrostatic interaction between two sites of BHET. The BHET structure was quite stable for the whole simulation time of 150 ns in the presence of [Ch]₃[PO₄] and pure water.

2.3. Root Mean Square Fluctuation (RMSF)

In order to have a deep insight into structural stability, one can analyze the stability of each residue over the simulation time. The flexibility and stability of each residue is investigated by RMSF. As shown in Figure 5, the RMSF values of PETase in 40% [Ch]₃[PO₄] are lower than in water, which is consistent with RMSD fluctuation in Figure 3.

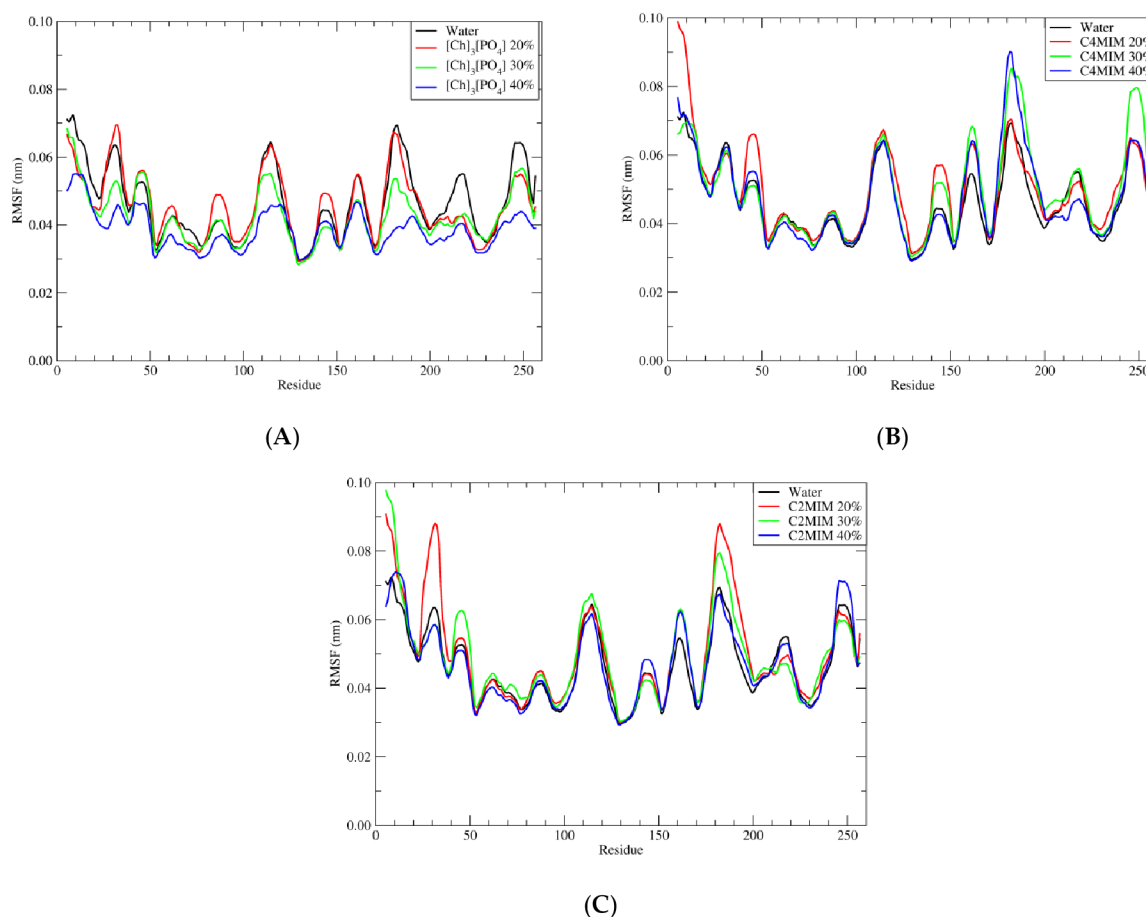


Figure 5. Root mean square fluctuation (RMSF) of wild-type of PETase with water and three different ionic liquids solutions in the presence of ligand BHET. (A) Pure water in black; 20% of [Ch]₃[PO₄] in red; 30% of [Ch]₃[PO₄] in green and 40% of [Ch]₃[PO₄] in blue. (B) Pure water in black; 20% of [C4MIM][Ac] in red; 30% of [C4MIM][Ac] in green and 40% of [C4MIM][Ac] in blue. (C) Pure water in black; 20% of [C2MIM][Ac] in red; 30% of [C2MIM][Ac] in green and 40% of [C2MIM][Ac] in blue.

The residues which are fluctuating more are at residue positions 100–120 and 170–180. Among these two domains, we have found that the residue Asn-183 has the highest value of RMSF and it is the most unstable one. The same residue has the highest RMSF also in the presence of [C4MIM][Ac] and [C2MIM][Ac] ionic liquid.

To understand this further, we performed a detailed inspection of the simulations and found that [Ch]₃[PO₄] with 40% concentration has a strong hydrogen bond interaction between the residue Asn-183 and PO₄³⁻. One hydrogen bond interaction between the hydrogen atom of residue Asn-183 of the PETase enzyme with the oxygen of phosphate group PO₄³⁻ was observed. This hydrogen bond interaction was with the bond distance of 1.8 Å to 3 Å. However, we noticed that it was not stable enough over the simulation. This makes the residue Asn-183 stable relatively when we have [C4MIM][Ac] and [C2MIM][Ac] as solvents. There was no eligible entity in [C4MIM][Ac] and [C2MIM][Ac] to have an interaction with residue Asn183 and, as a result, the residue was unstable in the presence of both [C4MIM][Ac] and [C2MIM][Ac] ionic liquids; therefore, producing the higher root mean square fluctuation value.

2.4. Radius of Gyration

Calculating the radius of gyration of a protein is a measurement of its compactness. Thus, if a protein is stably compact, it will maintain a relatively stable value of R_g over the simulation of time. However, if a protein unfolds during the simulation of time, the R_g value will fluctuate. Therefore, the measurement of the compactness of protein is investigated by the radius of gyration function. The radius of gyration of each simulated system is calculated and compared between simulations in water and simulations in ionic liquid. There were no structural distortions or unfolding of the secondary structure during 150 ns simulations. However, PETase in water possesses a low radius of gyration relatively with simulated ionic liquid systems. As shown in Figure 6, the protein in ionic liquids have a radius of gyration from 1.66 to 1.68 nm, which is larger than in water, where the radius of gyration was around 1.64 nm. This indicates that the protein has a slightly less compact structure in ILs than in water. This can be explained by interactions of the IL's ions with protein instead of the water molecules. The protein radius of gyration in ILs at different concentrations is comparable, except the [Ch]₃[PO₄] at 40%, where R_g is slightly lower at 1.66 compared with 1.67 in [C2MIM][Ac] and [C4MIM][Ac]. This is most likely due to local higher concentration of the [PO₄], which (in comparison to then [CXMIM] and [Ac]) is less likely to disrupt local geometry of the water molecules in the vicinity of the protein (see Hofmeister series [38]).

After analyzing the overall structure of PETase, we focused on the active site of PETase, where BHET ligand binds and is degraded into smaller units through the catalytic reaction. The catalytic triad is present on the protein surface. The triad is composed of Serine 131, Histidine 208, and Aspartic acid 177. We investigated the distance between our ligand (BHET) carbonyl carbon and oxygen of Ser-131. In order to understand the stability of the interaction between ligand and catalytic residue, the distance between the ligand and Ser-131 in the presence of water and all ionic liquids in all three ionic concentrations was calculated over the whole duration of MD simulation. As depicted in Figure 7, the distance between these two residues is stable over the simulation in water and in [Ch]₃[PO₄] as shown in Figure 7A.

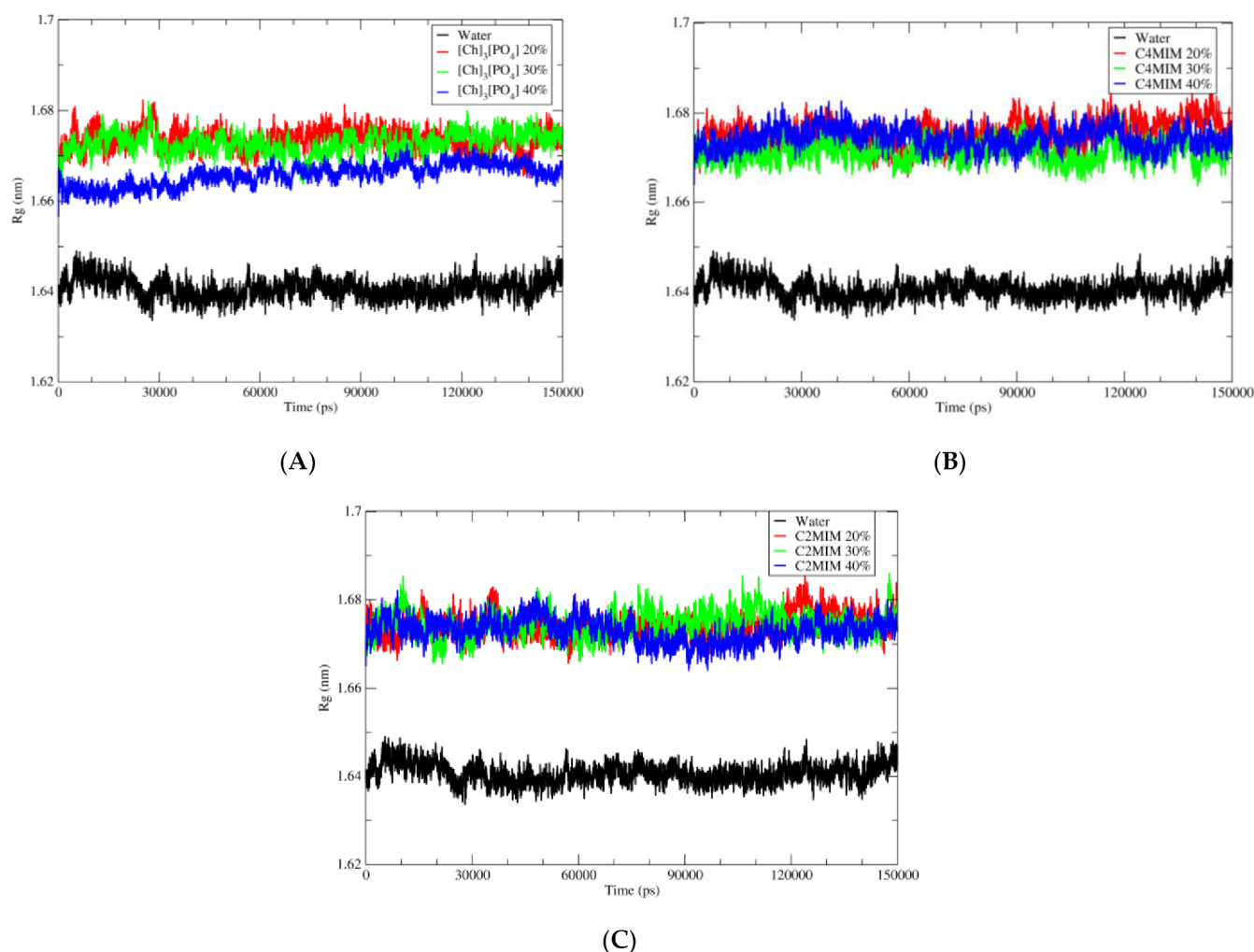


Figure 6. Radius of gyration (Rg) graph of wild-type PETase in complex with BHET ligand in the presence of different solvents. (A) Pure water in black; 20% of $[\text{Ch}_3][\text{PO}_4]$ in red; 30% of $[\text{Ch}_3][\text{PO}_4]$ in green and 40% of $[\text{Ch}_3][\text{PO}_4]$ in blue. (B) Pure water in black; 20% of $[\text{C4MIM}][\text{Ac}]$ in red; 30% of $[\text{C4MIM}][\text{Ac}]$ in green and 40% of $[\text{C4MIM}][\text{Ac}]$ in blue. (C) Pure water in black; 20% of $[\text{C2MIM}][\text{Ac}]$ in red; 30% of $[\text{C2MIM}][\text{Ac}]$ in green and 40% of $[\text{C2MIM}][\text{Ac}]$ in blue.

The black curve shows the distance in the water and the blue one with $[\text{Ch}_3][\text{PO}_4]$ at 40% concentration. This shows the stability of ligand during the simulation; hence the condition that is favorable for the reaction is maintained. Therefore, one can consider $[\text{Ch}_3][\text{PO}_4]$ ionic liquid as a possible medium for BHET hydrolysis. However, in the case of $[\text{C4MIM}][\text{Ac}]$ and $[\text{C2MIM}][\text{Ac}]$, the distance fluctuates significantly during the simulation, which implies the instability of ligand on the active site of PETase. Among the ionic liquids, $[\text{Ch}_3][\text{PO}_4]$ illustrated the best result for maintaining ligand stability at the catalytic site.

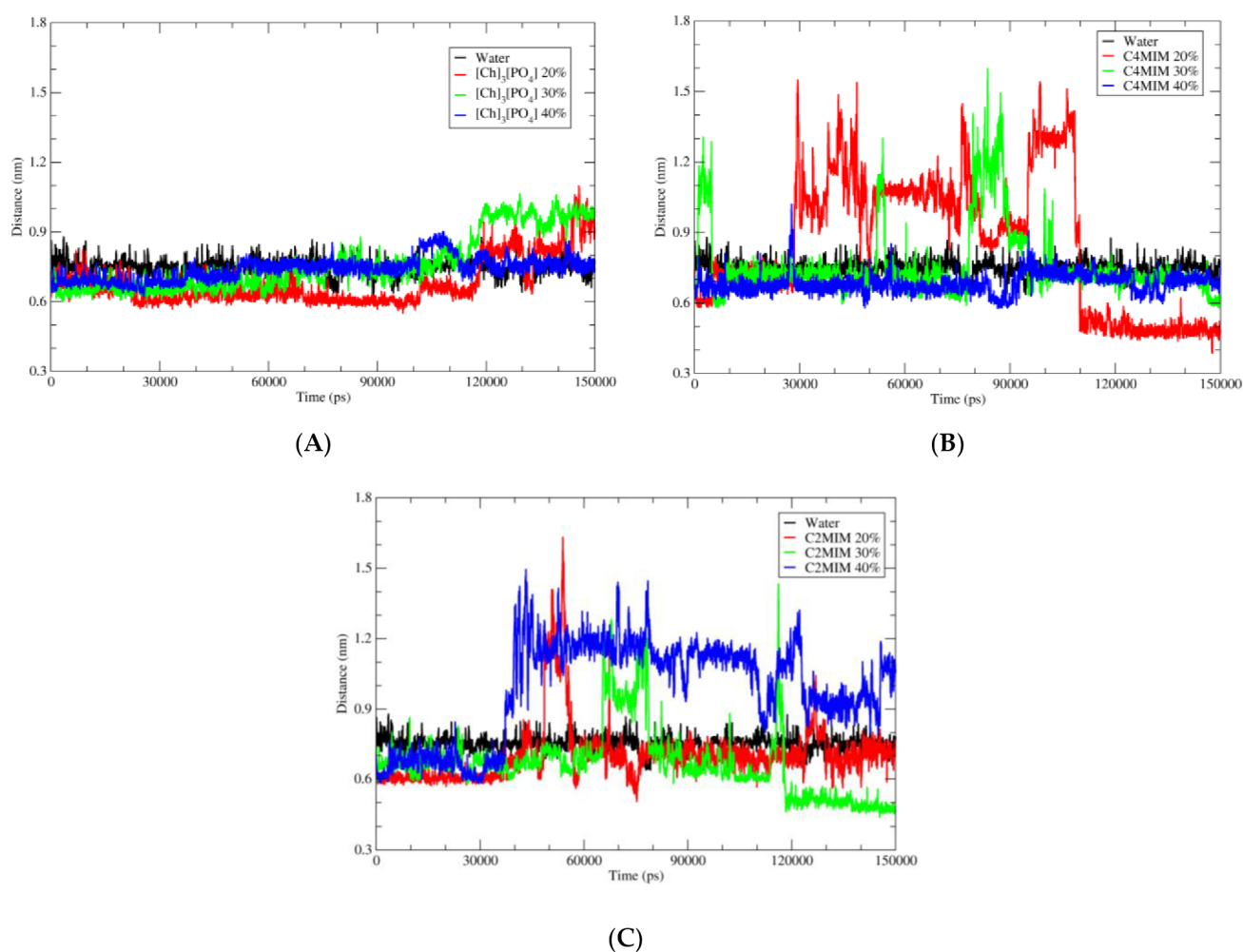


Figure 7. Distance between the C of carbonyl group of BHET with the O of Ser-131 in water and different ionic liquids solutions. (A) Pure water in black; 20% of $[\text{Ch}_3][\text{PO}_4]$ in red; 30% of $[\text{Ch}_3][\text{PO}_4]$ in green and 40% of $[\text{Ch}_3][\text{PO}_4]$ in blue. (B) Pure water in black; 20% of $[\text{C4MIM}][\text{Ac}]$ in red; 30% of $[\text{C4MIM}][\text{Ac}]$ in green and 40% of $[\text{C4MIM}][\text{Ac}]$ in blue. (C) Pure water in black; 20% of $[\text{C2MIM}][\text{Ac}]$ in red; 30% of $[\text{C2MIM}][\text{Ac}]$ in green and 40% of $[\text{C2MIM}][\text{Ac}]$ in blue.

2.5. Hydrogen Bonds and Hydrophobic Interaction

The solubility and stability of a protein are also dependent on its solvent interaction. The solvent interaction can stabilize or destabilize the amino acids of the protein. Moreover, the hydrogen bond interaction plays an important role in the overall stability of the protein structure. Thus, the number of H bonds with the protein demonstrates its structural stability.

As shown in Figure 8, the number of H bonds of water molecules, cholinium, and phosphate ions with protein residues were calculated in different ionic liquid concentrations. Here, 40%, 30%, and 20% concentrations of each system were calculated by adding the solvent values for a separate system.

Figure 8 illustrated that, when pure water was replaced with aqueous solutions of ionic liquids, the number of hydrogen bonds decreased, probably due to the bigger size of cation and anions. Furthermore, the number of H bonds in the 20% solution is higher than the one in the 40% solution. However, in the case of water- $[\text{C4MIM}][\text{Ac}]$ and water- $[\text{C2MIM}][\text{Ac}]$ (Supplementary data Figure S1A,B), the $[\text{C4MIM}]$ and $[\text{C2MIM}]$ cations do not play important role for H bonding with the PETase, as they do not have groups that promote H bonds. However, there is no significant change in H bonds for different concentrations of $[\text{C4MIM}][\text{Ac}]$ and $[\text{C2MIM}][\text{Ac}]$.

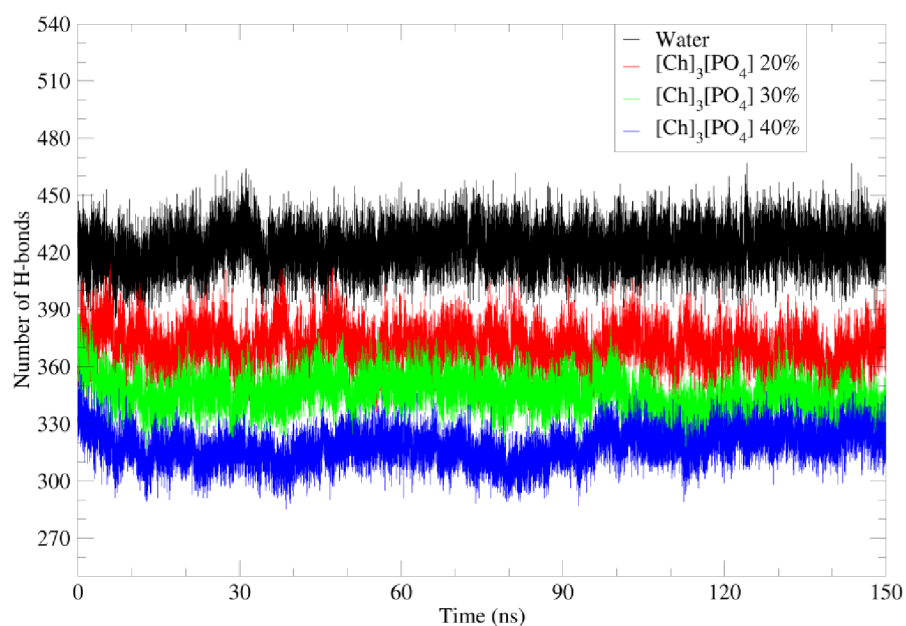


Figure 8. Number of hydrogen bonds of water and cholinium phosphate with amino acids of PETase in 40%, 30%, and 20% IL solutions. Pure water in black; 20% of [Ch]₃[PO₄] in red; 30% of [Ch]₃[PO₄] in green and 40% of [Ch]₃[PO₄] in blue.

Furthermore, the hydrophobic amino acids are also located at the surface of PETase, which are not solvated by water molecules. Therefore, they interact more with the hydrophobic part of [C4MIM], [C2MIM], and cholinium cations. The hydrophobic interaction took place between hydrophobic amino acids, such as A123, F26, P145, A197, P9, A11, F232, and F162, and methyl groups of cholinium, hydrocarbon (-CH₂-CH₃), or the imidazolium ring of [C4MIM] and [C2MIM] cation. Hence, cholinium cations (Figure 9), [C4MIM] and [C2MIM] (Supplementary data Figure S2A,B) are mainly distributed over the hydrophobic surface of PETase.

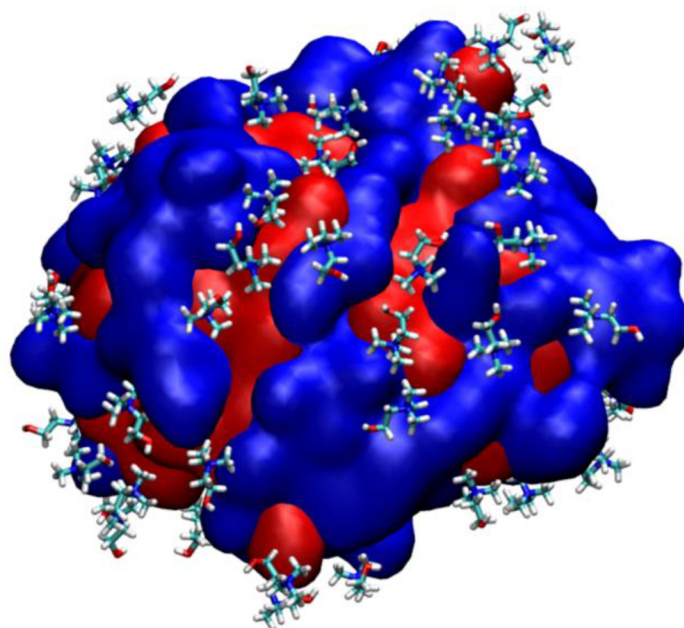


Figure 9. The interaction of cholinium cations with hydrophobic surface of PETase. The hydrophobic surface is colored in red and the hydrophilic surface is colored in blue.

2.6. Radial Distribution Function

The radial distribution function (RDF)—the probability of finding a particle from a reference particle over distance—is a powerful tool in MD simulations for understanding how the $(\text{CH}_3)_3\text{N}^+$ group of cholinium cation, the ring of imidazolium [C4MIM], and [C2MIM] are distributed around the side chain of the hydrophobic surface amino acids.

The RDF of the $(\text{CH}_3)_3\text{N}^+$ group of cholinium cation around the side chain of hydrophobic amino acids at the protein surface (such as A_123, F_26, P_145, A_197, and P_9), the RDF of the ring of [C4MIM] around the side chain of hydrophobic amino acids at the protein surface (such as A_123, A1_1, F_232, P_9, and F_162), and the RDF of the ring of [C2MIM] around side chain of hydrophobic amino acids at the protein surface (such as A_123, A_11, F_232, P_9, and F_162), were calculated, and the results are shown in Figure 10, Supplementary data Figure S3, and Supplementary data Figure S4, respectively.

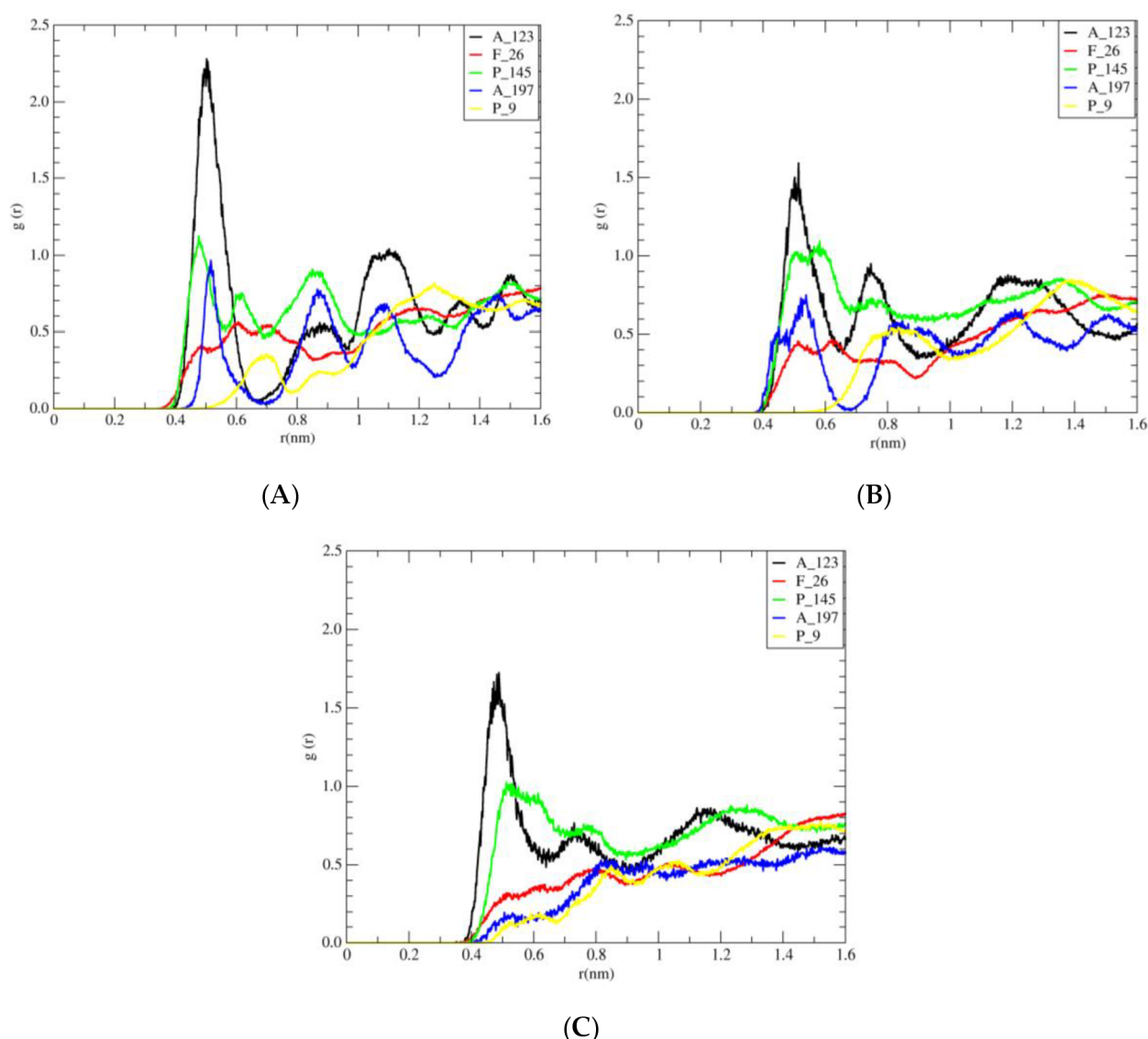


Figure 10. Radial distribution functions (RDFs) for atoms with (A) side chain of amino acids A_123 (in black), F_26 (in red), P_145 (in green), A_197 (in blue), and P_9 (in yellow) of the hydrophobic surface and nitrogen of cholinium cations in 40% of $[\text{Ch}]_3[\text{PO}_4]$. (B) Side chain of amino acids A_123, F_26, P_145, A_197, and P_9 of the hydrophobic surface and nitrogen of cholinium cations in 30% of $[\text{Ch}]_3[\text{PO}_4]$. (C) Side chain of amino acids A_123, F_26, P_145, A_197, and P_9 of the hydrophobic surface and nitrogen of cholinium cations in 20% of $[\text{Ch}]_3[\text{PO}_4]$.

As shown in Figure 10, in different concentrations (40%, 30%, and 20%), the height of the first peak (A_123) of the distribution function is larger than the rest of the amino acids. According to Figure S3, in different concentrations (40%, 30%, and 20% of [C4MIM][Ac]), the height of the first peak (A_123) in the radial distribution function is greater. As shown in Figure S4, in all designed systems of [C2MIM][Ac] in different concentrations 40%, 30%, and 20%, the height of the first peak (A_123) of the RDF is larger than the rest. Thus, in accordance with Figure 10 through Figure S4, the height of the first peak (A_123) for different ionic liquids is as follows:

Alkyl groups of [C2MIM] cation < Alkyl groups of [C4MIM] cation < methyl groups of cholinium cation.

On the other hand, the highest peak in RDF corresponds to the probability of methyl groups of cholinium cation around the methyl group of A_123 (Figure 10). From Figure 10, can be seen that methyl groups of cation showed insignificant differences of probability density around the rings of F_26 and P_9. As it was expected from A_123 and P145, the probability density of methyl groups of cholinium cation was more for the methyl group (side chain) of A_123 than for the ring of P_145.

Furthermore, by decreasing the concentration of [Ch]₃[PO₄], the density of cations around A_123 is also decreased. It can be also concluded that with the increase in the length of the alkyl chain from [C2MIM] to [C4MIM], the density of the cations around A_123 increased, but by increasing the concentration (from 20% to 40%) of [C2MIM][Ac] and [C4MIM][Ac], the change in the density of these cations is not significant. Thus, the effect of crowding on the stability of the hydrophobic surface is more pronounced in the presence of [Ch]₃[PO₄] than other ionic liquids.

3. Materials and Methods

Several different model systems were set up to perform molecular dynamics simulations of wild-type *Ideonella sakaiensis* PETase enzyme with the PDB code of 5XJH [39]. The simulation systems with three different concentration of three ILs of 1-ethyl-3-methylimidazolium acetate [C2MIM][Ac], 1-butyl-3-methylimidazolium acetate [C4MIM][Ac], and cholinium phosphate (choline phosphate) [Ch]₃[PO₄] were prepared. Recent studies reveal that [Ch]₃[PO₄] is a bi-functional media, capable of both high solubilization (solvent) and effective depolymerization (catalyst) of PET [4]. Furthermore, [Ch]₃[PO₄] is also an effective depolymerizer (catalysts). Furthermore, the lower cost of cholinium phosphate [Ch]₃[PO₄] ionic liquid has quite a good ability to dissolve PET (10 wt%) [4]. Hence, the initial structures with these ionic liquids were setup using PACKMOL [40]. As a control, the PETase enzyme was also simulated in pure aqueous media. The ligand presented in our study has two TPA rings, which are called BHET. Parametrization of the ligand and ILs were carried out using general amber force field GAFF [41], as this forcefield can accurately predict thermodynamic and transport properties of various ionic liquids [42], and we have successfully used it in our previous calculations with ILs [43,44]. Each system was placed in a cubic box, sized 12 nm, using PACKMOL program package. Each model system has been neutralized by counterions. The system was first equilibrated in canonical ensemble (NVT) for 500 ps at 300 K temperature followed by the NPT—the isothermal isobaric ensemble. The temperature was maintained at 300 K and the pressure was maintained at 1bar with compressibility of 4.6×10^{-5} /bar by weak coupling to temperature and pressure baths using the Berendsen method [45] with relaxation times of 0.1 ps. Van der Waals forces were evaluated with a Lennard-Jones potential, having 10 Å cut-off, and long-range electrostatic contributions were evaluated using the particle mesh Ewald method [46] with a direct interaction cut-off of 10.0 Å. A time step of 2 fs was employed. Lengths of all covalent bonds were constrained by the linear constraint solver algorithm (LINCS) [47]. All simulations were run with periodic boundary conditions for 150 ns. The MD simulations and related analyses were performed using the GROMACS program package [48–50]. Molecular graphics images were produced using VMD [51] software and all the graphs were prepared using xmgrace program.

4. Conclusions

In the current study, the structural basis of the possible co-solvent candidates for the stability of PETase were analyzed and their interaction patterns were compared. The in silico-based investigation, using MD simulations, provides new insights into the interacting residues of the protein with the ionic liquids and water. The effect of ionic liquids cholinium phosphate $[\text{Ch}]_3[\text{PO}_4]$, 1-butyl-3-methyl-imidazolium acetate $[\text{C4MIM}][\text{Ac}]$, 1-ethyl-3-methyl-imidazolium acetate $[\text{C2MIM}][\text{Ac}]$, and their water solutions on *Ideonella sakaiensis* PETase with BHET substrate were investigated. Moreover, after the careful structural and interactive analyses of the ligand with the PETase, it is concluded that among all the above mentioned ionic liquids, $[\text{Ch}]_3[\text{PO}_4]$ has the smallest effect of the structure of PETase and its interaction with the BHET substrate, which is comparable to the pure water solvent. This makes the water solution with $[\text{Ch}]_3[\text{PO}_4]$ a good candidate for the solvent used during BHET hydrolysis, which can be used for future investigation.

Supplementary Materials: The following supporting information can be downloaded online, Figure S1: The number of hydrogen bonds between amino acids of PETase and $[\text{C2MIM}][\text{Ac}]$, $[\text{C4MIM}][\text{Ac}]$; Figure S2: the interaction of $[\text{C4MIM}]$ (A) and $[\text{C2MIM}]$ (B) cations with hydrophobic surface of PETase; Figure S3: radial distribution functions (RDFs) for atoms of hydrophobic amino acids and $[\text{C4MIM}]$ cations; Figure S4: additionally, the radial distribution functions (RDFs) for atoms of hydrophobic amino acids and $[\text{C2MIM}]$ cations are included in the supplementary data file.

Author Contributions: Conceptualization, B.M., E.C., and D.Ř.; methodology, B.M. and D.Ř.; formal analysis, D.M., Z.Z., and S.K.P.; funding acquisition, D.Ř.; investigation, Z.Z. and D.M.; software, D.Ř. and B.M.; supervision, D.Ř.; visualization, Z.Z. and D.M.; writing—original draft preparation, Z.Z. and D.M.; writing—review and editing, B.M., D.Ř., E.C., F.F., and Z.Z. All authors have read and agreed to the published version of the manuscript.

Funding: This research work was supported by the Grant Agency of the University of South Bohemia (GAJU 017/2019/P) and by the Czech Science Foundation as the project GA21-15936S. Computational resources were supplied by the project “e-Infrastruktura CZ” (e-INFRA LM2018140), provided within the program Projects of Large Research, Development, and Innovations Infrastructures.

Institutional Review Board Statement: Not applicable.

Informed Consent Statement: Not applicable.

Data Availability Statement: The data presented in this study are available in article.

Acknowledgments: We appreciatively acknowledge the support from the Grant Agency of the University of South Bohemia (GAJU 017/2019/P) and by the Czech Science Foundation as the project GA21-15936S. The computational resources were supplied by the project “e-Infrastruktura CZ” (e-INFRA LM2018140), provided within the program Projects of Large Research, Development, and Innovations Infrastructures.

Conflicts of Interest: The authors declare no conflict of interest.

Sample Availability: Not applicable.

References

1. Cimpan, C.; Bjelle, E.L.; Stromman, A.H. Plastic packaging flows in Europe: A hybrid input-output approach. *J. Ind. Ecol.* **2021**, *25*, 1572–1587. [[CrossRef](#)]
2. Rochman, C.M.; Browne, M.A.; Halpern, B.S.; Hentschel, B.T.; Hoh, E.; Karapanagioti, H.K.; Rios-Mendoza, L.M.; Takada, H.; Teh, S.; Thompson, R.C. Classify plastic waste as hazardous. *Nature* **2013**, *494*, 169–171. [[CrossRef](#)]
3. Geyer, R.; Jambeck, J.R.; Law, K.L. Production, use, and fate of all plastics ever made. *Sci. Adv.* **2017**, *3*, e1700782. [[CrossRef](#)] [[PubMed](#)]
4. Sun, J.; Liu, D.; Young, R.P.; Cruz, A.G.; Isern, N.G.; Schuerg, T.; Cort, J.R.; Simmons, B.A.; Singh, S. Solubilization and Upgrading of High Polyethylene Terephthalate Loadings in a Low-Costing Bifunctional Ionic Liquid. *ChemSusChem* **2018**, *11*, 781–792. [[CrossRef](#)] [[PubMed](#)]
5. Todd, A.D.; McEneaney, R.J.; Topolkaraev, V.A.; Macosko, C.W.; Hillmyer, M.A. Reactive compatibilization of poly (ethylene terephthalate) and high-density polyethylene using amino-telechelic polyethylene. *Macromolecules* **2016**, *49*, 8988–8994. [[CrossRef](#)]

6. Shi, H.; Tang, A.; Liang, Q.; Jiang, Y. Synthesis and hydrophobic properties of F & Si containing poly (ethylene terephthalate). *RSC Adv.* **2016**, *6*, 106540–106546.
7. Wang, H.; Li, Z.; Liu, Y.; Zhang, X.; Zhang, S. Degradation of poly (ethylene terephthalate) using ionic liquids. *Green Chem.* **2009**, *11*, 1568–1575. [[CrossRef](#)]
8. Chaudhary, N.; Koiry, S.; Singh, A.; Tillu, A.; Jha, P.; Samanta, S.; Debnath, A.; Aswal, D.; Mondal, R.; Acharya, S. Electron beam induced modifications in flexible biaxially oriented polyethylene terephthalate sheets: Improved mechanical and electrical properties. *Mater. Chem. Phys.* **2017**, *189*, 237–244. [[CrossRef](#)]
9. Samak, N.A.; Jia, Y.; Sharshar, M.M.; Mu, T.; Yang, M.; Peh, S.; Xing, J. Recent advances in biocatalysts engineering for polyethylene terephthalate plastic waste green recycling. *Environ. Int.* **2020**, *145*, 106144. [[CrossRef](#)]
10. Wallace, N.E.; Adams, M.C.; Chafin, A.C.; Jones, D.D.; Tsui, C.L.; Gruber, T.D. The highly crystalline PET found in plastic water bottles does not support the growth of the PETase-producing bacterium *Ideonella sakaiensis*. *Environ. Microbiol. Rep.* **2020**, *12*, 578–582. [[CrossRef](#)]
11. Olivier-Bourbigou, H.; Magna, L.; Morvan, D. Ionic liquids and catalysis: Recent progress from knowledge to applications. *Appl. Catal. A Gen.* **2010**, *373*, 1–56. [[CrossRef](#)]
12. Moniruzzaman, M.; Nakashima, K.; Kamiya, N.; Goto, M. Recent advances of enzymatic reactions in ionic liquids. *Biochem. Eng. J.* **2010**, *48*, 295–314. [[CrossRef](#)]
13. Hadad, C.; Husson, E.; Van Nhien, A.N. Conversion of Chitin in Ionic Liquids. In *Encyclopedia of Ionic Liquids*; Springer: Singapore, 2020; pp. 1–6.
14. Bubalo, M.C.; Radošević, K.; Redovniković, I.R.; Slivac, I.; Srček, V.G. Toxicity mechanisms of ionic liquids. *Arch. Ind. Hyg. Toxicol.* **2017**, *68*, 171–179. [[CrossRef](#)] [[PubMed](#)]
15. Roosen, C.; Müller, P.; Greiner, L. Ionic liquids in biotechnology: Applications and perspectives for biotransformations. *Appl. Microbiol. Biotechnol.* **2008**, *81*, 607–614. [[CrossRef](#)] [[PubMed](#)]
16. Gorke, J.; Srienc, F.; Kazlauskas, R. Toward advanced ionic liquids. Polar, enzyme-friendly solvents for biocatalysis. *Biotechnol. Bioprocess Eng.* **2010**, *15*, 40–53. [[CrossRef](#)] [[PubMed](#)]
17. Halle, B. Protein hydration dynamics in solution: A critical survey. *Philos. Trans. R. Soc. Lond. Ser. B Biol. Sci.* **2004**, *359*, 1207–1224. [[CrossRef](#)] [[PubMed](#)]
18. Klibanov, A.M. Improving enzymes by using them in organic solvents. *Nature* **2001**, *409*, 241–246. [[CrossRef](#)]
19. Constatinescu, D.; Herrmann, C.; Weingärtner, H. Patterns of protein unfolding and protein aggregation in ionic liquids. *PCCP* **2010**, *12*, 1756–1763. [[CrossRef](#)] [[PubMed](#)]
20. Page, T.A.; Kraut, N.D.; Page, P.M.; Baker, G.A.; Bright, F.V. Dynamics of loop 1 of domain I in human serum albumin when dissolved in ionic liquids. *J. Phys. Chem. B* **2009**, *113*, 12825–12830. [[CrossRef](#)] [[PubMed](#)]
21. Akdogan, Y.; Junk, M.J.; Hinderberger, D. Effect of ionic liquids on the solution structure of human serum albumin. *Biomacromolecules* **2011**, *12*, 1072–1079. [[CrossRef](#)]
22. Micaelo, N.M.; Soares, C.M. Protein structure and dynamics in ionic liquids. Insights from molecular dynamics simulation studies. *J. Phys. Chem. B* **2008**, *112*, 2566–2572.
23. Klähn, M.; Lim, G.S.; Seduraman, A.; Wu, P. On the different roles of anions and cations in the solvation of enzymes in ionic liquids. *PCCP* **2011**, *13*, 1649–1662. [[CrossRef](#)] [[PubMed](#)]
24. Wang, H.; Gurau, G.; Rogers, R.D. Ionic liquid processing of cellulose. *Chem. Soc. Rev.* **2012**, *41*, 1519–1537. [[CrossRef](#)]
25. Xu, A.R.; Wang, F. Carboxylate ionic liquid solvent systems from 2006 to 2020: Thermal properties and application in cellulose processing. *Green Chem.* **2020**, *22*, 7622–7664. [[CrossRef](#)]
26. Tournier, V.; Topham, C.; Gilles, A.; David, B.; Folgoas, C.; Moya-Leclair, E.; Kamionka, E.; Desrousseaux, M.-L.; Texier, H.; Gavalda, S. An engineered PET depolymerase to break down and recycle plastic bottles. *Nature* **2020**, *580*, 216–219. [[CrossRef](#)]
27. Müller, R.J.; Schrader, H.; Profe, J.; Dresler, K.; Deckwer, W.D. Enzymatic degradation of poly (ethylene terephthalate): Rapid hydrolyse using a hydrolase from *T. fusca*. *Macromol. Rapid Commun.* **2005**, *26*, 1400–1405. [[CrossRef](#)]
28. Sinha, V.; Patel, M.R.; Patel, J.V. PET waste management by chemical recycling: A review. *J. Polym. Environ.* **2010**, *18*, 8–25. [[CrossRef](#)]
29. Liu, B.; He, L.; Wang, L.; Li, T.; Li, C.; Liu, H.; Luo, Y.; Bao, R. Protein crystallography and site-direct mutagenesis analysis of the poly (ethylene terephthalate) hydrolase PETase from *Ideonella sakaiensis*. *ChemBioChem* **2018**, *19*, 1471–1475. [[CrossRef](#)]
30. Yang, Y.; Yang, J.; Jiang, L. Comment on “A bacterium that degrades and assimilates poly (ethylene terephthalate)”. *Science* **2016**, *353*, 759. [[CrossRef](#)] [[PubMed](#)]
31. Yoshida, S.; Hiraga, K.; Takehana, T.; Taniguchi, I.; Yamaji, H.; Maeda, Y.; Toyohara, K.; Miyamoto, K.; Kimura, Y.; Oda, K. A bacterium that degrades and assimilates poly (ethylene terephthalate). *Science* **2016**, *351*, 1196–1199. [[CrossRef](#)]
32. Bornscheuer, U.T. Feeding on plastic. *Science* **2016**, *351*, 1154–1155. [[CrossRef](#)]
33. Han, X.; Liu, W.; Huang, J.-W.; Ma, J.; Zheng, Y.; Ko, T.-P.; Xu, L.; Cheng, Y.-S.; Chen, C.-C.; Guo, R.-T. Structural insight into catalytic mechanism of PET hydrolase. *Nat. Commun.* **2017**, *8*, 1–6. [[CrossRef](#)]
34. Palm, G.J.; Reisky, L.; Böttcher, D.; Müller, H.; Michels, E.A.; Walczak, M.C.; Berndt, L.; Weiss, M.S.; Bornscheuer, U.T.; Weber, G. Structure of the plastic-degrading *Ideonella sakaiensis* MHETase bound to a substrate. *Nat. Commun.* **2019**, *10*, 1–10. [[CrossRef](#)]
35. Marshall, I.; Todd, A. The thermal degradation of polyethylene terephthalate. *Trans. Faraday Soc.* **1953**, *49*, 67–78. [[CrossRef](#)]
36. Tokiwa, Y.; Calabia, B.P.; Ugwu, C.U.; Aiba, S. Biodegradability of plastics. *Int. J. Mol. Sci.* **2009**, *10*, 3722–3742. [[CrossRef](#)]

37. Austin, H.P.; Allen, M.D.; Donohoe, B.S.; Rorrer, N.A.; Kearns, F.L.; Silveira, R.L.; Pollard, B.C.; Dominick, G.; Duman, R.; El Omari, K. Characterization and engineering of a plastic-degrading aromatic polyestherase. *Proc. Natl. Acad. Sci. USA* **2018**, *115*, E4350–E4357. [[CrossRef](#)]
38. Baldwin, R.L. How Hofmeister ion interactions affect protein stability. *Biophys. J.* **1996**, *71*, 2056–2063. [[CrossRef](#)]
39. Joo, S.; Cho, I.J.; Seo, H.; Son, H.F.; Sagong, H.-Y.; Shin, T.J.; Choi, S.Y.; Lee, S.Y.; Kim, K.-J. Structural insight into molecular mechanism of poly (ethylene terephthalate) degradation. *Nat. Commun.* **2018**, *9*, 1–12. [[CrossRef](#)] [[PubMed](#)]
40. Martínez, L.; Andrade, R.; Birgin, E.G.; Martínez, J.M. PACKMOL: A package for building initial configurations for molecular dynamics simulations. *J. Comput. Chem.* **2009**, *30*, 2157–2164. [[CrossRef](#)]
41. Dickson, C.J.; Madej, B.D.; Skjevik, Å.A.; Betz, R.M.; Teigen, K.; Gould, I.R.; Walker, R.C. Lipid14: The amber lipid force field. *J. Chem. Theory Comput.* **2014**, *10*, 865–879. [[CrossRef](#)] [[PubMed](#)]
42. Sprenger, K.G.; Jaeger, V.W.; Pfaendtner, J. The General AMBER Force Field (GAFF) Can Accurately Predict Thermodynamic and Transport Properties of Many Ionic Liquids. *J. Phys. Chem. B* **2015**, *119*, 5882–5895.
43. D’Oronzo, E.; Secundo, F.; Minofar, B.; Kulik, N.; Pometun, A.A.; Tishkov, V.I. Activation/Inactivation Role of Ionic Liquids on Formate Dehydrogenase from *Pseudomonas* sp 101 and Its Mutated Thermostable Form. *Chemcatchem* **2018**, *10*, 3247–3259.
44. Shaposhnikova, A.; Kutty, M.; Chaloupkova, R.; Damborsky, J.; Smatanova, I.K.; Minofar, B.; Prudnikova, T. Stabilization of Haloalkane Dehalogenase Structure by Interfacial Interaction with Ionic Liquids. *Crystals* **2021**, *11*, 1052. [[CrossRef](#)]
45. Ryckaert, J.-P.; Ciccotti, G.; Berendsen, H.J. Numerical integration of the cartesian equations of motion of a system with constraints: Molecular dynamics of n-alkanes. *J. Comput. Phys.* **1977**, *23*, 327–341. [[CrossRef](#)]
46. Essmann, U.; Perera, L.; Berkowitz, M.L.; Darden, T.; Lee, H.; Pedersen, L.G. A smooth particle mesh Ewald method. *J. Chem. Phys.* **1995**, *103*, 8577–8593. [[CrossRef](#)]
47. Hess, B. P-LINCS: A parallel linear constraint solver for molecular simulation. *J. Chem. Theory Comput.* **2008**, *4*, 116–122. [[CrossRef](#)]
48. Berendsen, H.J.C.; Vandespoel, D.; Vandrunen, R. GROMACS—A message-passing parallel molecular-dynamics implementation. *Comput. Phys. Commun.* **1995**, *91*, 43–56.
49. Pronk, S.; Pall, S.; Schulz, R.; Larsson, P.; Bjelkmar, P.; Apostolov, R.; Shirts, M.R.; Smith, J.C.; Kasson, P.M.; van der Spoel, D.; et al. GROMACS 4.5: A high-throughput and highly parallel open source molecular simulation toolkit. *Bioinformatics* **2013**, *29*, 845–854. [[CrossRef](#)]
50. Van der Spoel, D.; Lindahl, E.; Hess, B.; Groenhof, G.; Mark, A.E.; Berendsen, H.J.C. GROMACS: Fast, flexible, and free. *J. Comput. Chem.* **2005**, *26*, 1701–1718. [[CrossRef](#)]
51. Humphrey, W.; Dalke, A.; Schulten, K. VMD: Visual molecular dynamics. *J. Mol. Graph.* **1996**, *14*, 33–38. [[CrossRef](#)]

PAPER 2

Preassembly and coupling of 5-hydroxytryptamine receptor type 7 (5-HT7R) and the stimulatory Gs protein: dynamics of the protein-protein interface models. Journal of Chemical Information and Modeling.

Zeenat Zara, Alessandro Nicoli, Natalia Kulik, David Reha, Alexey Bondar, Antonella Di Pizio,

PAPER 3

Ionic Liquid-Based Nano-Materials for Drug Delivery

Zeenat Zara, Saurabh Kumar Pandey, Babak Minofar

DOI: https://doi.org/10.1007/978-981-10-6739-6_71-1